Springer ThesesRecognizing Outstanding Ph.D. Research

Viola Folli

Nonlinear Optics and Laser Emission through Random Media



Springer Theses

Recognizing Outstanding Ph.D. Research

For further volumes: http://www.springer.com/series/8790

Aims and Scope

The series "Springer Theses" brings together a selection of the very best Ph.D. theses from around the world and across the physical sciences. Nominated and endorsed by two recognized specialists, each published volume has been selected for its scientific excellence and the high impact of its contents for the pertinent field of research. For greater accessibility to non-specialists, the published versions include an extended introduction, as well as a foreword by the student's supervisor explaining the special relevance of the work for the field. As a whole, the series will provide a valuable resource both for newcomers to the research fields described, and for other scientists seeking detailed background information on special questions. Finally, it provides an accredited documentation of the valuable contributions made by today's younger generation of scientists.

Theses are accepted into the series by invited nomination only and must fulfill all of the following criteria

- They must be written in good English.
- The topic should fall within the confines of Chemistry, Physics, Earth Sciences and related interdisciplinary fields such as Materials, Nanoscience, Chemical Engineering, Complex Systems and Biophysics.
- The work reported in the thesis must represent a significant scientific advance.
- If the thesis includes previously published material, permission to reproduce this must be gained from the respective copyright holder.
- They must have been examined and passed during the 12 months prior to nomination.
- Each thesis should include a foreword by the supervisor outlining the significance of its content.
- The theses should have a clearly defined structure including an introduction accessible to scientists not expert in that particular field.

Viola Folli

Nonlinear Optics and Laser Emission through Random Media

Doctoral Thesis accepted by Dipartimento di Fisica, Sapienza Università di Roma, Rome, Italy



Author
Dr. Viola Folli
Dipartimento di Fisica
Sapienza Università di Roma
Piazzale Aldo Moro 2
00185 Rome
Italy

Supervisor
Prof. Dr. Claudio Conti
Department of Physics
University of Rome–La-Sapienza
Rome
Italy

Springer Dordrecht Heidelberg New York London

Library of Congress Control Number: 2012937845

© Springer Science+Business Media Dordrecht 2012

This work is subject to copyright. All rights are reserved by the Publisher, whether the whole or part of the material is concerned, specifically the rights of translation, reprinting, reuse of illustrations, recitation, broadcasting, reproduction on microfilms or in any other physical way, and transmission or information storage and retrieval, electronic adaptation, computer software, or by similar or dissimilar methodology now known or hereafter developed. Exempted from this legal reservation are brief excerpts in connection with reviews or scholarly analysis or material supplied specifically for the purpose of being entered and executed on a computer system, for exclusive use by the purchaser of the work. Duplication of this publication or parts thereof is permitted only under the provisions of the Copyright Law of the Publisher's location, in its current version, and permission for use must always be obtained from Springer. Permissions for use may be obtained through RightsLink at the Copyright Clearance Center. Violations are liable to prosecution under the respective Copyright Law.

The use of general descriptive names, registered names, trademarks, service marks, etc. in this publication does not imply, even in the absence of a specific statement, that such names are exempt from the relevant protective laws and regulations and therefore free for general use.

While the advice and information in this book are believed to be true and accurate at the date of publication, neither the authors nor the editors nor the publisher can accept any legal responsibility for any errors or omissions that may be made. The publisher makes no warranty, express or implied, with respect to the material contained herein.

Printed on acid-free paper

Springer is part of Springer Science+Business Media (www.springer.com)

Supervisor's Foreword

The physics of disordered and nonlinear systems is one of the leading mainstreams in modern research. This topic is largely interdisciplinary and commits together a variety of different disciplines, like nonlinear waves, diffusive processes, quantum mechanics, photonics, and ultimately the whole field of nanotechnology, as reducing spatial dimensions always leads to enhanced field intensities (and hence nonlinear effects) while also introducing disorder because of fabrication tolerances.

Disorder and nonlinearity are also ubiquitous in the so-called science of complex systems, which deals with things like swarming, traffic, soft-matter, and many other frameworks, where one can identify a number of interacting agents (from ants to photons). Wave propagation in random media and, specifically, optical propagation in disordered systems, is well within the science of complex systems, even if this connection is so far only barely developed. When I first decided to assign a thesis on the Photonics of Complex Systems, I was looking for a smart student able to tackle the problem in its whole generality without losing in mathematical formalities and, hopefully, also able to realize some practical implementations either in numerical simulations or, even better, in experiments. This activity was to be placed within the project of the European Research Council âLight and Complexityâ aimed to create a general interdisciplinary amount of knowledge between the fields of statistical mechanics of disordered systems and photonics.

There was the possibility of making many different theses, either on nonlinear optics or on lasers; there was also the open choice between an experimental work or a theoretical one. When I first met Dr. Folli, I had not in mind the possibility she could be able of putting all of this in a single Ph.D. For such an achievement, there was the need of a very talented student with a background in fundamental physics, nonlinear waves, statistical mechanics, and a large amount of courage and imagination.

The overall work of Dr. Folli can be read with several perspectives: as a first attempt to conciliate different forms of localization in nonlinear random waves, as the application of methods of statistical mechanics to nonlinear optics, as the demonstration that disorder and nonlinearity may open new applications (e.g., two

level lasers), and last, but not least, as the opening of a new experimental line: lasing in shaken matter.

Dr. Folli has hence written a work which can be considered as a paradigmatic model for a thesis in Complex Photonics, and the amount of the presented results is certainly impressive for the content, the degree of inter-disciplinarity, and the novelty. This thesis will certainly stimulate a number of developments in the field.

Rome, 17 February 2012

Prof. Dr. Claudio Conti

Acknowledgments

It is with great pleasure that I thank all those people who have contributed to make this thesis possible and successful.

I would like to express my sincere gratitude to my special guide, Prof. C. Conti, for his assistance and support in all my "amazing" adventures through my Ph.D. experience. It is been a privilege for me to work and collaborate with him. With his advice and his great patience, he guided my enthusiasm and awakened my curiosity. His approach to science was the best way to stimulate and promote creativity in my work. Physics is about giving space to the imagination by fitting and linking new ideas with established rules. Thus my supervisor's guidance provided the necessary technical support to encourage abstract ideas in becoming concrete physical strategies. A rolling stone gathers no moss.

I am grateful to Prof. G. Ruocco and Prof. R. Caminiti, especially for their coordination and agility in moving through the bureaucracy of my Ph.D. work. I wish to thank Prof. S. Trillo and Prof. E. Del Re for useful discussions and suggestions concerning the soliton theory and the scale-free regime.

I would like to remember all my colleagues of room 114 and Ph.D. room. Working within a friendly and lovely environment has been of great importance for me, especially during the unforgettable year of 2009. Spending time together at the University and outside of it, our friendship has grown through the years. A heartfelt thank you Silvia Gentilini and her cheerful laugh that always helped me "to stay in peace", to Neda Gofraniha and her tenacious personality. Guido Bolognesi has been a fabulous dining companion who has spent time by listening to me: "You're not LISTENING TO ME!"...he is the right friend. Thank you to Marco Leonetti, the scientist, and to Stefano Cazzato now doing research in North Europe! I also acknowledge Md Deen Islam for his technical expertise in solving any type of issue, from scientific equipment to coffee machine repairs.

Beyond Physics and academia, these years have been made joyful due to all of my friends whose kindly presence has brightened my road. In particular, thanks from the heart to my dear Giacinta who not only gave me her valuable advice, but also encouraged and supported my choices with her special vision of life. I thank her family, my second family.

viii Acknowledgments

Lastly and most importantly, I would like to thank my parents for their appreciation and encouragement in all the steps through my Ph.D. journey. Ever since I was young, their presence has strengthened me and all my successes are due to their vigilant and motivational care.

This thesis is dedicated to my family, especially to my special little girl.

Dr. Viola Folli

Contents

| 1 | Intr | oduction | | | | | | |
|-----|---|---|--|--|--|--|--|--|
| | 1.1 | Light and Nonlinearity | | | | | | |
| | 1.2 | Light and Disorder | | | | | | |
| | 1.3 | Overview of This Thesis | | | | | | |
| | Refe | prences | | | | | | |
| | | | | | | | | |
| Par | t I | Non-Resonant Systems | | | | | | |
| 2 | Nonlinear Schroedinger Equation | | | | | | | |
| | 2.1 | Introduction 9 | | | | | | |
| | 2.2 | Local Case | | | | | | |
| | | 2.2.1 Plane Wave Solution | | | | | | |
| | | 2.2.2 Modulation Instability | | | | | | |
| | | 2.2.3 The Bound States | | | | | | |
| | 2.3 | Nonlocal Case | | | | | | |
| | | 2.3.1 Plane Wave Solution | | | | | | |
| | | 2.3.2 Modulation Instability | | | | | | |
| | | 2.3.3 The Bound States | | | | | | |
| | | 2.3.4 Highly Nonlocal Limit | | | | | | |
| | Refe | erences | | | | | | |
| 3 | Weakly Disordered Nonlinear Schroedinger Equation 2 | | | | | | | |
| | 3.1 | Introduction | | | | | | |
| | 3.2 | The Model | | | | | | |
| | 3.3 | Soliton Perturbation Theory in Nonlocal Media | | | | | | |
| | 3.4 | Application to the Disordered Nonlocal NLS | | | | | | |
| | 3.5 | Nonparaxial Corrections | | | | | | |
| | Refe | erences | | | | | | |

x Contents

| | Disordered Nonlinear Schroedinger Equation | | | | | | |
|-----|---|--|--|--|--|--|--|
| | 4.1 Introduction | | | | | | |
| | 4.2 Anderson Localization | . 30 | | | | | |
| | The Model | | | | | | |
| | 4.4 Highly Nonlocal Limit | . 32 | | | | | |
| | 4.5 Instability of Anderson States | . 33 | | | | | |
| | 4.6 Nonlocal Responses | . 34 | | | | | |
| | 4.7 Numerical Results | . 36 | | | | | |
| | 4.8 Beating of Anderson Localizations | . 37 | | | | | |
| | References | . 38 | | | | | |
| 5 | Scale-Free Nonlinearity in Disordered Ferroelectrics | | | | | | |
| | 5.1 Diffusive Nonlinearity in Disordered Ferroelectrics | . 41 | | | | | |
| | 5.2 Scale-Free Solitons | . 43 | | | | | |
| | 5.3 Scale-Free Instability | . 44 | | | | | |
| | 5.3.1 Absence of Modulational Instability | . 44 | | | | | |
| | 5.3.2 Theory of Scale-Free Instabilities | | | | | | |
| | 5.3.3 Defocusing Instability | . 46 | | | | | |
| | 5.3.4 Fragmenting Instability | . 47 | | | | | |
| | References | . 49 | | | | | |
| | | | | | | | |
| Paı | t II Resonant Systems | | | | | | |
| 6 | The Maxwell-Bloch Equations | . 53 | | | | | |
| | | | | | | | |
| | 6.1 Introduction | . 53 | | | | | |
| | 6.2 Generalities | . 53 . 54 | | | | | |
| | 6.2 Generalities | . 53 . 54 . 57 | | | | | |
| | 6.2 Generalities | . 53 . 54 . 57 . 59 | | | | | |
| | 6.2 Generalities | . 53 . 54 . 57 . 59 | | | | | |
| 7 | 6.2 Generalities | 53 . 54 . 57 . 59 . 60 | | | | | |
| | 6.2 Generalities | . 53 . 54 . 57 . 59 . 60 | | | | | |
| | 6.2 Generalities | 53 54 57 59 60 61 | | | | | |
| | 6.2 Generalities . 6.3 The Numerical Approach . 6.4 The Soliton Solution of the MB Equations . References . Disordered Maxwell-Bloch Equations . 7.1 Introduction . | 53 54 57 59 60 61 61 | | | | | |
| | 6.2 Generalities | . 53 . 54 . 57 . 59 . 60 . 61 . 63 . 65 | | | | | |
| | 6.2 Generalities | . 53 . 54 . 57 . 59 . 60 . 61 . 63 . 65 . 69 | | | | | |
| 7 | 6.2 Generalities | . 53 . 54 . 57 . 59 . 60 . 61 . 63 . 65 . 69 | | | | | |
| 7 | 6.2 Generalities 6.3 The Numerical Approach 6.4 The Soliton Solution of the MB Equations References Disordered Maxwell-Bloch Equations 7.1 Introduction 7.2 Soliton Perturbation Theory in Resonant Media 7.3 Anderson Localization in Resonant Media References Glassy Behavior of Laser | . 53 . 54 . 57 . 59 . 60 . 61 . 63 . 65 . 69 | | | | | |
| 7 | 6.2 Generalities 6.3 The Numerical Approach 6.4 The Soliton Solution of the MB Equations References Disordered Maxwell-Bloch Equations 7.1 Introduction 7.2 Soliton Perturbation Theory in Resonant Media 7.3 Anderson Localization in Resonant Media References Glassy Behavior of Laser 8.1 Introduction | . 53 . 54 . 57 . 59 . 60 . 61 . 63 . 65 . 69 . 71 . 72 | | | | | |
| 7 | 6.2 Generalities . 6.3 The Numerical Approach 6.4 The Soliton Solution of the MB Equations References . Disordered Maxwell-Bloch Equations . 7.1 Introduction . 7.2 Soliton Perturbation Theory in Resonant Media . 7.3 Anderson Localization in Resonant Media . References . Glassy Behavior of Laser . 8.1 Introduction . 8.2 The Model . 8.3 Averaged Free Energy . | . 53 . 54 . 57 . 59 . 60 . 61 . 63 . 65 . 69 . 71 . 72 . 73 | | | | | |
| 7 | 6.2 Generalities . 6.3 The Numerical Approach 6.4 The Soliton Solution of the MB Equations References . Disordered Maxwell-Bloch Equations . 7.1 Introduction . 7.2 Soliton Perturbation Theory in Resonant Media . 7.3 Anderson Localization in Resonant Media . References . Glassy Behavior of Laser . 8.1 Introduction . 8.2 The Model . 8.3 Averaged Free Energy . | . 53 . 54 . 57 . 59 . 60 . 61 . 63 . 65 . 69 . 71 . 72 . 73 . 74 | | | | | |

Contents xi

| 9 | The Granular Laser | | | | | |
|----|--------------------|---------|------------------------------------|-----|--|--|
| | 9.1 | Introd | uction | 81 | | |
| | 9.2 | Introd | uction to Random Laser | 82 | | |
| | 9.3 | Exper | imental Setup and Procedures | 86 | | |
| | | 9.3.1 | Continuous Wave Analysis | 87 | | |
| | | 9.3.2 | Laser Emission Analysis | 90 | | |
| | | 9.3.3 | Oscillation Amplitude Calibration | 91 | | |
| | 9.4 | The D | Diffusive Random Laser | 92 | | |
| | | 9.4.1 | Continuous Wave Analysis | 92 | | |
| | | 9.4.2 | Laser Emission Analysis | 93 | | |
| | 9.5 | The G | Granular Random Laser | 95 | | |
| | | 9.5.1 | Continuous Wave Analysis | 96 | | |
| | | 9.5.2 | Laser Emission Analysis | 98 | | |
| | | 9.5.3 | Emission at Constant Power | 105 | | |
| | | 9.5.4 | Shot-to-Shot Variation | 106 | | |
| | | 9.5.5 | Sample with Doubled Radius (2 mm) | 107 | | |
| | | 9.5.6 | The Two-Dimensional Granular Laser | 108 | | |
| | | 9.5.7 | The Heterogeneous Granular Sample | 111 | | |
| | Refe | erences | | 112 | | |
| 10 | Con | clusion | S | 115 | | |

Chapter 1 Introduction

Fortunately, we are living in a nonlinear world. While linearization beautifies physics, nonlinearity provides excitement in physics

Y. R. Shen

1

The real world embraces nonlinearity and disorder and works with their mutual interplay. All the natural and artificial bodies are nonlinear and disordered, especially in the interaction with strong fields, the pivotal topic of this thesis. Here, we will explore several features of this interplay: we will discuss new intriguing phenomena (like the use of nonlinearity to control the stability of light localizations, the emission through two-levels laser action, the first observation of competitive laser spectra by granular media, etc.), that open up novel avenues for research in several fields, from medical imaging to nonlinear optics. In this preface, we give an overview about these two mechanisms, with special emphasis on localization phenomena.

1.1 Light and Nonlinearity

Electrons, the principal players in determining the optical properties of a medium, cannot be truly considered harmonic oscillators when subject to intense electromagnetic fields. ¹ Hence, the nonlinear response of the optical media must be included in Maxwell 's equations, which govern the propagation of electromagnetic waves:

$$\nabla \times \mathbf{E}(\mathbf{r}, t) = -\partial_t \mathbf{B}(\mathbf{r}, t)$$

$$\nabla \times \mathbf{H}(\mathbf{r}, t) = +\partial_t \mathbf{D}(\mathbf{r}, t),$$
(1.1)

V. Folli, Nonlinear Optics and Laser Emission through Random Media, Springer Theses, DOI: 10.1007/978-94-007-4513-1_1,
© Springer Science+Business Media Dordrecht 2012

¹ The restoring force, related to the Coulomb field of the ion core and that binds the electron to its equilibrium position, is not simply elastic and, hence, the energy levels are no longer equidistant.

2 1 Introduction

where **E**, **B** and **H** are respectively the electric, magnetic induction and magnetic fields. The constitutive relationships define the coupling between the fields and the medium. For what concerns the electric field²:

$$\mathbf{D}(\mathbf{r},t) = \epsilon_0 \mathbf{E}(\mathbf{r},t) + \mathbf{P}(\mathbf{r},t), \tag{1.2}$$

where \mathbf{D} is the electric displacement and \mathbf{P} is the electric polarization. The polarization is usually a complicated nonlinear function of the electric field that fully describes the response of the medium to the applied field. In principle, the combined resolution of the Maxwell's and the constitutive equations with the appropriate boundary conditions gives all the information on the matter-radiation interaction. This is only possible for a limited class of phenomena. The remaining universe must be treated via approximations. For example, the following power-series expansion of the electric polarization in term of the electric field, only valid for sufficiently weak fields, allows to distinguish the linear contribution in the matter response with respect to the nonlinear one:

$$\mathbf{P} = \chi^{(1)} \mathbf{E} + \chi^{(2)} \mathbf{E} \mathbf{E} + \chi^{(3)} \mathbf{E} \mathbf{E} \mathbf{E} + \cdots, \tag{1.3}$$

and enables to solve the resulting linear system of equations $[\chi^{(1),(2),(3)}]$ are the susceptibility tensors]. The most interesting manifestations of the light-matter interaction however occur on higher order than the linear and this thesis wants to address these regimes.

We will discuss about the nonlinearity in relation to the formation of localized wave-forms. In fact, first we investigate the non-resonant regime, where the spatial nonlinearity (terms higher than the first in the power expansion of polarizability) can compensate for the diffraction effects related to the finite size of the transverse beam, through an optically induced change of the refractive index. Analytically, the relevant wave equation for the electric field is

$$\nabla \times \nabla \times \mathbf{E}(\mathbf{r}, t) + 1/c^2 \partial_{tt} \mathbf{E}(\mathbf{r}, t) = \mu_0 \partial_{tt} \mathbf{P}(\mathbf{r}, t), \tag{1.4}$$

where c is the light velocity and μ_0 the magnetic constant, and admits spatially localized solutions, the so-called *solitons*, 3 which can propagate without altering their

I was observing the motion of a boat which was rapidly drawn along a narrow channel by a pair of horses, when the boat suddenly stopped—not so the mass of water in the channel which it had put in motion; it accumulated round the prow of the vessel in a state of violent agitation, then suddenly leaving it behind, rolled forward with great velocity, assuming the form of a large solitary elevation, a rounded, smooth and well-defined heap of water, which continued its course along the channel apparently without change of form or diminution of speed. I followed it on horseback, and overtook it still rolling on at a rate of some eight or nine miles an hour, preserving its original figure some thirty feet long and a foot to a foot

We assume no free charges present and no magnetization of the medium.

³ The first reported observation of solitons was made by J. S. Russel in 1984 by studying water waves but, once first observed and understood, the solitary waves are found in every branch of the physics of wave propagation [1–5]. He wrote

shapes. Secondly we address the resonant interaction between radiation and matter, in which case the solitary wave can be still observed (e.g. in the so called the Self-Induced Transparency [6, 7]) but its manifestation is due to a different mechanism. In fact, the conservation of the light pulse shape is no longer related to a compensation phenomenon between the diffraction and the modulation of the refractive index in the Maxwell's equations, but to a "synchronized swinging" between absorption and stimulated emission. Furthermore, the electric field is much more intense and the perturbation series above is no longer valid. The material response is calculated from the ab-initio Bloch equations, determining the polarization density, and the complete set of Maxwell's and Bloch's equations defines the interaction processes. In the corpus of this thesis, we will investigate both the non-resonant and resonant nonlinearities and both kinds of solitary waves in presence of randomness.

1.2 Light and Disorder

Disorder is everywhere. It is "invasive" and one should learn to harness it to own interests, avoiding unrealistic approximations that rule out fascinating questions. Without taking into account randomness, related to the presence of scatterers, imperfections or fluctuations in the refractive index, the most relevant physical phenomena observed in complex systems remain unexplored, like turbulence, chaotic dynamics, light and electronics localizations, frustrated dynamics of spin-glass materials, etc. In last years, there has been a massive growth of interest in the study of light propagation in random media, both for practical purposes (mostly in the medical research field) and for basic research. We support this latter point and we aimed at understanding the role of disorder in the propagation of light in nonlinear systems. In fact, disorder is the main actor along with nonlinearity in "trapping" light. In other words, the randomness in the material, when strong enough, permits light to stay localized in narrow spatial regions, the Anderson localized states of light [8]. By varying the strength and the characteristics of disorder, one can confine light practically in any point. The aim of this dissertation is to understand when and how nonlinearity and disorder can compete or cooperate in order to stabilize light localization.

⁽Footnote 3 continued)

and a half in height. Its height gradually diminished, and after a chase of one or two miles I lost it in the windings of the channel. Such, in the month of August 1834, was my first chance interview with that singular and beautiful phenomenon which I have called the Wave of Translation

[—]Report of the fourteenth meeting of the British Association for the Advancement of Science, York, September 1844 (London 1845), pp. 311–390, Plates XLVII–LVII.

4 1 Introduction

1.3 Overview of This Thesis

The chapter organization of this thesis consists of two distinct parts. Part I extends from Chaps. 2–5 and is related to non-resonant regime of interaction between light and matter in a nonlinear disordered framework. Part II extends over Chaps. 6–9 and makes an *excursus* on the nonlinearity-disorder topic in resonant media.

- Part I—Chap. 2: a theoretical background of nonlinear optics. The Nonlinear Schroedinger Equation, the ikon of all the studies on solitary waves is analyzed in the local and nonlocal case of the matter response with a focus on the formation of solitons.
- Part I—Chap. 3: we add disorder by first introducing fluctuations in the refractive index. An analytical perturbative approach is developed and a numerical algorithm is implemented to study the dynamics of solitary waves. The role of nonlocality is examined.
- Part I—Chap. 4: increasing the strength of disorder, we create a second kind of light localization: the Anderson states. The competitive interplay by nonlinearity and disorder is analyzed, by invoking the limit of high nonlocality. The developed analytical perturbative approach is found in agreement with the numerical results.
- Part I—Chap. 5: the spatial scale-length of the interplay between nonlinearity and
 disorder is varied by studying the disordered ferroelectric materials. We analyze
 the family of localized wave-forms, emerging in these materials, and we use the
 linearization techniques to reveal a new kind of light instability.
- Part II—Chap. 6: the basic theory for the study of resonant media. We present the general equations, describing ab-initio matter-radiation interaction: the Maxwell-Bloch's system and the numerical approach via the discretization of the system and the use of Finite-Difference-Time-Domain (FDTD) algorithm.
- Part II—Chap. 7: we retrace the steps of Part I by adding disorder in the Maxwell-Bloch's equations, both perturbative and structural, and studying the propagation of the solitary waves. The difference with the first part is that now the material responds on the same time-scale of the pulse time-life and the nonlinearity plays a role much more pronounced.
- Part II—Chap. 8: we use the theory of spin glasses to analytically solve the problem of nonlinear disordered systems in interaction with resonant light when a large number of localized modes is present.
- Part II—Chap. 9: in this chapter, we present the experimental section. The emission
 spectra dependence on the strength of disorder is analyzed. We exploit one of the
 paradigms of the statistical mechanics of disordered systems: granular matter. Its
 properties principally depend on the dynamical effects, and hence can be controlled
 by using mechanical solicitations, as shear or shaking. We experimentally observe
 that the random laser characteristics can be varied and controlled by the state of
 motion of the granular.

References 5

References

- 1. Dodd R (1982) Solitons and nonlinear wave equations. Academic, London
- 2. Drazin PG, Johnson RS (1989) Solitons: an introduction. Cambridge University Press, New York
- 3. Hasegawa A, Matsumoto M (2002) Optical solitons in fibers. 3rd edn. Springer, New York
- 4. Kivshar YS, Agrawal GP (2003) Optical solitons. Academic, New York
- 5. Trillo S, Torruealls W (eds) (2001) Spatial solitons. Springer-Verlag, Berlin
- 6. McCall SL, Hahn EL (1969) Phys Rev 183:457
- 7. Maimistov A (1990) Present state of self-induced transparency theory. In: Physics reports North-Holland
- 8. Anderson PW (1958) Phys. Rev. 109:1492

Part I Non-Resonant Systems

Chapter 2 Nonlinear Schroedinger Equation

The main aim of this thesis is the study of the interaction between nonlinearity and disorder, the pivotal processes underlying the localization of light. Knowing how the manipulation of an optical system by modifying the mutual competition between disorder and nonlinearity can result in localized wave-forms is an intriguing challenge and a significant target of modern optics. In this section, we discuss the Nonlinear Schroedinger equation (NLS), a paradigmatic universal nonlinear model that describes several physical phenomena in the framework of several disciplines, from the nonlinear optics to the quantum condensate. In a simple way, this equation allows to understand how the nonresonant nonlinearity (specifically the Kerr effect) can promote the formation of localized wave-forms through the balance of two opposite effects: wave dispersion and nonlinear response. The NLS represents the starting point to study the complex interplay between nonlinearity and disorder.

2.1 Introduction

We start by the Maxwell's Equations. They describe the propagation of an electromagnetic wave in a medium with refractive index n. In the time domain they read as,

$$\nabla \times \mathbf{E} = -\mu_0 \partial_t \mathbf{H}$$

$$\nabla \times \mathbf{H} = \epsilon_0 n^2 \partial_t \mathbf{E},$$
(2.1)

where x, y, z are the spatial coordinates while t is the temporal variable. The vectors \mathbf{E} and \mathbf{H} are respectively the electric and the magnetic fields. The relative electric permittivity is ϵ_r and the relative magnetic permeability is μ_r . The refractive index is $n = \sqrt{\epsilon_r \mu_r}$, and depends by the relative values of the considered material; ϵ_0 is the electric constant and μ_0 is the magnetic constant. We study the propagation of an electromagnetic field into a dielectric medium in which no current and no charges are present. From Eq. (2.1), we obtain the wave equation for the electric field:

$$\nabla \times \nabla \times \mathbf{E} = -\mu_0 \epsilon_0 n^2 \partial_t^2 \mathbf{E}. \tag{2.2}$$

We write the monochromatic solution of Eq. (2.2) as:

$$\mathbf{E}(\mathbf{x}, \mathbf{y}, \mathbf{z}, \mathbf{t}) = Re[\mathbf{E}(\mathbf{x}, \mathbf{y}, \mathbf{z})e^{-i\omega t}]$$
 (2.3)

and by using the paraxial approximation (we are considering a z-collimated laser beam) for which it is possible to approximate $\nabla \times \nabla \times \mathbf{E} = \nabla (\nabla \cdot \mathbf{E}) - \nabla^2 \mathbf{E} \approx -\nabla^2 \mathbf{E}$, we write the Helmholtz equation for the electric field:

$$\nabla^2 \mathbf{E} + \frac{\omega^2}{c^2} n^2 \mathbf{E} = 0. \tag{2.4}$$

In an homogeneous medium with $n(r) = n_0$, the simplest solution of Eq. (2.4) in one-dimensional case is the plane wave $\mathbf{E}(z) = Ee^{ikz}\hat{\mathbf{x}}$, for which the Helmholtz equation gives the wave vector $k = \frac{\omega}{c}n_0$. We want to treat the interaction of light in a nonlinear medium, in which the permittivity and the permeability depend on the electromagnetic field. In this specific case, for sake of simplicity, we consider the case in which $\mu_r = 1$ while the electric permittivity is a function of the electric field $\epsilon = \epsilon(E)$. If the medium is nonlinear, we can write $n(r) = n_0 + \Delta n(r)$. We let the general solution amplitude to be space-dependent because nonlinearity can spatially modulate the propagating field:

$$\mathbf{E}(\mathbf{x}, \mathbf{y}, \mathbf{z}) = E(x, y, z)e^{ikz}\hat{\mathbf{x}}.$$
 (2.5)

By inserting Eq. (2.5) in Eq. (2.4) and within the paraxial approximation, for which the longitudinal variation is slow enough and $\partial_z^2 E \approx 0$, we write the amplitude equation:

$$2ik\partial_z E + \nabla_\perp^2 E + 2k^2 \frac{\Delta n}{n_0} E = 0$$
 (2.6)

where we have neglected the higher order term in Δn and we have used the relation $k=\frac{\omega}{c}n_0$. The Eq. (2.6) represents the propagation of a laser beam, collimated along \hat{z} (paraxial approximation), in the presence of an index modulation Δn induced by the nonlinear effects. The power flux is related to the z-component of the Poynting vector, $P_z=\frac{nE^2}{2Z_0}=I$, where $Z_0=\sqrt{\mu_0/\epsilon_0}$ is the impedance of the vacuum. We hence define an optical field A for which the optical intensity is $I=|A|^2$, in this way the complex envelope is related to E by $A=\sqrt{n/2Z_0}E$. The equation for A is simply obtained from which for E:

$$2ik\partial_z A + \nabla_\perp^2 A + 2k^2 \frac{\Delta n}{n_0} A = 0.$$
 (2.7)

In the following, we put particular attention to the one-dimensional case (that corresponds to take $\nabla_{\perp}^2 = \partial_x^2$), in order to simplify the successive analysis of the interplay between nonlinearity and disorder.

¹ Once the disorder is added to the system, the permittivity, and hence the refractive index, will become explicitly dependent on the spatial coordinate, $\epsilon = \epsilon(r, E)$.

2.2 Local Case

2.2 Local Case

In this section, we consider the simplest example of nonlinear system, the Kerr medium. In this kind of material, only the cubic nonlinearity in the paraxial approximation is retained. The refractive index linearly increases with the beam intensity. The refractive index perturbation depends only on the intensity in a given point $\Delta n(r) = n_2 I(r)$, and:

$$n(r) = n_0 + n_2 I(r). (2.8)$$

Equation (2.7) becomes:

$$2ik\partial_z A + \partial_x^2 A + 2k^2 \frac{n_2}{n_0} |A|^2 A = 0.$$
 (2.9)

This is the well-known nonlinear Schroedinger equation (NLS), a universal nonlinear equation describing several nonlinear phenomena, including the Bose-Einstein condensation when it is expressed in the adimensional form, by rescaling the coordinates $z \to 2kx_0^2z$, $x \to x_0x$ and the field amplitude $A \to \sqrt{n_0/(2k^2x_0^2|n_2|)}\psi$:

$$i\partial_z \psi + \partial_x^2 \psi \pm |\psi|^2 \psi = 0, \tag{2.10}$$

where the sign plus (minus) is associated to the self-focusing $n_2 > 0$ (self-defocusing $n_2 < 0$) character of the medium.

2.2.1 Plane Wave Solution

Equation (2.10) admits a plane wave stationary solution for which the field is not dependent on x. By writing $\psi(z) = \psi_0 \exp(i\beta z)$ and inserting this solution in (2.10), we obtain that $\beta = \psi_0^2$ such that

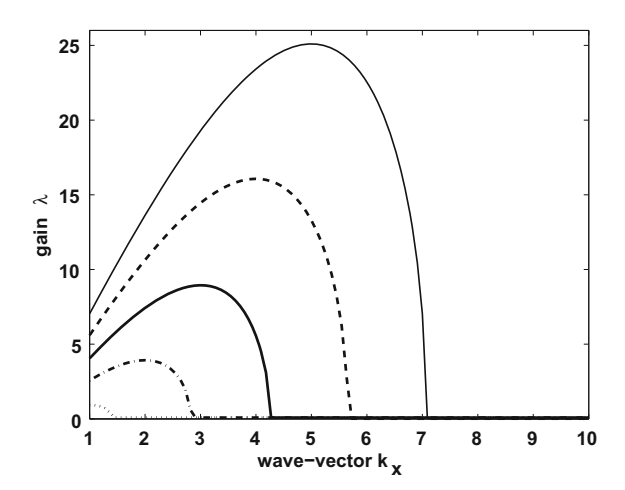
$$\psi(z) = \psi_0 \exp(iCIz), \tag{2.11}$$

where *C* is a constant and *I* is the dimensional intensity. This physically means that, during its propagation in the nonlinear medium, the plane wave field has an intensity dependent phase.

2.2.2 Modulation Instability

The plane wave solution is unstable when a small transverse perturbation is applied. Let us analyze the stability properties of (2.11) and write it as:

Fig. 2.1 Gain versus wave-vector for various plane-wave amplitudes $\psi_0 = 1$ (dotted line), $\psi_0 = 2$ (dot-dashed line), $\psi_0 = 3$ (continuous- bold line), $\psi_0 = 4$ (dashed line), $\psi_0 = 5$ (continuous-thin line)



$$\psi(z, x) = [\psi_0 + p(z, x)]e^{i\psi_0^2 z}, \qquad (2.12)$$

where $p(z, x) = \alpha_+(z)e^{ik_xx} + \alpha_-^*(z)e^{-ik_xx}$. We put this solution in (2.10) and by linearizing, we obtain an equation system for α_{\pm} :

$$i\dot{\alpha}_{+} - k_{x}^{2}\alpha_{+} + \psi_{0}^{2}(\alpha_{-} + \alpha_{+}) = 0$$

$$-i\dot{\alpha}_{-} - k_{x}^{2}\alpha_{-} + \psi_{0}^{2}(\alpha_{-} + \alpha_{+}) = 0,$$
(2.13)

where k_x is the wave-vector. We assume that $\alpha_{\pm} = \hat{\alpha}_{\pm} e^{\lambda z}$ and obtain the equation for the gain λ :

$$\lambda^2 = k_x^2 (2\psi_0^2 - k_x^2). \tag{2.14}$$

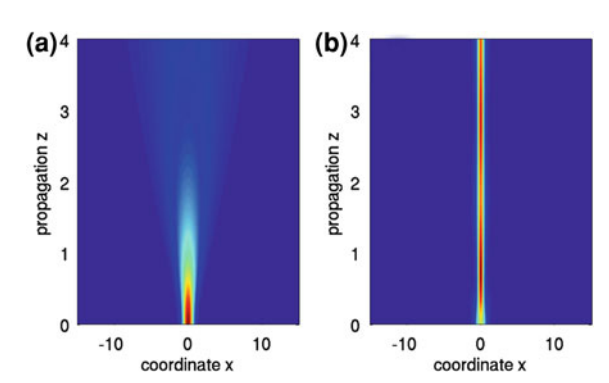
When (for a specific range of k_x), the second term is positive, we have an unstable growth of the introduced periodic perturbation, despite it can be chosen as small as we want. The perturbation hence grows exponentially during the wave propagation. The gain of the perturbation has a maximum growth rate for a fixed value of the wave vector, $k_x = \psi_0$, as it can be seen in Fig. 2.1. There exists a value of the period of the perturbation that grows more successfully than others. This leads to the formation of a periodical pattern of field distribution for which there are alternating regions where the field is much more intense.

In Fig. 2.2, we show the numerical simulations for a plane-wave solution of the NLS equation when a small perturbation is added to the unperturbed solution. We see that an initial homogeneous field distribution, describing the front wave of the plane wave, breaks into a periodical pattern. It is important to stress that, as it can be seen by Eq. (2.14), the modulation instability at which the light beam is subject, is managed by the self-focusing nonlinearity (through the ψ_0^2 intensity term) and the diffraction, related to the wave-vector k_x .

Fig. 2.2 Numerical simulations of the nonlinear Schroedinger equation start from a plane-wave perturbed with 1% perturbation noise. The figure shows that, starting from an homogenous field distribution, periodical pattern emerges, eventually developing into an ensemble of localized waves (solitons)

4
3.5
3
x 2.5
2.5
0
-15
-10
-5
0
coordinate x

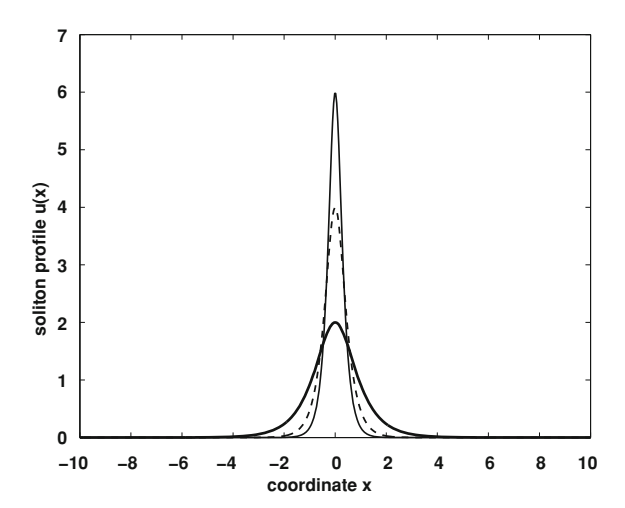
Fig. 2.3 Propagation of a one-dimensional Gaussian beam by integrating the nonlinear Schroedinger equation through the beam propagation method, in the diffraction case (a) obtained for a low power input, and in the self-trapped case (b) when the input beam is high



2.2.3 The Bound States

As we have seen in the previous section, the plane-wave solution is unstable under transverse spatial perturbation. So, the NLS solution cannot be obtained by applying small perturbations to the plane-wave solution. We must look for new stationary solutions. It can be shown that in nonlinear Kerr media, the nonlinear term in Eq. (2.10) curves the wave phase-front in a way related to the sign of the nonlinear term. We are considering attractive Kerr media for which the positive sign of the nonlinear term involves a convergent effect on the propagating wave. For a beam with a finite transverse extent, we expect that a stable solution can be derived by balancing the diffraction mechanism (a spreading of the propagating beam, a concave curvature of the phase-front) with the nonlinear focusing mechanism. Figure 2.3 shows this mechanism. In panel (a), we consider a low intensity beat. By Eq. (2.10), the nonlinear term can be neglected and the diffraction causes the beam dispersion. In panel (b), the input beam has higher intensity, the nonlinear compensation yields to the formation of a self-trapped beam. The simplest localized solution for Eq. (2.10)

Fig. 2.4 1D kerr soliton shape for three different amplitude values $u_0 = 2$ (continuous-bold line), $u_0 = 4$ (dashed line), $u_0 = 6$ (continuous-thin line)



takes the form $\psi(x, z) = u(x)e^{i\beta z}$, with

$$u(x) = u_0 \operatorname{sech}(x/w_0), \tag{2.15}$$

where the width is $w_0 = \frac{u_0}{\sqrt{2}}$ and $\beta = u_0^2/2$ is directly related to the amplitude of the wave. It is important to observe that the balance of the nonlinearity with the diffraction term results into a flat phase-front and that, in order to exist, the localized solution has to satisfy a fixed relation between the width of the beam (associated to the diffraction) and the beam amplitude u_0 , determining the strength of the nonlinearity. As shown in Fig. 2.4, by increasing the amplitude (and hence the power $P = \int dx |u|^2$) of the input beam, the soliton width shrinks such that $u_0w_0 = \text{constant}$. This relationship is known as the "existence curve" of the solitary waves.

2.3 Nonlocal Case

Over the years, the role of a nonlocal nonlinear response, with special emphasis on the optical spatial solitons (OSS) [1], appeared with an increasing degree of importance [2–8]; on one hand because it must be taken into account for the quantitative description of experiments and, on the other hand, because it is a leading mechanism for stabilizing multidimensional solitons [9]. Nonlocality in nonlinear wave propagation is found in those physical systems exhibiting long range correlations, like nematic liquid crystals (LC) [3], photorefractive media (PR) [10], thermal [4, 11, 12] and thermo-diffusive [13] nonlinear susceptibilities, soft-colloidal matter (SM) [14], BEC [15, 16], and plasma-physics [17, 18].

Let us consider a typical nonlocal nonlinear medium in which the change in the refractive index is related to the intensity of the wave in a finite region, it is a nonlocal

2.3 Nonlocal Case 15

function of the wave field. This effect can be represented in general form, for the focusing case, as

$$\Delta n(x, I) = \int_{-\infty}^{+\infty} dx' K(x - x') I(x', z),$$
 (2.16)

where K(x-x') is the response function. Its form depends on the specific nonlinearity under consideration and it is associated to a length-scale σ that measures the degree of nonlocality. Thanks to the paraxial approximation, the nonlocal response along z can be typically neglected. In a local system, σ tends to zero, the response is punctual $R(x-x')=\delta(x-x')$ and the refractive index locally changes with the light intensity (in Kerr media). In general, however, there always exists a degree of nonlocality in the physical systems that support the wave propagation. The local approximation can be done when the spatial correlations in the optical response are much smaller of the wavelength (below 100 nm). By inserting Eq. (2.16) in (2.7) and repeating the rescaling of the physical variables, we obtain the adimensional nonlocal nonlinear Schroedinger equation:

$$i\partial_z \psi + \partial_x^2 \psi + \psi K * |\psi|^2 = 0, \tag{2.17}$$

where $K * |\psi|^2$ is the convolution integral that measures the correlation between the optical field and the punctual response K of the nonlinear medium. In the Fourier domain, the convolution integral becomes $\tilde{\rho} = S(k_x)|\tilde{\psi}|^2$ where the tilde denotes the Fourier transform and $S(k_x)$ is the "structure factor" (that is the Fourier transform of K(x)). It is often useful to write Eq. (2.17) as a system of two differential equations:

$$i\partial_z \psi + \nabla_x^2 \psi + \rho \psi = 0$$

$$\mathcal{G}(\rho) = |\psi|^2.$$
(2.18)

where K is the Green function of the differential operator \mathcal{G} .

2.3.1 Plane Wave Solution

Hereafter, we will consider the general nonlocal Kerr nonlinearity with a nonlocal exponential response function:

$$K(x) = \frac{1}{2\sigma} \exp\left(-\frac{|x|}{\sigma}\right),\tag{2.19}$$

where σ , as we have seen above, represents the degree of the nonlocality. The expression for the structure factor

$$S(k_x) = \frac{1}{1 + \sigma^2 k_x^2} \tag{2.20}$$

is obtained as the Fourier transform of the response function. In this case, we have that the differential operator $\mathcal G$ acts on ρ as $-\sigma^2\rho_{xx}+\rho$. This corresponds, for example, to the re-orientational nonlinearity of nematic liquid crystals or to the thermal nonlinearity in lead-glasses [3, 4]. By calculating the corresponding Green function, the solution for ρ takes the form $\rho=\int \frac{e^{-|x-x'|/\sigma}}{2\sigma}|\psi|^2(x')dx'$. As in the local case, the plane wave

$$\psi(z) = \psi_0 e^{i\beta z}$$

$$\rho = \rho_0,$$
(2.21)

where $\psi_0 = \text{constant}$, is a solution of the Eq. (2.22) if $\beta = \rho_0$ and $\rho_0 = \psi_0^2$.

2.3.2 Modulation Instability

The modulation instability theory can be developed through the same procedures used in the local case. Let us start by considering the nonlocal nonlinear Schroedinger equation for an exponential nonlocal response

$$i\partial_z \psi + \nabla_x^2 \psi + \rho \psi = 0$$

$$-\sigma^2 \rho_{xx} + \rho = |\psi|^2,$$
 (2.22)

and add a small perturbation for the amplitude and the density of the form

$$\psi(z, x) = [\psi_0 + p(z, x)]e^{i\psi_0 z}$$

$$\rho(x) = \rho_0 + r(x),$$
(2.23)

where $p(z, x) = \alpha_+(z)e^{ik_xx} + \alpha_-^*(z)e^{-ik_xx}$ while $r(x) = r_+e^{ik_xx} + r_-^*e^{-ik_xx}$. By inserting the expression for ρ in the second equation of (2.22), one obtains:

$$r_{\pm} = \psi_0 S(k_x)(\alpha_+ + \alpha_-).$$
 (2.24)

By linearizing the first equation of (2.22), the dispersion relation give us the following growth rate for the perturbation:

$$\lambda = |k_x| \sqrt{2\psi_0^2 S(k_x) - k_x^2},\tag{2.25}$$

it should be noted that the local limit result (2.14) returns for $\sigma \to 0$, $S(k_x) \to 1$.

In Fig. 2.5, we show the dependence of the growth rate of the transverse perturbation by the wave-vector for the local case ($\sigma=0$) and the nonlocal case ($\sigma=1$). As it can be seen, the nonlocality tends to shrink the bandwidth of the modulation instability phenomenon and to reduce the maximum growth rate of the perturbation [see Fig. 2.6]. This effect will be strongly taken into account in the next chapters where we will study the interplay between nonlinearity and disorder and where the nonlocality will help us to understand and analytically solve the physical involved phenomena.

2.3 Nonlocal Case 17

Fig. 2.5 Gain versus wave-vector for $\sigma = 0$, the local case (*dashed line*) and for $\sigma = 1$, the nonlocal case (*continuous line*)

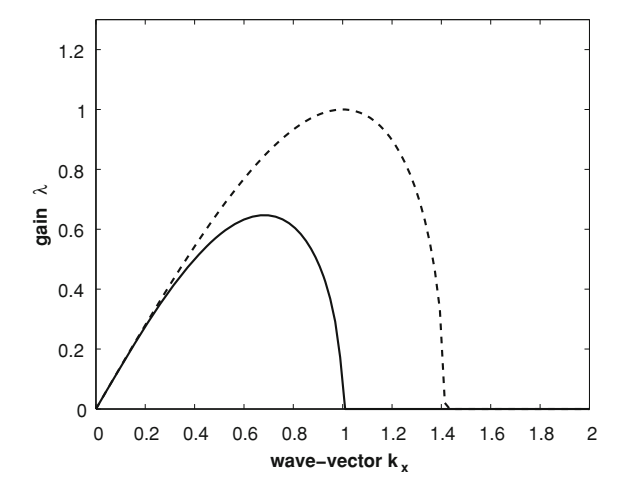
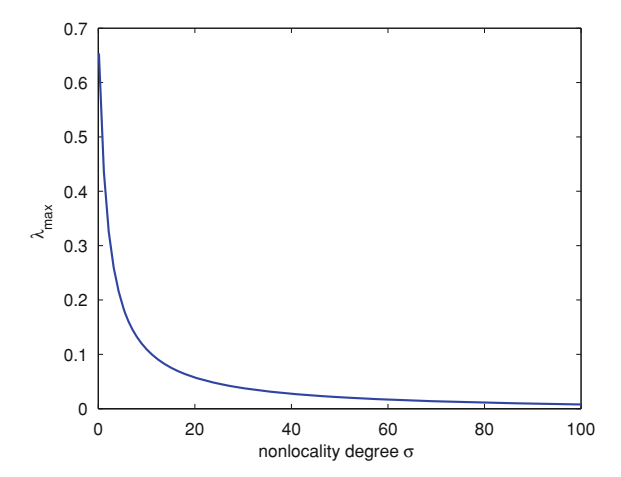


Fig. 2.6 Maximum gain versus the nonlocality degree



2.3.3 The Bound States

Now, we focus on the stable solutions $\psi(x, z) = u(x)e^{i\beta z}$ of the nonlocal nonlinear Schroedinger equation in the case of exponential response:

$$-\beta u + u_{xx} + u\rho = 0, \tag{2.26}$$

where $\rho(x) = \int dx' K(x - x') u^2(x')$ and, as seen above, $K(x) = e^{-|x|/\sigma}/2\sigma$. The exact solutions, at variance with what happens in the local case, cannot be found analytically.

In Fig. 2.7, we show the numerically obtained profiles for u(x) and $\rho(x)$. It can be noticed that, as the nonlocality increases, the response ρ widens with respect to the field profile. This leads to the possibilty of an analytical approach typically denoted

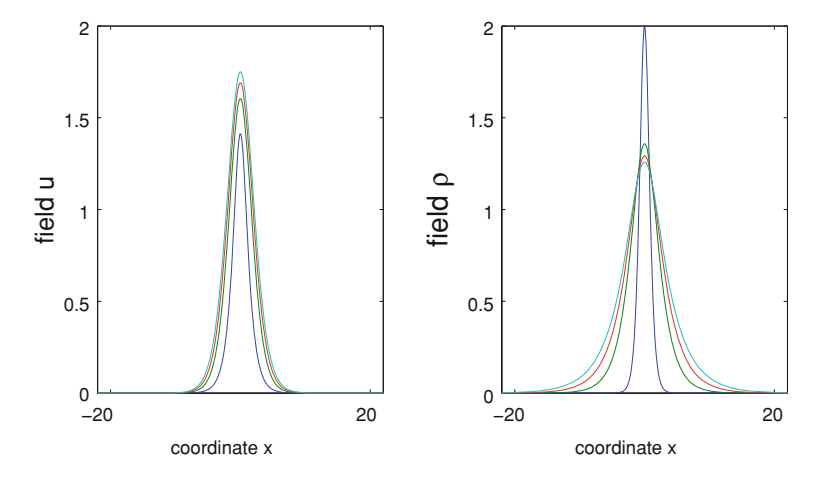


Fig. 2.7 The field profile u(x) and the response function $\rho(x)$ for different degrees of nonlocality, for $\beta = 1$. Shown is the local case (*blue line*), $\sigma = 3$ (*green line*), $\sigma = 7$ (*red line*) and $\sigma = 10$ (*cyan line*)

as the highly nonlocal limit described in the following paragraph, where the response function is approximated by a parabolic profile.

2.3.4 Highly Nonlocal Limit

In this section, we analyze the limit of a strongly nonlocal response. This is the case in which the local response distribution, induced by the optical field, is much broader than the spatial extension of the field itself (see Fig. 2.8. u(x) samples the response function at $x' \approx 0$ in the integral,

$$\rho(x) = \int dx' K(x - x') u^2(x') \simeq K(x) P, \tag{2.27}$$

where $P = \int dx' u^2(x')$ is the power of the soliton. We can then expand the nonlocal response K(x) (which is a bell shaped function) in Taylor series:

$$K(x) \simeq K_0 - \frac{1}{2}K_2x^2,$$
 (2.28)

where K_0 and K_2 are positive constants and the minus sign takes into account the focusing solution. In the parabolic approximation, an analytical solution exists. The equation for u(x) takes the following form:

$$-\beta u + u_{xx} + P(K_0 - \frac{K_2}{2}x^2)u = 0.$$
 (2.29)

2.3 Nonlocal Case 19

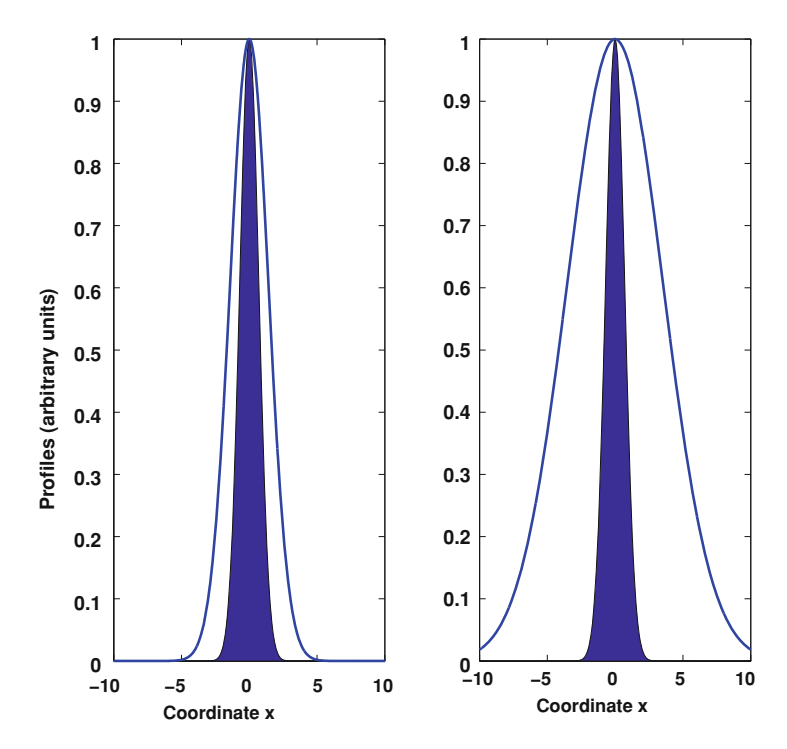


Fig. 2.8 The pulse profile (*filled curve*) and the response function profile (*continuous line*) for the local case (*left* panel) and the highly nonlocal case (*right* panel)

Equation (2.29) admits a Gaussian solution,

$$u(x) = u_0 \exp(-x^2/2x_0^2)$$
 (2.30)

where $u_0 = \sqrt{\frac{P}{x_0\sqrt{\pi}}}$. The spatial extension of the localized wave is related to the soliton power by the relationship,

$$x_0^4 P = \frac{2}{K_2} = \text{constant},$$
 (2.31)

that is also known as the "existence curve" of the nonlocal solitons.

The highly nonlocal limit will allow to solve the disordered version of this kind of systems and the nonlocality, as we will see, play a crucial role in the management of the localized light phenomena, acting as a filter between nonlinearity and disorder, and averaging out several effects related to randomness.

References

- 1. Trillo S, Torruealls W (eds) (2001) Spatial solitons. Springer-Verlag, Berlin
- 2. Snyder AW, Mitchell DJ (1997) Science 276:1538
- 3. Conti C, Peccianti M, Assanto G (2003) Phys Rev Lett 91:073901
- 4. Rotschild C, Cohen O, Manela O, Segev M, Carmon T (2005) Phys Rev Lett 95:213904
- 5. Rasmussen PD, Bang O, Królikowski W (2005) Phys Rev E 72:066611
- 6. Buccoliero D, Desyatnikov AS, Krolikowski W, Kivshar YS (2007) Phys Rev Lett 98:053901
- 7. Kartashov YV, Torner L (2007) Opt Lett 32:946
- 8. Ouyang S, Guo Q (2009) Opt Express 17:5170
- 9. Królikowski W, Bang O (2000) Phys Rev E 63:016610
- 10. Segev M, Crosignani B, Yariv A, Fischer B (1992) Phys Rev Lett 68:923
- 11. Ghofraniha N, Conti C, Ruocco G, Trillo S (2007) Phys Rev Lett 99:043903
- 12. Conti C, Fratalocchi A, Peccianti M, Ruocco G, Trillo S (2009) Phys Rev Lett 102:083902
- 13. Ghofraniha N, Conti C, Ruocco G, Zamponi F (2009) Phys Rev Lett 102:038303
- 14. Conti C, Ruocco G, Trillo S (2005) Phys Rev Lett 95:183902
- 15. Parola A, Salasnich L, Reatto L (1998) Phys Rev A 57:R3180
- 16. Perez-Garcia VM, Konotop VV, Garcia-Ripoll JJ (2000) Phys Rev E 62:4300
- 17. Litvak AG, Sergeev AM (1978) JETP Lett 27:517
- 18. Pecseli HL, Rasmussen JJ (1980) Plasma Phys 22:421

Chapter 3 Weakly Disordered Nonlinear Schroedinger Equation

By using a perturbational approach, we analyze the evolution of solitary waves in a nonlocal medium in the presence of perturbative disorder. An increasing degree of nonlocality may largely hamper the Brownian motion of self-trapped wave-packets. The result is valid for any kind of nonlocality and in the presence of non-paraxial effects. We compare the analytical predictions with numerical simulations based on stochastic partial differential equations.

3.1 Introduction

In the last sections of the Chap. 2, we have explored the effect of the nonlocality in the NLS equation. We have seen that the nonlocality acts as a spatial filter on the wave propagation, limiting modulation instability. In fact, the modulation of the refractive index by the nonlinearity in the Fourier space can be written as $\tilde{\Delta}n(k) = S(k)\tilde{I}(k)$, where k is the wave-vector, S is the structure factor (the Fourier transform of the spatial response) and \tilde{I} is the Fourier intensity profile of the solitary wave (SW). As the intensity of the beam increases (for the existence curve, the wave shrinks), \tilde{I} widens. In the product $\tilde{\Delta}n(k)$ however, S(k) filters out the "in excess field" by limiting all the instability phenomena. The nonlocality is present in physical systems displaying long-range correlations (see references in Chap. 2) and hence it must be often taken into consideration. However, it is important to note that considering a nonlocal response implies taking into account disorder. In fact, as detailed below, the large spatial region that interacts with the propagating electromagnetic field into a nonlocal medium commonly includes material fluctuations that get in the system a certain degree of disorder. Here, we analyze the evolution of solitary waves in a nonlocal nonlinear medium in the presence of disorder. We expect that, as the degree of nonlocality increases, the effect of the random fluctuations of the material will also increase and the soliton propagation will be mostly influenced in its Brownian motion. However we find that the random walk of the soliton displacement is obstructed by

the high nonlocality that averages out all the short-range correlations and reduces the soliton fluctuations induced by the presence of disorder.

In the following, we start our analysis by adding disorder in the NLS equation, by a linear random potential term: $V(x, y, z, t)\psi$ that corresponds to take a refractive-index perturbation as $\Delta n(r, I) = \Delta n(I) + \Delta n_{ran}(r)$, where $\Delta n_{ran}(r, t)$ takes into account the effect of the spatial randomness due to the material fluctuations.¹

3.2 The Model

For sake of notation, we write the evolution coordinate as z. The model we consider is written as

$$i\partial_z \psi + \nabla_x^2 \psi + \rho \psi = 0 \tag{3.1}$$

$$\mathcal{G}(\rho) = |\psi|^2 + \eta(x, z) \tag{3.2}$$

where ψ is the relevant wave field, x is the position vector, \mathcal{G} is a linear differential operator, which does not include derivatives with respect to the evolution coordinate z; for example, for the exponential nonlocality, $\mathcal{G}(\rho) = -\nabla_x^2 \rho + \sigma^2 \rho$, with σ^2 the degree of nonlocality [1]. In (3.2) $\eta(x,z)$ is a Langevin noise such that $\langle \eta(x,z)\eta(x',z')\rangle = \eta_N^2 \delta(x-x')\delta(z-z')$. The origin of η depends on the specific physical problem: (i) temperature (nematic director) ρ fluctuations for thermal (LC) media; (ii) SM particle density ρ fluctuations; (iii) space-charge field ρ fluctuations for PR (eventually induced by modulation of the background field); (iv) finite-temperature results into terms like η for plasmas and BEC [2].

In the Fourier domain (3.2) is written as $\tilde{\rho} = S(q)(|\tilde{\psi}|^2 + \tilde{\eta})$, where the tilde denotes the Fourier transform, S(q) is the "structure factor" [3], and the corresponding Green function is denoted by K(x), such that

$$i\partial_z \psi + \nabla_x^2 \psi + V(x, z)\psi + \psi K * |\psi|^2 = 0,$$
 (3.3)

where $V(x, z) = K*\eta$ is a colored random noise (the asterisk "*" denoting the x-convolution integral). The local regime corresponds to $K(x) = \delta(x)$, while in the highly nonlocal regime $K(x) = K_0$ [4]. Letting $\phi = \psi \exp(i\beta z)$, Eq. (3.3) is written as

¹ We stress that there exist two typologies of disorder: the first one, considered in this chapter, is the random fluctuations of the physical variables related to the medium response. This disorder depends on the spatial variable and on the evolution coordinate and it can be treated as a perturbation. The other one is the so-called structural disorder. It is much stronger with respect to the first one and permits also several forms of light localization. The former one is expected to describe material fluctuations as, e.g. due to the temperature, the latter accounts for externally induced potentials, as considered in the Chap. 4.

3.2 The Model 23

$$i\partial_z \phi + \nabla_x^2 \phi - \beta \phi + \phi K * |\phi|^2 = is(x, \psi, \psi_x, \psi_{xx}, \dots, z)$$
(3.4)

where s is taken as a perturbation term, depending on ψ and its transverse derivative at any order, and β is the nonlinear wave-vector. Equation (3.4) is a generalization of (3.3), accounting for any kind of perturbation, e.g. in the presence of material losses $s = -\alpha \phi$, with α the loss coefficient. Equation (3.3) corresponds to $s = V \phi$.

3.3 Soliton Perturbation Theory in Nonlocal Media

Soliton perturbation theory was previously developed for one dimensional (1D) solitons of the integrable local nonlinear Schroedinger (NLS) equation (see, e.g. [5]), and it is based on the knowledge of the exact soliton solutions. Here this approach is generalized to a non-integrable model, in the presence of an arbitrary nonlocality, and then applied to the SW Brownian motion. The SW profile is given, in the absence of the perturbation (s = 0), by the real-valued solution u(x) of

$$-\beta u + \nabla_x^2 u + u \int K(x - x')u^2(x')dx' = 0.$$
 (3.5)

To simplify the notation, we consider hereafter the 1D case, while the results below equally apply to the multi-dimensional case. The un-perturbed SW is written as

$$\phi_0 = u(x - X + 2\Omega z, \beta) \exp(i\theta - i\Omega x - i\Omega^2 z)$$
(3.6)

where *X* is the center of the self-trapped wave, θ is the phase, and 2Ω is the velocity. The analysis can be limited to SW with $\Omega = 0$. By letting $\phi = \phi_0 + \phi_1$, the linearized evolution equation is

$$\partial_z \phi_1 = \mathcal{L}(\phi_1) + s, \tag{3.7}$$

with

$$\mathcal{L}(\phi_1) = -i\beta\phi_1 + i\phi_{1,xx} + i\phi_0 K * (\phi_0\phi_1^* + \phi_0^*\phi_1) + i\phi_1 K * |\phi_0|^2.$$
(3.8)

Without loss of generality, the first order perturbation can be decomposed in a term representing a small variation of the solitary-wave parameters and the remaining part, denoted as the radiation term ϕ_r . The former is proportional to the derivatives of ϕ_0 with respect to the various parameters, X, Ω , θ , β , and ϕ_1 is written as

$$\phi_1 = f_X \delta X + f_\theta \delta \theta + f_\theta \delta \beta + (f_\Omega - X f_\theta) \delta \Omega + \phi_r, \tag{3.9}$$

while having introduced the auxiliary functions

$$f_{\theta} = i\phi_{0}$$

$$f_{\beta} = \partial_{\beta}\phi_{0}$$

$$f_{X} = \partial_{X}\phi_{0}$$

$$f_{\Omega} = -i(x - X)\phi_{0},$$
(3.10)

and being $\delta X(z)$, $\delta \theta(z)$, $\delta \beta(z)$ and $\delta \Omega(z)$ the z-dependent perturbations to SW parameters.

We introduce the adjoint functions \hat{f} given by $\hat{f}_{\theta} = if_{\beta}$, $\hat{f}_{\beta} = -if_{\theta}$, $\hat{f}_{\Omega} = -if_{X}$, $\hat{f}_{X} = if_{\Omega}$, and such that $(\hat{f}_{a}, f_{b}) = \mathcal{N}_{a}\delta_{a,b}$ with a and b two SW parameters $(X, \Omega, \theta, \text{ or } \beta)$ and introducing the scalar product $(\hat{f}, f) = \Re \int (\hat{f})^{*} f dx$. It is $\mathcal{N}_{\theta} = \mathcal{N}_{\beta} = (1/2)(dP/d\beta) = P'/2$ and $\mathcal{N}_{X} = \mathcal{N}_{\Omega} = (1/2)P$, with $P = (\phi_{0}, \phi_{0})$ the SW power.

Following the original argument in [6], f and \hat{f} are localized around the SW position X, as a consequence, their scalar products with ϕ_r are vanishing because the radiation term spreads for long times, and $(\hat{f}, \phi_r) = 0$. This assumption is confirmed by the agreement with the numerical simulations reported below.

We apply the operator \mathcal{L} on the auxiliary functions, obtaining:

$$\mathcal{L}(f_{\theta}) = 0$$

$$\mathcal{L}(f_{\beta}) = i\phi_0 \equiv f_{\theta}$$

$$\mathcal{L}(f_X) = 0$$

$$\mathcal{L}f_{\Omega} = 2e^{i\theta}u_X \equiv 2f_X.$$
(3.11)

By using the following relation for the adjoint operator, $\hat{\mathcal{L}}(if) = -i\mathcal{L}(f)$, we are able to write the action of $\hat{\mathcal{L}}$ on the adjoint auxiliary functions:

$$\hat{\mathcal{L}}(\hat{f}_{\theta}) = -if_{\theta}$$

$$\hat{\mathcal{L}}(\hat{f}_{\beta}) = 0$$

$$\hat{\mathcal{L}}(\hat{f}_{X}) = 2if_{X}$$

$$\hat{\mathcal{L}}\hat{f}_{Q} = 0.$$
(3.12)

and then, projecting these relations over the adjoining functions Eq. (3.7), we derive the following equations for the dynamics of the SW parameters:

$$\delta\dot{\theta} - X\delta\dot{\Omega} = \delta\beta + \frac{2S_{\theta}}{P'}, \qquad \delta\dot{\beta} = \frac{2S_{\beta}}{P'},$$

$$\delta\dot{X} = -2\delta\Omega + \frac{2S_{X}}{P}, \qquad \delta\dot{\Omega} = \frac{2S_{\Omega}}{P},$$
(3.13)

where $S_{\alpha} = (\hat{f}_{\alpha}, s)$, and the dot is the derivative with respect to the evolution coordinate z.

3.4 Application to the Disordered Nonlocal NLS

Equation (3.13) hold for any s; for a random perturbation in the density ρ , as given by $\eta(x, z)$ above, we can write:

$$s = iV(x, z)ue^{i\theta}, (3.14)$$

where $V(x, z) = \int K(x - x') \eta(x', z) dx'$ and η is the random potential seen above. The Eq. (3.13) become

$$\delta \dot{\theta} = X \delta \Omega + \delta \beta + \frac{1}{P'} \frac{d}{d\beta} \int u^2(x - X)(K * f) dx,$$

$$\delta \dot{\beta} = 0, \quad \delta \dot{X} = -2\Omega,$$

$$\delta \dot{\Omega} = -\frac{2}{P} \int u(x - X)u_X(x - X)(K * f) dx,$$
(3.15)

from which

$$\delta\Omega(z) = -\frac{2}{P} \int_0^t \int \int u(x - X) \quad u_x(x - X) K(x - x') f(x', z') dx' dx dz'.$$
(3.16)

Writing $\delta\Omega(z)\delta\Omega(z')$ after (3.16) and averaging over disorder leads to

$$\langle \delta \Omega(z) \delta \Omega(z') \rangle = \frac{4\langle f \rangle}{P^2} C \min(z, z')$$
 (3.17)

where

$$C = \int \int \int u(x_1 - X)u_x(x_1 - X)u(x_3 - X)$$

$$\times u_x(x_3 - X)K(x_1 - x_2)K(x_3 - x_2)dx_1dx_2dx_3$$
 (3.18)

The deviation from the mean position is found as

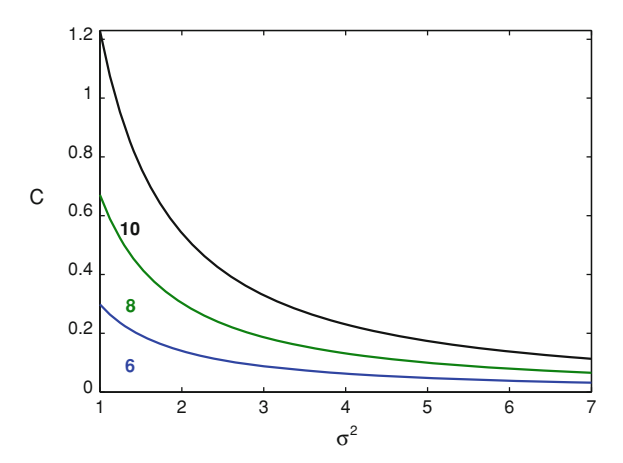
$$\delta X(z) = -2 \int_0^z \delta \Omega(z') dz'$$
 (3.19)

from which $\langle \delta X \rangle = 0$ and

$$\langle \delta X(z)^2 \rangle = 4 \int_0^z \int_0^z \langle \Omega(z_1) \Omega(z_2) \rangle dz_1 dz_2 = \frac{16\eta_N^2 C}{3P^2} z^3.$$
 (3.20)

The previous result is the nonlocal counterpart of the so-called Gordon–Haus effect, firstly introduced for describing the random fluctuations of solitons in amplified lightwave systems [5, 6]. Equation (3.20) states that the random fluctuations, measured by $\langle \delta X(z)^2 \rangle$, grow with the cubic of the propagation distance, and decay with the square

Fig. 3.1 Amplitude of the fluctuations C for the exponential nonlocality versus σ^2 , after Eq. (3.20), for various soliton powers P



of the SW power. A significant role is played by quantity C, which, in general, depends on the specific soliton and nonlocality profile. In the local regime $K(x-y) = \delta(x-y)$ it is

$$C = \int \left[u(x_1 - X)u_x(x_1 - X) \right]^2 dx_1. \tag{3.21}$$

The relevant result is found in the highly nonlocal limit $K(x) \to K_0$, which gives, for a bell-shaped soliton profile [u(x) = u(-x)],

$$C = K_0^2 \left[\int u(x_1 - X)u_X(x_1 - X)dx_1 \right]^2 = 0, \tag{3.22}$$

irrespectively of the specific shape of K(x). As a result, in the highly nonlocal regime the random fluctuations of the fundamental soliton vanish. Physically, this corresponds to the fact that the noise is filtered out by a narrow S(q) as the degree of nonlocality increases. We stress that this results is independent on the specific kind of nonlocality. For example, with reference to the exponential nonlocality $S(q) = (1+\sigma^2q^2)^{-1}$ [1], we show in Fig. 3.1 the C parameter Vs σ^2 for various P (note that β changes along each curve, because σ^2 varies) as calculated after the bound-state solutions of Eq. (3.5). As expected when σ^2 increases ($\sigma^2 = 0$ corresponds to the local case), the predicted fluctuation decreases. Equation (3.5) is also valid in the two-dimensional case for each transverse coordinate.

To validate the previous analytical results, we resorted to the numerical integration of the stochastic partial differential equation resulting from a 1D exponential nonlocality; we adopted a pseudo-spectral stochastic Runge-Kutta [7, 8]. Figure 3.2 a shows a typical evolution starting from a bound state and displaying the random deviation of the SW. In Fig. 3.2b, we report various trajectories for a fixed SW power. Figure 3.3 shows the calculated standard standard deviation for various degrees of nonlocality: the analytical prediction after Eq. (3.20) is indistinguishable from the numerical results.

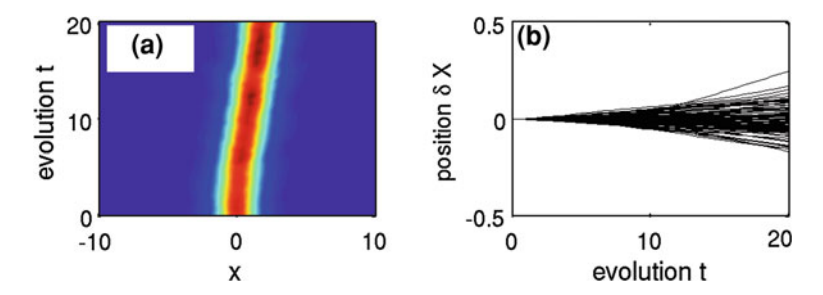
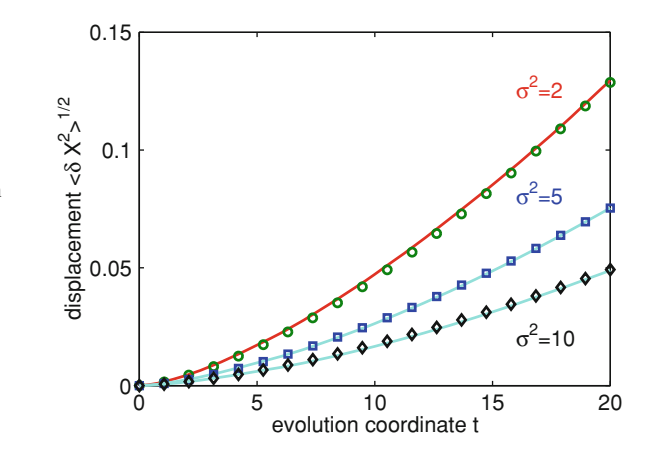


Fig. 3.2 a Typical dynamics of a solitary wave [Eq. (3.3)] as obtained from the numerical solutions of (3.4) in the presence of randomness and exponential nonlocality (P=6, $\sigma^2=5$, $\eta_N=0.01$); **b** Center of mass trajectories of the same bound-state (P=6, $\sigma^2=5$) for 100 disorder realizations ($\eta_N=0.01$)

Fig. 3.3 Comparison of the numerically (continuous lines, P=6, $\eta_N=0.01$) and theoretically (circles for $\sigma^2=2$, squares for $\sigma^2=5$ and diamonds for $\sigma^2=10$) calculated standard deviation of the solitary wave position versus the evolution coordinate for three degrees of nonlocality and 100 disorder realizations



3.5 Nonparaxial Corrections

Before concluding, we consider the effect of non-paraxiality on the SW fluctuations. Ultra-thin nonlocal OSS were considered in [3, 9]; in this framework, non-paraxiality at the lowest order is described by the perturbation $s = -\epsilon \psi_{xxxx}$, where $\epsilon = (\lambda/4\pi nw_0)$ is ratio, within some numerical constants, between the wavelength and the spatial beam waist [3] and is determined by taking into account the next order terms in the expansion of the traverse operator of the backward scalar wave equation of the optical field A and normalizing it: $i\partial_z A + \sqrt{k^2 + \nabla_\perp^2} A + \frac{\omega \Delta n}{c} A = 0$. It turns out that Eq. (3.20) still holds true in the ultra-focused regime, with the addition of a linear increase of the phase along propagation:

$$\delta\theta_{\text{non-paraxial}} = -z \frac{2\epsilon}{P'} \int u_{\beta} u_{xxxx} dx,$$
 (3.23)

corresponding to the perturbation to the SW nonlinear wave-vector due to the non-paraxial term. This analysis shows that even in the non-paraxial regime, the nonlocality limits the fluctuations of the beam.

In this chapter, we are concerned with solitons (the "localized product" of the non-linearity) evolving in a weakly disordered medium. As known by [10], the refractive index fluctuations act as random forces that push and pull the baricenter of the solitary wave, causing its Brownian motion. We have theoretically shown that nonlocality largely affects the dynamics of a soliton in the presence of disorder; this results in a random walk of the soliton position, which is hampered by the filtering action of the nonlocal regime, and ideally vanishes for a infinite degree of nonlocality. These results are expected to be specifically relevant for Bose-Einstein condensates, liquid crystals and soft-colloidal matter, and suggest to employ highly nonlocal media for routing information by self-trapped beams in order to moderate the effect of randomness.

References

- 1. Królikowski W, Bang O (2000) Phys Rev E 63:016610
- 2. Stoof H (1999) J Low Temp Phys 114:11
- 3. Conti C, Ruocco G, Trillo S (2005) Phys Rev Lett 95:183902
- 4. Snyder AW, Mitchell DJ (1997) Science 276:1538
- Iannone E, Matera F, Mecozzi A, Settembre M (1998) Nonlinear optical communication networks. Wiley, New York
- 6. Gordon JP, Haus HA (1986) Opt Lett 11:665
- 7. Werner MJ, Drummond PD (1997) J Comput Phys 132:312
- 8. Qiang J, Habib S (2000) Phys Rev E 62:7430
- 9. Conti C, Peccianti M, Assanto G (2004) Phys Rev Lett 92:113902
- 10. Kartashov YV, Vysloukh VA, Torner L (2008) Phys. Rev. A 77:051802

Chapter 4 Disordered Nonlinear Schroedinger Equation

Here, we deal with the nonlinear Schroedinger equation in the presence of structural disorder. The strength of disorder allows the formation of light localizations, the Anderson states. The effect of focusing and defocusing nonlinearities, present in the model equation, on Anderson localization in highly nonlocal media is theoretically and numerically investigated. A perturbative approach is developed to solve the nonlocal nonlinear Schroedinger equation in the presence of a random potential. We find closed form expressions showing that nonlocality stabilizes Anderson states. Numerical analysis validates the theoretical results. A regime in which multiple Anderson localizations are excited and compete by nonlocality is also outlined.

4.1 Introduction

In this chapter, we investigate the effect of a generic random potential (not necessary perturbative) on the nonlinear Schroedinger equation (NLS). The disorder is called structural and is strong enough to allow light localization in a different way with respect to the solitary waves (SW), due to nonlinearity. Indeed, a sufficient strength of disorder fosters the transition from a diffusive regime to a wave-function exponentially decaying over a characteristic distance *l*; this scenario is commonly referred to as Anderson localization (AL) [1]. By an analytical point of view, when the nonlinearity is absent, the considered equation reduces to the Anderson model, the system admits exponentially localized states. When the nonlinearity is present, the resulting equation is the NLS with a random potential term. This model cannot be analytically solved and problems arise also in the numerical computations. As shown below, including nonlocality can allow to address various issues concerning the disordered NLS: first, the nonlocality in the nonlinear response can largely affect the localized wave-forms, depending on the degree of nonlocality σ [2–6]. In addition, the interplay between the disorder induced localization length l and the characteristic length of nonlocality σ has never been considered before. Finally, as seen, in the highly-nonlocal limit, the NLS equation can be easily linearized and it will be possible to derive closed form expressions to analytically describe the role of nonlinearity on Anderson localizations.

4.2 Anderson Localization

Anderson localization is a general phenomenon for wave propagation in random media. If the strength of disorder is enough, a spatial confinement of light in relatively narrow regions takes place, caused by interference effects due to multiple scattering. A transition from a diffusive regime to a localized state occurs and the transport properties of the medium drastically change. Originally the Anderson transition was referred to a particular issue in the study of the conductance of electrons, the metalinsulator transition. The diffusion of electrons into a metallic system can be described through the multiple scattering phenomena by impurities of the solid. The meanfree path measures the average length between two consecutive electronic collisions during its motion into the material and it decreases as the disorder is growth. By increasing the strength of disorder over a critical value, the diffusive motion of the electrons is halted and the material turns into an insulating state. The concept of electronic spatial confinement was first introduced by Anderson [1] in 1958 in order to explain the absence of diffusion. Later, a similar explanation was applied in the study of the photons transport in disordered systems [7-14] and the light localization due to the disorder was experimentally observed [9, 15]. This phenomenon is also present in the physics of Bose-Einstein condensation [16, 17]

The Anderson model is written in terms of the following Hamiltonian,

$$H_0 = -\partial_x^2 + V(x); \tag{4.1}$$

where V(x) is a random potential, the eigenstates are written as

$$H_0\psi_n = \beta_n\psi_n \tag{4.2}$$

with $(\psi_n, \psi_m) = \delta_{nm}$. The Eq. (4.1) simply describes a free-particle moving in a random potential. When the disorder is strength enough, H_0 sustains exponentially localized states in a finite region, corresponding to negative eigenvalues β_n . The fundamental state can be approximated by:

$$\psi_0(x) = \frac{1}{\sqrt{l}} e^{-|x - x_0|/l} \tag{4.3}$$

where the average localization length l is determined by the strength of the random potential V_0 and describes the spatial extension of the region of light localization, while x_0 is the location of the eigenfunction with eigenvalue β_0 . In the following, without loss of generality, we assume that the horizontal axis has been shifted such that $x_0 = 0$. The (4.3) states are called Anderson localizations and the characteristic localized shape is shown in Fig. 4.1 for the ground state in the case of a Gaussianly distributed random potential. In Fig. 4.2a, b we report the numerically calculated

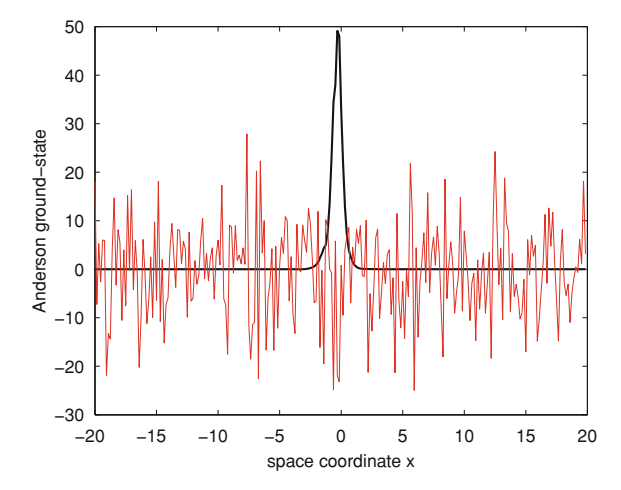


Fig. 4.1 The *black line* represents the ground-state, as retrieved by a Gaussian random potential (*red line*)

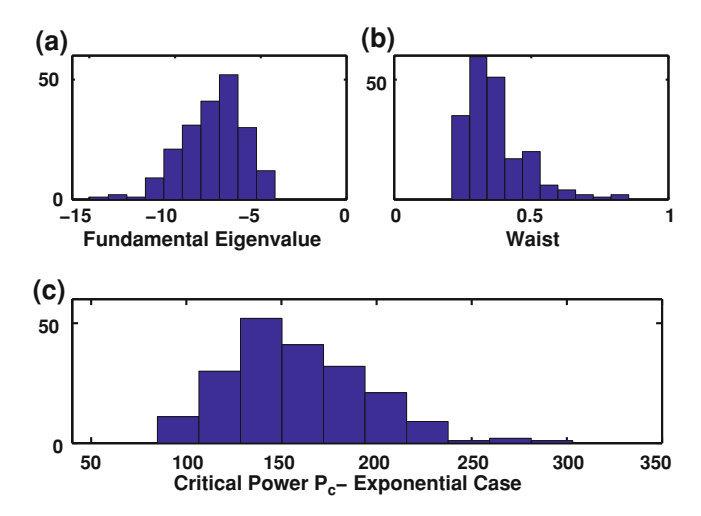


Fig. 4.2 Histogram over 200 realizations of disorder for the ground-state β_0 (**a**), the corresponding waist (**b**), critical power (**c**) ($V_0 = 10$, $\sigma = 10$)

distribution of eigenvalue β_0 and the localization lengths (calculated as the standard deviation or *waist*) for a Gaussianly distributed V(x) with zero mean and standard deviation V_0 .

In order to understand the link between the energies β_0 of the bound states and the relative localization lengths l, from Eq. (4.2) one can calculate the average value of the Hamiltonian on ψ_0 : $\langle \beta_0 \rangle = \langle (\psi_0, H_0 \psi_0) \rangle \cong -1/l^2$. The lowest energy state has the highest degree of localization and hence the localization length is also a direct measurement of the eigenstates stability.

4.3 The Model

When both disorder than Kerr nonlocal nonlinearity are taken into account, then the model describing the underlying field propagation phenomena is the random nonlocal nonlinear Schroedinger equation that reads as

$$i\psi_z + \psi_{xx} = V(x)\psi - s\psi \int_{-\infty}^{+\infty} \chi(x' - x)|\psi(x')|^2 dx'$$
 (4.4)

where $\psi = \psi(x,z)$, V(x) is the random potential and $\chi(x)$ is the response function of the nonlocal medium normalized such that $\int \chi(x) dx = 1$; $s \pm 1$ corresponds to a focusing (s = 1) or defocusing (s = -1) nonlinearity. In this chapter, we consider both the nonlinearities because the comparison can help to understand the role of nonlocality on the Anderson localization stability. Equation (4.4) applies to a variety of physical problems, including nonlinear optics and Bose Einstein condensation [18].

4.4 Highly Nonlocal Limit

Equation (4.4) does not admit an analytical solution. Doing the highly nonlocal approximation can be a valid approach to solve the problem. The nonlocality is described by $\chi(x)$, which is typically bell-shaped with a characteristic length σ . For an average localization length l much shorter than the nonlocality degree σ of the medium, the response function $\chi(x'-x)$ can be expanded around the localization center, x'=0, and one has in (4.4)

$$\psi \int_{-\infty}^{+\infty} \chi(x' - x) |\psi(x')|^2 dx' = \psi P \chi(x). \tag{4.5}$$

In such *highly nonlocal limit* (HNL), the nonlinearity is reduced to a linear term that can be initially treated as a perturbation to the Anderson model, an interaction Hamiltonian $H_{\text{int}} = s\chi(x)P$, where $P = \int_{-\infty}^{+\infty} |\psi(x)|^2 dx$ is overall energy, or beam power, which is conserved during evolution. Hence in the HNL, the random NLS (4.4) can be written through the Hamiltonian:

$$H = H_0 + PH_{\text{int}},\tag{4.6}$$

being P the expansion term (we deal with a Kerr nonlinearity perturbation). Now, we can simply solve the whole linear model in the framework of the standard perturbative theory. We stress that this limit is valid in the regime of a wave dominated by a single localization, which, without loss of generality, is taken centered at $x_0 = 0$. This also holds true as far as during the dynamics, additional localization are generated among those located in proximity of x = 0. Conversely, if two distant localizations are excited, $\chi(x)$ will be composed by two nonlocal responses centered in the two

Anderson states, this case will be investigated elsewhere. The HNL allows to apply the standard perturbation theory of quantum mechanics for deriving closed form expressions for the effect of nonlinearity on the Anderson states. We write the general solution as an expansion in *P*:

$$\psi = \sqrt{P} \left(\psi_0 + P \psi^{(1)} + P^2 \psi^{(2)} + \cdots \right), \tag{4.7}$$

where we take at the leading order $\psi = \sqrt{P}\psi_0$ to focus on the effect of nonlocal nonlinearity on the fundamental state. By following the standard perturbation theory, we obtain the correction to the Anderson ground state (at second order in P) eigenvalue:

$$\beta_0(P) = \beta_0 + s P \chi_{00} + P^2 \sum_{n \neq 0} \frac{|\chi_{n0}|^2}{\beta_0 - \beta_n},$$
(4.8)

with the matrix elements of the nonlocality given by

$$\chi_{nm} = \int \chi(x)\psi_n(x)\psi_m(x)dx. \tag{4.9}$$

We first observe that as the degree of nonlocality increases, $\chi(x)$ can be treated as a constant in (4.9), such that $\chi_{mn} = \chi(0)\delta_{nm}$. This shows that the perturbation to the Hamiltonian is diagonal, therefore, in the HNL, the effect of the nonlocality is to shift the eigenvalue such that

$$\beta_0(P) = \beta_0 + s\chi(0)P. \tag{4.10}$$

We stress that this equation is valid at any order in P: the overall Hamiltonian $H = H_0 + H_{\text{int}}$ is diagonal in the same states of H_0 , hence Anderson localizations turn out to be eigenstates also in the presence of the nonlocality. These localizations are hence expected to be extremely robust in the focusing case with respect to the nonlinearity.

In (4.10), χ (0) depends on the specific $\chi(x)$, and will explicitly contain the degree of nonlocality, as detailed below.

4.5 Instability of Anderson States

The effect of nonlinearity on Anderson states becomes relevant when the term linear in P is comparable with β_0 (higher order corrections vanish in the HNL); this allows to define through Eq. (4.8), the critical power P_c :

$$P_{c} = \frac{|\beta_{0}|}{\int_{-\infty}^{+\infty} |\psi_{0}(x)|^{2} \chi(x) dx}.$$
 (4.11)

In the specific case of a defocusing medium (s=-1), this is the power needed to change the sign of the eigenvalue $\beta_0(P)$, from negative to positive; such that the localization is destroyed. Conversely, for a focusing medium (s=1), this can be interpreted as the power were the average degree of localization is strongly affected by nonlinearity, indeed as $l(P) \cong 1/\sqrt{\langle \beta(P) \rangle}$, one has

$$l(P) \cong \frac{l}{\sqrt{1 + sP/\langle P_c \rangle}} \tag{4.12}$$

such that at critical power, the localization length is reduced by a factor $\sqrt{2}$ for the focusing case s=1, and diverges for the defocusing case s=-1. This shows that for $P>P_c$ no localized states are expected for s=-1, as the corresponding eigenvalue changes sign. This trends applies as far as additional effects, like the excitation of further localizations, occurs, as discussed below. From Eq. (4.11), we obtain the expression for P_c in the HNL, $P_c \equiv \hat{P}_c = |\beta_0|/|\chi(0)|$ with $\langle \hat{P}_c \rangle \cong \sigma/2l^2 \left[\chi(0) = 1/2\sigma \right]$ for an exponential nonlocality]. Because of the Cauchy-Schwarz inequality, one has $\int_{-\infty}^{+\infty} |\psi_0(x)|^2 \chi(x) dx < 1$, and one readily sees that for a finite nonlocality $P_c < \hat{P}_c$; as the nonlocality increases the power needed to destabilize the Anderson states grows.

A useful measure to quantify the effect of a nonlocal nonlinearity on Anderson states is the residual value of $\beta(P)$ at the critical power P_c , which can be written as

$$\delta\beta(\sigma) = \frac{\beta_0(s P_c)}{\beta_0} = \sum_{n \neq 0} \frac{|\chi_{n0}|^2}{|\chi_{00}|^2 (1 - \beta_n/\beta_0)}.$$
 (4.13)

 $\delta\beta$ only depends on the disorder realization and on the degree of nonlocality; $\delta\beta=0$ if higher order corrections $O(P^2)$ to $\beta(P)$ are vanishing. As it is determined by the off-diagonal elements χ_{n0} , $\delta\beta$ can be taken as the "residual coupling" due to the nonlocal nonlinearity, which vanishes in the HNL limit. In Fig. 4.3, we numerically show [for an exponential $\chi(x)$, see below] that $\delta\beta$ goes to zero when increasing σ : as the nonlocality increases the nonlinear coupling of ψ_0 with other states is moderated, hence it tend to behave as an eigenstate of the system even if nonlinearity is present (however, its degree of localization may be largely affected).

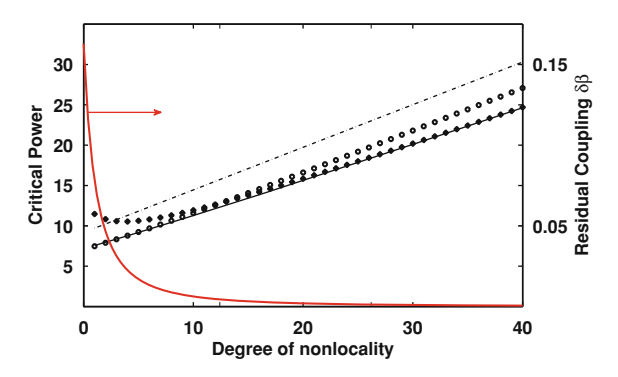
4.6 Nonlocal Responses

The critical power Eq. (4.11) for a few specific cases of the response function $\chi(x)$ [2] is given by:

Rectangular:

$$\chi = \frac{1/(2\sigma) \ for \ |x| < \sigma}{0 \ elsewhere} \tag{4.14}$$

Fig. 4.3 Left axis: critical power for exponential (dashed line), Gaussian (continuous line) quadratic (dots) and rectangular (diamonds) response functions, for a single realization of the disorder; right, residual coupling $\delta\beta$ Vs degree of nonlocality, averaged over 10 disorder realizations ($V_0=1$)



and hence,

$$P_c = 2\sigma |\beta_0|/(1 - e^{-2\sigma/l});$$
 (4.15)

Exponential:

$$\chi(x) = e^{-|x|/\sigma}/(2\sigma),\tag{4.16}$$

and hence,

$$P_c = |\beta_0|(2\sigma + l);$$
 (4.17)

Gaussian:

$$\chi(x) = e^{-x^2/\sigma^2} / \sqrt{\pi \sigma^2},$$
 (4.18)

and hence.

$$P_c = l|\beta_0| \exp(-\sigma^2/l^2) \operatorname{Erfc}(\sigma/l); \tag{4.19}$$

Quadratic:

$$\chi(x) = \chi(0) + \chi_2 x^2, \tag{4.20}$$

[e.g. for a Gaussian $\chi(0) = 1/\sqrt{\pi\sigma^2}$ and $\chi_2 = -\chi(0)/\sigma^2$],

$$P_c = |\beta_0|/|\chi(0)|(1 - l^2/2\sigma^2), \tag{4.21}$$

the last response function (4.20) is frequently used to approximate any bell-shaped nonlocal response.

In all of these cases, the critical power is linearly dependent on the unperturbed eigenvalue of the state. So, the higher the strength of the disorder V_0 , the lower β_0 , the higher the power needed to affect the localization.

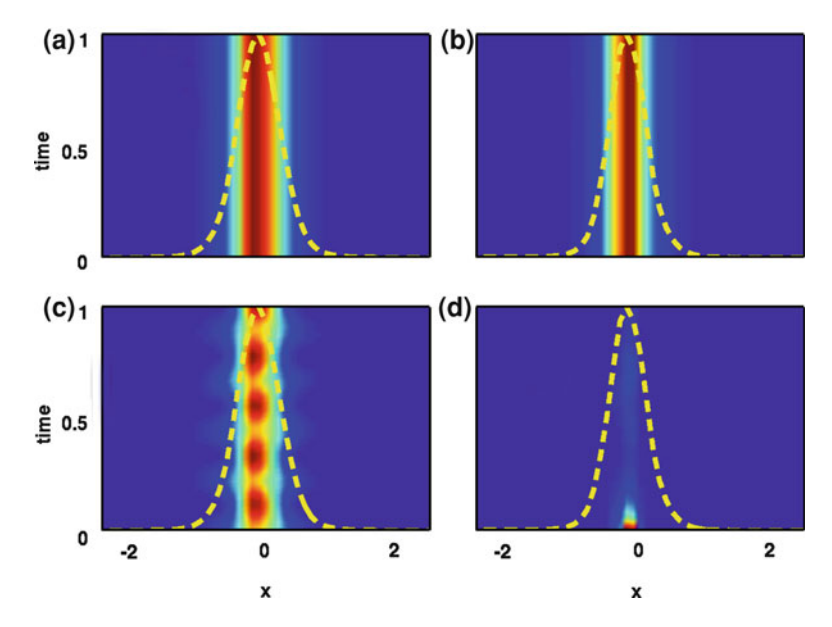


Fig. 4.4 Evolution of the ground-state intensity for a fixed disorder realization, for $\sigma = 10$, $V_0 = 10$; focusing (attractive) case s = 1, for $P = 0.04P_{cr}$ (a) and for $P = 4P_{cr}$ (c); defocusing (repulsive) case s = -1, for $P = 0.04P_{cr}$ (b) and for $P = 4P_{cr}$ (d). The superimposed dashed line in the panels represents the ground-state at the initial time

In Fig. 4.3, we report the behavior of the critical power as a function of the nonlocality degree σ for the analyzed response functions. Furthermore, we emphasize that the critical power, directly depending on the unperturbed eigenvalue, has a statistical distribution depending on the disorder configuration. For a given σ and V_0 , one has a distribution of critical powers, as shown in Fig. 4.2c.

4.7 Numerical Results

We numerically solved Eq. (4.4) for fixed disorder configurations: we first obtain the eigenstates, then by using a pseudo-spectral Runge-Kutta algorithm, we evolve the Anderson localizations in a nonlocal medium with a given $\chi(x)$ [an exponential response hereafter, similar results are obtained for other $\chi(x)$].

Figure 4.4 shows the dynamics of the ground-state intensity: for $P < P_c$ the state remains almost unperturbed [panels (a), attractive case; panel (b), repulsive case]. By increasing the power beyond the critical threshold, we observe two different phenomena. In the focusing case, the state becomes more localized (c), displaying fluctuations due to the beating between the ground state and other localized modes, as detailed below. In the defocusing case, we observe the breaking of the Anderson

4.7 Numerical Results 37

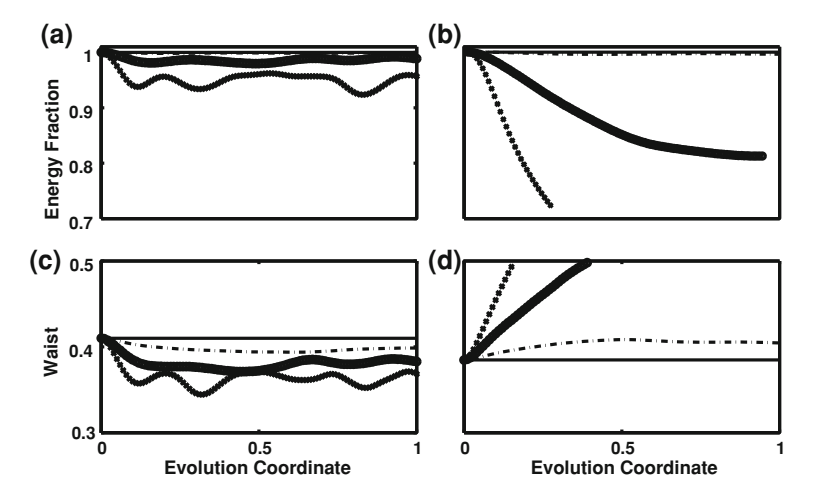


Fig. 4.5 Energy fraction and wavefunction waist for focusing (**a**), (**c**) and defocusing (**b**), (**d**) cases, for various powers, $P = 0.04P_{cr}$ (continuous line), $P = 0.64P_{cr}$ (dashed line), $P = 2P_{cr}$ (dotted line), $P = 4P_{cr}$ (diamond line), ($\sigma = 10$, $V_0 = 10$). Results averaged over 10 disorder realizations; the vertical axis is limited in panels (**b**, **d**) to improve the comparison among the various cases

localization. In Fig. 4.4, we report on a single realization of the disorder; in the following we consider various realizations, for each of them the critical power is calculated.

Figure 4.5 shows the fraction energy in the ground state and of its localization length for various powers. At any instant z, we expand ψ in terms of the eigenmodes:

$$\psi = \sum_{n} a_n(z)\psi_n(x) \exp(-i\beta_n z)$$
 (4.22)

where $\sum_n |a_n|^2 = P$. We define the ground state energy fraction of Fig. 4.5 as $E_0(z) = |a_0(z)|^2/P$ with $E_0(z=0) = 1$. In the focusing case (s=1), the localized shape is not substantially affected (Fig. 4.5a); conversely for s=-1 there is a drastic change in the energy distribution as $P > P_c$. These trends are also confirmed by the localization length, which decreases for s=1 [see panel (4.5c)], while in the defocusing case, the perturbation delocalizes the eigenmode. Note that these results are obtained when considering Eq. (4.4), hence for a finite degree of nonlocality.

4.8 Beating of Anderson Localizations

We consider the case of a residual coupling between the fundamental mode and an additional state located in its spatial proximity (all the other states are expected to have vanishing χ_{0n} , corresponding to a low overlap, because of distant locations with respect to the localization length). We derive the following coupled mode-theory equations in the HNL of (4.4), while assuming that only two modes are excited

$$i\dot{a}_0 = P\chi_{0a}a_a \exp(-i\Delta\beta z) + P\chi_{00}a_0 \tag{4.23}$$

$$i\dot{a}_a = P\chi_{0a}a_0\exp(i\Delta\beta z) + P\chi_{aa}a_a, \tag{4.24}$$

with $\Delta\beta=\beta_q-\beta_0$. We assumed that there is some other mode with index n=q, which is mostly coupled with the initial fundamental one n=0. The solutions to Eq. (4.24) is written, with obvious notation, as $a_{0,q}=\hat{a}_{0,q}\exp\left(\pm i\frac{\Delta\beta}{2}z+i\kappa z\right)$ and two possible values κ_\pm for κ are found. The general solutions is readily found, here we only report the HNL regime, when $\chi_{00}=\chi_{qq}$, and at the lowest order in χ_{0q} one finds

$$\Delta \kappa = \kappa_+ - \kappa_- = \sqrt{\frac{\Delta \beta^2}{4} + P^2 \chi_{0q}^2}$$
 (4.25)

and the wave intensity $|\psi(x)|^2$ oscillates with period $2\pi/\Delta\kappa$ that decreases with power, as also numerically verified (not reported). We stress that this result is expected to be mostly relevant in the focusing case, as in the defocusing case the Anderson localization is inhibited by the nonlinearity hence all the modes tend to be delocalized; we note indeed that the critical power for higher order modes is lower than the fundamental one. In the focusing case, the degree of localization is enhanced, therefore a regime in which only few modes interact (and in particular only two modes) can be achieved.

In conclusion, in this chapter we have investigated the way structural disorder and nonlinearity interact in the highly nonlinear limit. By increasing the degree of nonlinear nonlocality, the stability of Anderson localizations increases, these states turn out to be very robust with respect to the nonlinear effects. Mainly related to the fact that the nonlinear nonlocality reduces the coupling between Anderson states (a rather counter-intuitive result, which however is confirmed by our numerical analysis), such an interplay between disorder and nonlinearity can be exploited for light trapping and can be extended to several related problems, as quantum phase diffusion and coherence [19], ultrashort pulses in fibers [20], second harmonic generation [21] and Bose-Einstein condensation [17].

References

- 1. Anderson PW (1958) Phys Rev 109:1492
- 2. Bang O, Krolikowski W, Wyller J, Rasmussen JJ (2002) Phys Rev E 66:046619

References 39

- 3. Rasmussen P, Bang O, Królikowski W (2005) Phys Rev E 72:066611
- 4. Maucher F, Krolikowski W, Skupin S (2010) ArXiv e-prints, pp 1008-1891
- 5. Conti C, Peccianti M, Assanto G (2003) Phys Rev Lett 91:073901
- 6. Snyder AW, Mitchell DJ (1997) Science 276:1538
- Sheng P (ed) (1990) Scattering and localization of classical waves in random media. World Scientific, Singapore
- 8. Soukoulis CM (ed) (2001) Photonic crystals and light localization in the 21st century. Kluwer, Dordrecth
- 9. Wiersma DS, Bartolini P, Lagendijk A, Righini R (1997) Nature 390:671
- 10. John S (1987) Phys Rev Lett 58:2486
- 11. Conti C, Fratalocchi A (2008) Nat Phys 4:794
- Shadrivov IV, Bliokh KY, Bliokh YP, Freilikher V, Kivshar YS (2010) Phys Rev Lett 104:123902
- 13. Kartashov YV, Vysloukh VA (2005) Phys Rev E 72:026606
- 14. Schwartz T, Bartal G, Fishman S, Segev M (2007) Nature 446:52
- 15. Billy J et al (2008) Nature 453:891
- 16. Roati G (2008) Nature 453:895
- 17. Modugno G (2010) Rep Prog Phys 73:102401
- 18. Folli V, Conti C (2010) Phys Rev Lett 104:193901
- 19. Batz S, Peschel U (2011) Phys Rev A 83:033826
- 20. Conti C, Schmidt M, Russell P, Biancalana F (2010) Arxiv preprint arXiv:1010.0331
- 21. Conti C, D'Asaro E, Stivala S, Busacca A, Assanto G (2010) Opt Lett 35:3760

Chapter 5 Scale-Free Nonlinearity in Disordered Ferroelectrics

So far in this work, we have considered disorder and nonlinearity as two phenomena living on the same spatial scale-length, which compete for what concerns the stability of localized wave-forms. The structural disorder of Chap. 4 or the material fluctuations of Chap. 3 are of the same order of magnitude of the beam waist. In this chapter, the emerging phenomena of the interaction between nonlinearity and disorder are explored when the randomness lies on a much smaller scale-length with respect to the spatial scale of the solitonic regime. At first analysis, light propagation through such a system should not display any kind of nonlinear effect: the light beam should not feel the disordered atomic configuration and hence should propagate unperturbed in such a kind of materials. On the contrary, we consider a specific effect when disorder is the cause of the nonlinear response to the electromagnetic field: this is a result of the mutual interaction between nonlinearity and disorder that gives a positive feedback for the activation of solitary waves. Recently, the observation of a novel class of optical spatial solitons [1, 2] has been reported in disordered out-of-equilibrium ferroelectrics [3, 4]. In this kind of media, the diffusion-driven photorefractive nonlinearity [5] can be largely enhanced to sustain "scale-free" nondiffractive beams, which can have arbitrary amplitude and waist (within the limit of validity of the paraxial approximation). In this chapter, we will discuss this kind of light localization and we will unveil the existence of a "scale-free" instability, characterized by the remarkable absence of a dominant spatial scale during, at variance with what happens in standard MI, where there is a wave-vector which is mostly amplified with respect to the others.

5.1 Diffusive Nonlinearity in Disordered Ferroelectrics

Here, we review the basic phenomenology underlying the photorefractive diffusive nonlinearity, which gives rise to scale-free phenomena.

The photorefractive effect appears in materials exhibiting both the electro-optic effect than the photo-generation of free-carriers. The electro-optic phenomenon

appears when the refractive index depends on the local low-frequency electric-field [6]. In this context, we study isotropic photorefractive crystals in which the dependence of the refractive index perturbation Δn on the electric field is quadratic,

$$\Delta n = -\frac{n_0^3}{2} g \epsilon_0^2 \chi^2 E_{DC}^2, \tag{5.1}$$

where n_0 is the refractive index of the isotropic medium, g is the component of the second-order electro-optic tensor, χ is the susceptibility related to the low-frequency electric field E_{DC} .

Now, we obtain the explicit expression of the low-frequency electric-field. When the light beam enters the crystal, the neighboring electrons absorb the light and can be excited in the conduction band of the semiconductor from the impurity levels. The free electrons can diffuse through the medium and the free-charge diffusion current density can be written as:

$$\mathbf{J} = \frac{D}{a} \nabla \rho, \tag{5.2}$$

where D is the diffusion coefficient, ρ is the charge density and q is the electron charge. The migration of the free-charges is balanced by the drift current:

$$\mathbf{J}_{drift} = \mu \rho \mathbf{E}_{DC},\tag{5.3}$$

where μ is the electron mobility. At equilibrium, one obtains the low-frequency electric field by setting Eq. (5.2) equal to Eq. (5.3):

$$\mathbf{E}_{DC} = \frac{k_B T}{q} \frac{\nabla \rho}{\rho},\tag{5.4}$$

with $k_BT = D/\mu$, where k_B is the Boltzmann constant and T is the temperature of the system. Being the charge density proportional to the photon density, Eq. (5.4) can be written in term of the field intensity,

$$\mathbf{E}_{DC} = \frac{k_B T}{q} \frac{\nabla I}{I},\tag{5.5}$$

and hence, the electro-optic effect induced by the photo-generation of free-carriers is

$$\Delta n(I) = -\frac{n_0^3}{2} g \epsilon_0^2 \chi^2 \frac{(k_B T)^2}{q^2} \frac{(\nabla I)^2}{I^2}.$$
 (5.6)

By inserting Eq. (5.6) in Eq. (2.7), we obtain the nonlinear equation for the photore-fractive diffusive nonlinearity:

$$2ik\frac{\partial A}{\partial z} + \nabla_{\perp}^{2}A - \frac{L^{2}}{\lambda^{2}}\frac{(\partial_{x}|A|^{2})^{2} + (\partial_{y}|A|^{2})^{2}}{4|A|^{4}}A = 0,$$
(5.7)

where we neglected the term in $(\partial_z I)^2$ in Eq. (5.5) because of the paraxial approximation; being $I = |A|^2$ the optical intensity and L is a characteristic length of the diffusive nonlinearity

$$L = 4\pi n^2 \epsilon_0 \sqrt{g} \chi_{PNR}(k_B T/q), \qquad (5.8)$$

where g > 0, due to the focusing nature of the nonlinearity and χ_{PNR} is the mean low frequency susceptibility (χ above) that is mainly due to the so-called polar nanoregions (PNR), a metastable effect obtained when the considered system is rapidly cooled below a characteristic temperature. These regions exhibit a huge polarizability, as demonstrated in [3], and they are the main reason allowing to observe the propagation of self-localized wave-forms.

We rewrite Eq. (5.7) in dimensionless units as

$$i\frac{\partial\psi}{\partial z} + \frac{1}{2}\nabla_{xy}^2\psi - \sigma\frac{(\partial_x|\psi|^2)^2 + (\partial_y|\psi|^2)^2}{|\psi|^4}\psi = 0,$$
 (5.9)

where $x = X/W_0$, $y = Y/W_0$ and $z = Z/Z_0$, with $Z_0 = kW_0^2/2$ the diffraction length, W_0 an arbitrary beam waist, and $\sigma = L^2/8\lambda^2$, with $\sigma = 1/8$ for $L = \lambda$. The Eq. (5.9) admits solitonic solutions that, as we will see below, are "scale-free".

5.2 Scale-Free Solitons

The Eq. (5.9) depends on the ratio L/λ that describes the mutual competition between the diffractive effects and the nonlinearity. The wavelength λ controls the distortion of the laser beam through the diffraction while the strength of nonlinearity is dictated by the characteristic length L, related to the formation of the PNR and not directly connected to the beam waist in the scale-free regime. When $L \geq \lambda$, the nonlinear optical response is no longer negligible and the formation of self-trapped beams of arbitrary intensity and waist, marked by a flat "existence curve", is observable.

When $L = \lambda$, the scale-free solution is a Gaussian function $\psi(x, y, z) = \psi_0(x, y)e^{i\beta z}$, with

$$\psi_0(x, y) = \psi_0 \exp\left(-\frac{x^2 + y^2}{w_0^2}\right) \tag{5.10}$$

where $\beta = -2/w_0^2$. Both w_0 that ψ_0 are arbitrary constants. For $L > \lambda$, the scale-free solutions become $\psi(x, y, z) = \psi_0(x, y)e^{i\gamma^2\beta z}$ with:

$$\psi_0(x, y) = \psi_0 \left[\cosh\left(\sqrt{2} \frac{x}{w_0}\right) \cosh\left(\sqrt{2} \frac{y}{w_0}\right) \right]^{-\gamma^2}$$
 (5.11)

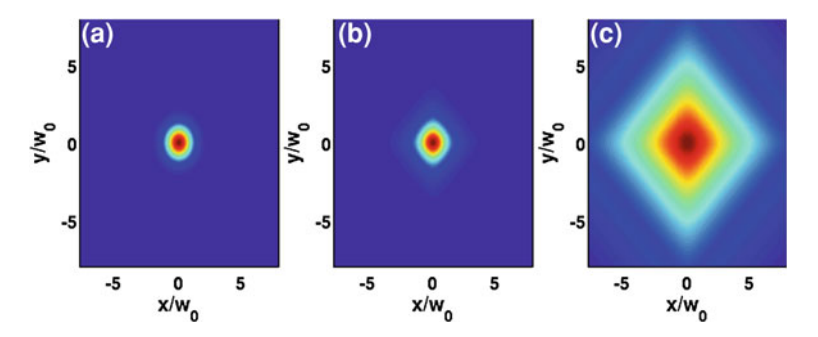


Fig. 5.1 Scale-free solutions for $L = \lambda$, that is $\sigma = 0.125$ (*Gaussian shape*) (a), and for $L > \lambda$ (generalized solution) in the weakly nonlinear regime $\sigma = 0.25$ (b), and in the *high* nonlinear regime $\sigma = 1$ (c)

and

$$\frac{1}{\gamma} = \sqrt{\left(\frac{L}{\lambda}\right)^2 - 1}.\tag{5.12}$$

As it can be seen in Fig. (5.1), when we increase the strength of the nonlinearity with respect to diffraction, the general solution (5.11) develops a square profile, losing its radial symmetry.

5.3 Scale-Free Instability

In this section, we consider one-dimensional solitons, also called the diffraction-free stripe solutions, $\psi(x, z) = \psi_0(x)e^{i\beta z}$,

$$\psi_0(x) = \psi_0 \exp\left(-\frac{x^2}{w_0^2}\right),\tag{5.13}$$

with $\beta = -1/w_0^2$, and ψ_0 and w_0 arbitrary independent parameters, such that this self-trapped beam exists at any intensity level and for any waist (within the validity of the paraxial approximation).

5.3.1 Absence of Modulational Instability

We then consider perturbations to the exact solution, which is written as

$$\psi = [\psi_0(x) + p(x, y, z)] \exp(i\beta z). \tag{5.14}$$

The linearized evolution equation for the perturbation p reads, with obvious notation, as

$$i\partial_z p + \frac{1}{2}\nabla_{xy}^2 p - 4\sigma \left[\frac{\psi_{0x}^2}{\psi_0^2} p + \psi_{0x} \left(\frac{p+p^*}{\psi_0}\right)_x\right] = \beta p.$$
 (5.15)

From (5.15), one readily sees that if $\psi_0(x) = \psi_0(w_0 \to \infty)$ no instability is expected (i.e. no solution such that p exponentially grows with z); showing indeed that the scale-free model (5.9) is not exhibiting the standard MI. This result is in striking contrast with the well known fact that MI always accompanies the existence of solitary waves solutions, as for Kerr, saturable or quadratic nonlinearities [1, 2]. Conversely, in the scale-free model, one has self-trapped bright beams, but no instability for the plane-wave solutions; we show in the following that another kinds of instability may indeed occur.

5.3.2 Theory of Scale-Free Instabilities

We first note that (5.15) does not imply an exponential growth for a perturbation whose spatial profile in the x direction is the same as the pump beam ψ_0 , i.e. for p such that

$$p = \psi_0(x)\alpha_+(z)e^{ik_yy} + \psi_0(x)\alpha_-(z)^*e^{-ik_yy}, \tag{5.16}$$

indeed the term containing p^* in (5.15) disappears, so that there is no instability. Note that as Eq. (5.15) does not contain coefficients explicitly dependent on y, p can be expressed as a plane wave expansion with respect to y without loss of generality. We then write the perturbation as

$$p = \psi_1(x)\alpha_+(z)e^{ik_yy} + \psi_1(x)\alpha_-(z)^*e^{-ik_yy},$$
 (5.17)

with $\psi_1(x)$ a spatial profile, different from $\psi_0(x)$. To keep the treatment as simple as possible, we limit to the Gaussian case for $L=\lambda$ ($\sigma=1/8$), and we take the profile for the perturbation ψ_1 as a Gaussian with waist different from that of the pump ψ_0 , i.e.

$$\psi_1 = \mathcal{N}_1 \exp(-\frac{x^2}{w_1^2}) \tag{5.18}$$

where $\mathcal{N}_1^2 = \sqrt{2/\pi w_1^2}$, such that $(\psi_1, \psi_1) = 1$, with the scalar product $(a, b) = \int_X a^*b$. We use Eq. (5.17) in (5.15) and project over ψ_1 , which corresponds to make an expansion in an Hermite-Gauss basis with respect to x and only retaining the first term of the expansion. We find the coupled equations for the amplitudes α_{\pm} after (5.17):

$$\pm 2i\dot{\alpha}_{\pm} + \left(-k_y^2 + \frac{1}{w_0^2} - \frac{1}{w_1^2}\right)\alpha_{\pm} + \frac{w_1^2 - w_0^2}{w_0^4}\alpha_{\mp} = 0.$$
 (5.19)

Note that the last term coupling α_{\pm} in (5.19) is that responsible for the instabilities and it is proportional to $w_1^2 - w_0^2$, hence for $w_1 = w_0$, we recover the result stated above, i.e. the absence of instability for a perturbation with the same x – size of the pump beam. Analogously, the instability disappears for $w_0 \to \infty$, corresponding to the plane-wave case, also discussed above.

For $w_1 \neq w_0$, one finds that (5.19), admits exponentially amplified solutions, which are written as $\alpha_{\pm} = \hat{\alpha}_{\pm} \exp(\lambda z)$, with the gain λ given by

$$4\lambda^{2}(k_{y}, w_{1}) = \frac{(w_{1}^{2} - w_{0}^{2})^{2}}{w_{0}^{8}} - \left(k_{y}^{2} - \frac{1}{w_{1}^{2}} + \frac{1}{w_{0}^{2}}\right)^{2};$$
 (5.20)

letting $r = w_1/w_0$, one has

$$4\lambda^{2}(k_{y}, r)w_{0}^{4} = (r^{2} - 1)^{2} - \left[(k_{y}w_{0})^{2} + 1 - 1/r^{2} \right]^{2}.$$
 (5.21)

The most unstable perturbation corresponds to the values r and k_y that maximes λ^2 . As detailed below, the analysis of Eq. (5.21) allows to identify two kinds of instabilities: with respect to perturbations with waist greater than the pump beam (r > 1), and the opposite case (r < 1), denoted hereafter as *defocusing* and *fragementing* instabilities, respectively.

5.3.3 Defocusing Instability

For a perturbation with $w_1 > w_0$, the condition $\lambda^2 > 0$ predicts the maximum gain at $k_y = 0$ and given by

$$\lambda_D = \frac{\sqrt{(r^2 - 1)^2 - (1 - 1/r^2)^2}}{2w_0^2}.$$
 (5.22)

 λ_D is positive only for r>1, and is shown in Fig. 5.2a. This maximum gain is not limited, and grows with r, thus revealing a self-propelling instability, such that if a perturbation with waist greater than the beam is superimposed, the beam tends to spread (the perturbation gains energy) and the spreading rate increases with the waist of the beam. Note that the gain is maximum at $k_y=0$, denoting an instability that does not tend to alter the striped shape of the beam by introducing periodical modulations. This process is also more pronounced for small waists, as the maximum gain λ_D goes like w_0^{-2} . We show in Fig. 5.3, an example of this instability, as obtained by numerically solving Eq. (5.9). The evolution reveals a defocusing of the beam, which is hence unstable, and is compared with the linear case $\sigma=0$ (linear propagation); for $\sigma>0$, the effect is more pronounced as the waist w_0 is reduced.

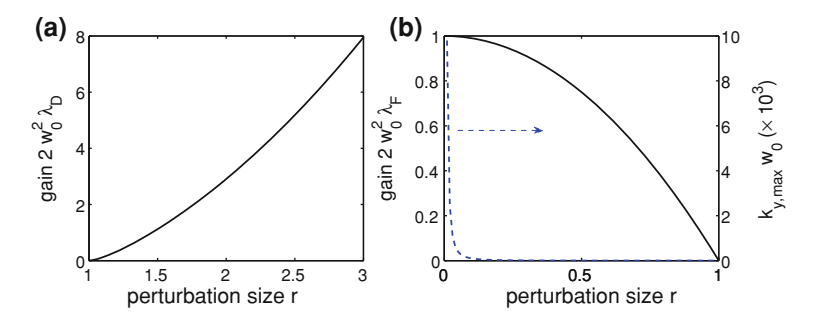


Fig. 5.2 a Gain versus the ratio of the waist between the perturbation and the pump for r > 1 (maximum gain attained at $k_y = 0$); **b** *Left* scale: gain versus r for r < 1; *right* scale: corresponding maximally amplied period

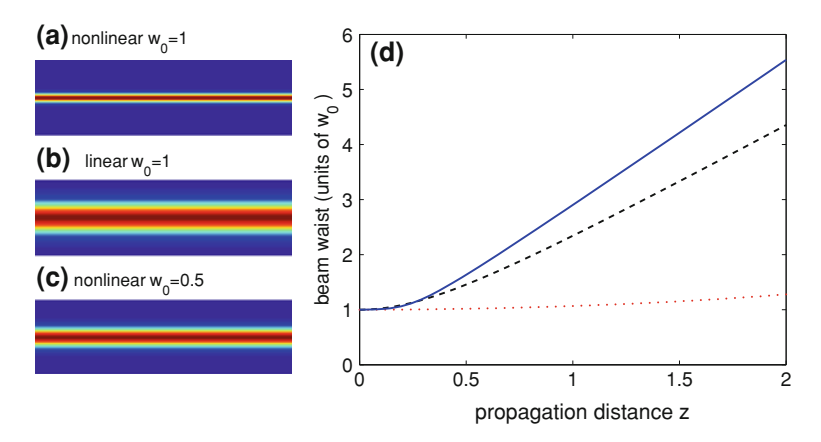


Fig. 5.3 Simulation of the defocusing instability after Eq. (5.9). **a** Output beam at z=4 for $\sigma=0.125$, with a striped beam with $w_0=1$; **b** as in **a** with $\sigma=0$ (linear propagation); **c** as in **a** with $w_0=0.5$; **d** beam waist in the x directions for **a**, dotted line, for **b**, dashed line, for **c**, continuous line

5.3.4 Fragmenting Instability

For r < 1 (perturbation smaller than the pump, i.e. $w_1 < w_0$), the gain is maximum at a $k_y > 0$, fixed by r, and given by

$$k_{y,\text{max}} = \frac{\sqrt{1/r^2 - 1}}{w_0}. (5.23)$$

The corresponding maximum growth rate λ_R is

$$\lambda_F = \frac{1 - r^2}{2w_0^2}. (5.24)$$

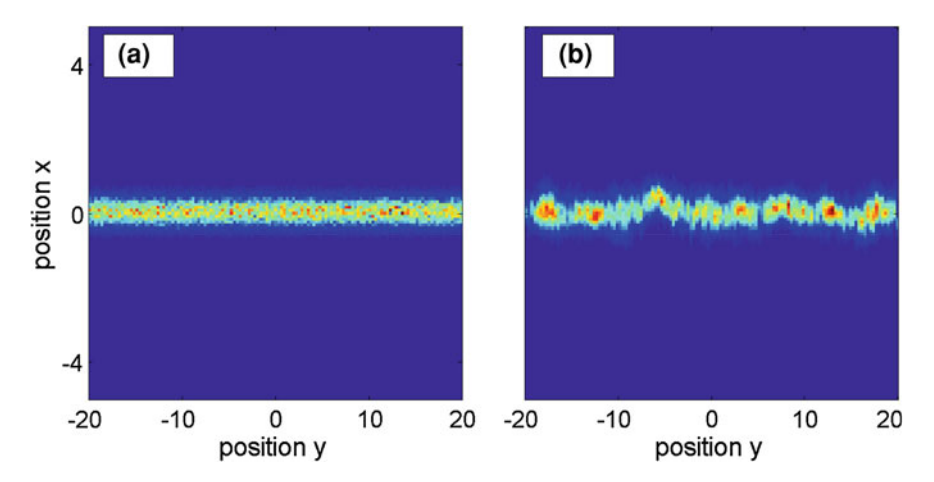


Fig. 5.4 Simulation of the fragmenting instability. The stripe solution is perturbed by a Gaussian noise with 10% noise; **a** input beam; **b** out beam at z = 10 ($w_0 = 1$, $\sigma = 0.125$)

However, as r < 1, the maximum gain corresponds to r = 0 (vanishing w_1) with diverging $k_{y,\text{max}}$, denoting the tendency of the beam to break up into very tiny spots, with no preferential spatial scale, in great contrast with the standard MI. Additionally, we note that, for a fixed r, the gain scales as the inverse squared waist, hence the more focused is the beam, the more pronounced in the instability. This is another remarkable difference with standard MI; e.g. in Kerr media as the pump power is increased, the gain increases as well; conversely in the scale-free model, the power does not affect the gain, which, on the contrary, increases when decreasing the beam spot. Note also that the gain level for the fragmenting instability is lower than for the defocusing one and is limited by the upper value $\lambda_F(r=0) = 1/(2w_0^2)$, need longer propagation distances are needed to appreciate its development. A notable outcome is that tiny details superimposed to the pump are amplified upon propagation. In Fig. 5.4, we show an example of the fragmenting instability, by the evolution of a stripe perturbed by a Gaussian noise with 10% amplitude with respect to the pump.

In conclusion, in this chapter, we have focused our attention on localized scale-free wave-forms resulting from a new kind of interaction between nonlinearity and disorder. The existence of novel kind of instabilities in nonlinear beam propagation was outlined. The overall picture show that the specific kind of nonlocality, which characterizes the scale-free model, furnishes peculiar mathematical and physical properties that largely distinguish the considered nonlinear optical process from previously investigated systems. The capability of the predicted unstable processes to amplify tiny beam perturbations, at any spatial scale (withing the paraxial approximation) looks to open interesting perspectives for imaging applications.

References 49

References

- 1. Kivshar YS, Agrawal GP (2003) Optical solitons. Academic, New York
- 2. Trillo, S, Torruealls, W (eds) (2001) Spatial solitons. Springer, Berlin
- 3. DelRe E, Spinozzi E, Agranat A, Conti C (2010) Nat. Photonics 5:39
- 4. Conti C, Agranat A, DelRe E (2011) Arxiv preprint arXiv 1102.4945
- 5. Crosignani B, Degasperis A, DelRe E, Di Porto P, Agranat AJ (1999) Phys Rev Lett 82:1664
- 6. Yariv A (1991) Quantum electronics. Saunders College, San Diego

Part II Resonant Systems

Chapter 6 The Maxwell-Bloch Equations

The last 40 years have witnessed an intensive and targeted growth of interest in the field of nonlinear optics [1], as a fascinating new field of research both with a vastness of applications in several systems related to communications, optical computing, etc. Furthermore, the analytical techniques, involved in the study of nonlinear optical phenomena, can be applied in other branches of the nonlinear physics, being tools of general character, as the perturbative approach used several times in the present thesis. The continuous development of ultra-short pulsed lasers allowed a sophisticated enlargement of the analysis of nonlinear optics on a wide range of systems, specifically concerning the matter-radiation interaction in the highly nonlinear regime.

In order to obtain the exact informations about the light behavior into a nonlinear medium, it is often necessary to employ numerical approaches. The choice of the more accurate numerical modeling is dependent on the specific nonlinear phenomenon.

In recent years, relevant attention was dedicated to the transient regime of light-matter interaction on nanometer spatial scales, in which it is essential to exactly know the time-dependent response of the medium. The natural solution for this kind of problems, particularly in the resonant media, is a time-domain algorithm, employing a first-principles approach. In this respect, continuing the subject of this thesis, we analytically and numerically develop a methodical technique that permits to study the interaction of ultra-short pulses with matter in the presence of disorder, both in the perturbative (analytical solution) and in the non-perturbative regime (numerical approach).

6.1 Introduction

The pivotal compass of the present chapter is to understand how to proceed in the study of transient coherent phenomena. In fact, ultra-short pulses, emitted by the lasers of last generation, have a time duration on the order of the femtoseconds. These

pulses can be considerably shorter than the relaxation times of the light absorbing atoms and they are characterized by highly intense fields, which result in a nonlinear reaction in the matter response. These phenomena are usually transient and coherent, hence we have to develop time domain algorithms. Furthermore, we stay in a parameter region in which the usual approximations cannot be considered valid, ¹ we must use first principles modeling, without making assumptions and retain a quantum treatment of the matter. In what follows, we will see as the *ab-initio* numerical simulations on the Maxwell-Bloch equations allow to true physics to emerge. In the first section, we derive the Maxwell-Bloch equations that couples the Maxwell equation with a two-states quantum system. In the second section, we explain the numerical method, the Finite Differences Time Domain algorithm (FDTD), by following the guideline of Ziolkowski and coworkers [2–4]. Finally, we look for the solitary-wave solutions.

6.2 Generalities

In this first section, we sketch the pivotal steps for the derivation of Maxwell-Bloch system [2], in which we start by the Maxwell's equations in matter (coupled via the polarization) and by the Bloch's system, describing the atomics dynamics of a N-levels system, through the density matrix formalism and the pseudo-spin equation. Finally, we connect each with each other by expressing the polarization in terms of pseudo-spin vectors. Let us start by writing the Maxwell's Equation in matter:

$$\partial_t \mathbf{H} = -\frac{1}{\mu_0} \nabla \times \mathbf{E}$$

$$\partial_t \mathbf{E} = \frac{1}{\epsilon_0} \nabla \times \mathbf{H} - \frac{1}{\epsilon_0} \partial_t \mathbf{P},$$
(6.1)

where **E** and **H** are respectively the magnetic and the electric field, the polarization $\mathbf{P}(\mathbf{r},\mathbf{t}) = -Ne\mathbf{q}(\mathbf{r},\mathbf{t})$ depends on the electronic charge e, on the atomic density N and on the $q(\mathbf{r},\mathbf{t})$, which is the displacement of an electron from its equilibrium position, \mathbf{r} . In the quantum mechanical description, it is expressed as the expectation value of the position operator, $\mathbf{q} = \langle \psi | \mathbf{Q} | \psi \rangle$ and ψ is the quantum wave function. The wave-function ψ obeys to the Schroedinger Equation:

$$i\hbar\partial_t\psi = \hat{H}\psi,\tag{6.2}$$

where the Hamiltonian is $\hat{H} = \hat{H}_0 + \hat{H}_{int}$. \hat{H}_0 is the unperturbed diagonal Hamiltonian describing the atom behavior when no external field are present. \hat{H}_{int} is

¹ The Slowly Varying Envelope Approximation (SVEA) assumes that the spatial and temporal variations on scale comparable to the wavelength or the optical cycle of the field envelope of the forward (the back-reflected wave is neglected: in the disordered case considered here, this assumption is not longer valid) traveling wave can be neglected.

6.2 Generalities 55

the light-matter interaction Hamiltonian and can be expressed in terms of the electric field and the position operator:

$$\hat{H}_{\text{int}} = -|e|\mathbf{E} \cdot \mathbf{Q}. \tag{6.3}$$

 \hat{H}_{int} is the quantized potential energy of a dipole with momentum $\mathbf{p} = e\mathbf{Q}$ in an external field \mathbf{E} .

We generalize the Schroedinger equation through the density-of-states operator ρ in order to calculate the observables (the expectation values) also when the system does not admit a wave function description, through the relation $\mathbf{q} = \langle \hat{Q} \rangle = Tr\{\rho \hat{Q}\}$. The density-of-states matrix evolve in time according to the Liouville equation:

$$i\hbar\partial_t\hat{\rho} = [\hat{H}, \hat{\rho}].$$
 (6.4)

In order to obtain the expression for \mathbf{q} to pass to the polarization equation, we have to solve the Liouville equation (6.4) and use the calculated density to obtain the expectation value of the operator \hat{Q} . We solve (6.4) by expanding the Hamiltonian in the adjoint representation of the Lie algebra SU(N), where N is the number of the atomic levels. By studying the rotational symmetry of the SU(N), group, it has been shown that both $\hat{\rho}$ and \hat{H} can be expressed in terms of N^2-1 generators, λ_i , of the SU(N) group:

$$\hat{\rho}(t) = \frac{1}{N}\hat{I} + \frac{1}{2}\sum_{j=1}^{N^2 - 1} s_j(t)\hat{\lambda}_j
\hat{H}(t) = \frac{1}{2}\hbar \left[\frac{2}{N} \left(\sum_{k=1}^{N} \omega_k \right) \hat{I} + \sum_{j=1}^{N^2 - 1} \gamma_j(t)\hat{\lambda}_j \right],$$
(6.5)

where,

$$s_{i}(t) = Tr\hat{\rho}(t)\hat{\lambda}_{i}$$

$$\gamma_{i}(t) = \frac{1}{\hbar}Tr\hat{H}(t)\hat{\lambda}_{i},$$
(6.6)

for definition, with $[\hat{\lambda}_i, \hat{\lambda}_j] = 2i\epsilon_{ijk}\hat{\lambda}_k$, where ϵ_{ijk} is the antisymmetric tensor. By inserting Eq. (6.5) in Eq. (6.4), we obtain:

$$\dot{s}_1(t)\hat{\lambda}_1 + \dot{s}_2(t)\hat{\lambda}_2 + \dot{s}_3(t)\hat{\lambda}_3 = \sum_i \gamma_i(t) \sum_j s_j(t)\epsilon_{ijk}\hat{\lambda}_k. \tag{6.7}$$

The ortogonality condition for the SU(2) group gives $Tr\hat{\lambda}_i\hat{\lambda}_j=2\hat{\delta}_{ij}$. For a two-level system, the SU(2) group is represented by the Pauli matrices as generators $\hat{\lambda}_i$. The Eq. (6.7) becomes

$$\dot{s}_1 = \gamma_2 s_3 \epsilon_{231} + \gamma_3 s_2 \epsilon_{321}
\dot{s}_2 = \gamma_1 s_3 \epsilon_{132} + \gamma_3 s_1 \epsilon_{312}
\dot{s}_3 = \gamma_1 s_2 \epsilon_{123} + \gamma_2 s_1 \epsilon_{213}.$$
(6.8)

At last, we calculate the components of $\gamma(t)$ by explicit the total Hamiltonian. The unperturbed contribution for a two-level system with energies: $E_0=0$ and $E_1=\hbar\omega_0$, where ω_0 is the atomic transition resonance frequency between the ground state and the excited one,

$$\hat{H}_0 = \begin{pmatrix} 0 & 0 \\ 0 & \hbar \omega_0. \end{pmatrix} \tag{6.9}$$

Under the dipole approximation,² the interaction term is $\hat{H}_{int} = -|e|\hat{Q} \cdot \mathbf{E}(\mathbf{R}, \mathbf{t})$, where **R** is the atomic baricenter position. \hat{H}_{int} has to be calculated on the atomic levels, $|0\rangle$, $|1\rangle$. The displacement operator is off-diagonal:

$$\hat{Q} = q_0 \begin{pmatrix} 0 & 1 \\ 1 & 0, \end{pmatrix} \tag{6.10}$$

where q_0 is the typical atomic length scale on order of $q_0=10^{-10}\,\mathrm{m}$. The total Hamiltonian can be written as:

$$\hat{H} = \hbar \begin{pmatrix} 0 & -\Omega_R \\ -\Omega_R & \omega_0, \end{pmatrix} \tag{6.11}$$

where we have introduced the Rabi frequency $\Omega_R = \frac{|e|q_0}{\hbar} E$. Finally, known \hat{H} , the $\gamma(t)$ vector is

$$\gamma(t) = \{-2\Omega_R, 0, -\omega_0\}. \tag{6.12}$$

By replacing Eq. (6.12) in Eq. (6.8), we obtain the "Pseudo-Spin" equations, representing the evolution of the density-of-state matrix elements:

$$\dot{s}_1 = \omega_0 s_2
\dot{s}_2 = 2\Omega_R s_3 - \omega_0 s_1
\dot{s}_3 = -2\Omega_R s_2,$$
(6.13)

with the normalization condition $|s_1|^2 + |s_2|^2 + |s_3|^2$. Physically, s_1 is the dispersive component of the polarization (the in-phase term), s_2 is the absorptive one (the quadrature component), while s_3 represents the population inversion between the two atomic levels. In order to comprehensively describe the underlying near-resonant physics, we have to include the "dissipative" terms. We phenomenologically take into account the damping effects by introducing diagonal terms related to characteristic decay rates:

$$\partial_t \begin{pmatrix} s_1 \\ s_2 \\ s_3 \end{pmatrix} = \begin{pmatrix} 0 & \omega_0 & 0 \\ -\omega_0 & 0 & 2\Omega_R \\ 0 & -2\Omega_R & 0 \end{pmatrix} \begin{pmatrix} s_1 \\ s_2 \\ s_3 \end{pmatrix} - \begin{pmatrix} \frac{1}{T_2} & 0 & 0 \\ 0 & \frac{1}{T_2} & 0 \\ 0 & 0 & \frac{1}{T_1} \end{pmatrix} \begin{pmatrix} s_1 \\ s_2 \\ s_3 - s_{30} \end{pmatrix}$$
(6.14)

² The electromagnetic field can be considered constant on the atomic scale.

6.2 Generalities 57

where T_1 is the excited-state lifetime, T_2 is the dephasing time and s_{03} represents the initial profile of the atomic population (in the active medium $s_{03} = 1$).

We do some assumptions on the electromagnetic field that is a uniform planewave, propagating along \hat{z} and polarized along \hat{x} : $\mathbf{E}(\mathbf{r},t) = E_x(z,t)\hat{\mathbf{x}}$ and $\mathbf{H}(\mathbf{r},t) = H_y(z,t)\hat{\mathbf{y}}$, so the dipole is aligned along the electric field direction and the polarization is $\mathbf{P} = P_x\hat{\mathbf{x}} = -N|e|Tr(\hat{\rho}\hat{Q})_{\hat{x}}$. In fact, the single component of \hat{Q} is $\hat{Q}_x = q_0\hat{\lambda}_1$ that gives

$$P_x = -N|e|q_0 s_1, (6.15)$$

by using the SU(2) representation (6.5). The coupling of the Maxwell's equations (6.1) to the Bloch's system (6.14) through (6.15) gives: *Maxwell Equations*:

$$\partial_t H_y = -\frac{1}{\mu_0} \partial_z E_x$$

$$\partial_t E_x = -\frac{1}{\epsilon_0} \partial_z H_y + \frac{N|e|q_0}{\epsilon_0} \omega_0 s_2 - \frac{N|e|q_0}{\epsilon_0 T_2} s_1.$$
(6.16)

Bloch Equations:

$$\dot{s}_1 = -\frac{1}{T_2} s_1 + \omega_0 s_2
\dot{s}_2 = -\omega_0 s_1 - \frac{1}{T_2} s_2 + 2 \frac{|e|q_0}{\hbar} E_x s_3
\dot{s}_3 = -2 \frac{|e|q_0}{\hbar} E_x s_2 - \frac{1}{T_1} (s_3 - s_{30}).$$
(6.17)

The resulting system of equations is resolved through the numerical approach, sketched in the following section.

6.3 The Numerical Approach

We now introduce the parallel finite difference time domain (FDTD) technique in order to obtain the exact solution for the Maxwell Bloch equations. In the next chapter, we generalize the obtained results to a random medium.

We follow the discretization approach of [2], based upon a predictor-corrector iterative scheme that gives the solution of the Maxwell-Bloch equations with each time update.

We use the standard grid finite-differences discretizations of the spatial and temporal derivatives (the unique approximation of the FDTD algorithm). The electric and magnetic field components are arranged on this spatio-temporal grid with steps $\Delta z/2$ and $\Delta t/2$. Being numerically complicated to treat the exponential decay of

 s_1 , s_2 and s_3 , we factorize out it by imposing $s_i(z,t) = e^{-t/T_2}u_i(z,t)$ with i = 1, 2 and $s_3(z,t) = s_{03} + e^{-t/T_1}u_3(z,t)$. The MB equations become:

$$\partial_t E_x = -\frac{1}{\epsilon_0} \partial_z H_y + A u_1 - B u_2$$

$$\partial_t u_1 = \omega_0 u_2$$

$$\partial_t u_2 = \omega_0 u_1 + C_+ E_x u_3 + D E_x$$

$$\partial_t u_3 = -C_- E_x u_2,$$
(6.18)

where
$$A(t) = \frac{N|e|q_0}{\epsilon_0 T_2} e^{-t/T_2}$$
, $B(t) = \frac{N|e|q_0}{\epsilon_0} \omega_0 e^{-t/T_2}$, $C_+(t) = 2 \frac{|e|q_0}{\hbar} e^{-t(1/T_1 - 1/T_2)}$, $C_-(t) = 2 \frac{|e|q_0}{\hbar} e^{-t(1/T_2 - 1/T_1)}$.

The magnetic field equation is solved at the steps $(m + \frac{1}{2})\Delta z$ and $(n + \frac{1}{2})\Delta t$. The electric field and the matter equations are solved for $m\Delta z$ and $n\Delta t$. So, the FDTD discretized Maxwell-Bloch equations are:

Discretized Maxwell-Bloch Equations:

$$H_{y}(m+\frac{1}{2},n+\frac{1}{2}) = H_{y}(m+\frac{1}{2},n-\frac{1}{2}) - \frac{\Delta t}{\mu_{0}\Delta z} \left[E_{x}(m+1,n) - E_{x}(m,n) \right]$$
(6.19)

$$E_{x}(m, n+1) = E_{x}(m, n) - \frac{\Delta t}{\epsilon_{0} \Delta z} \left[H_{y}(m + \frac{1}{2}, n + \frac{1}{2}) - H_{y}(m - \frac{1}{2}, n + \frac{1}{2}) \right] - A(n + \frac{1}{2}) \frac{1}{2} \left[u_{1}(m, n+1) + u_{1}(m, n) \right] \Delta t + B(n + \frac{1}{2}) \frac{1}{2} \left[u_{2}(m, n+1) + u_{2}(m, n) \right] \Delta t$$

$$(6.20)$$

$$u_1(m, n+1) = u_1(m, n) + \omega_0 \frac{1}{2} [u_2(m, n+1) + u_2(m, n)] \Delta t$$
 (6.21)

$$u_{2}(m, n+1) = u_{2}(m, n) - \omega_{0} \frac{1}{2} \left[u_{1}(m, n+1) + u_{1}(m, n) \right] \Delta t + C_{+}(n + \frac{1}{2})$$

$$\frac{1}{2} \left[E_{x}(m, n+1) + E_{x}(m, n) \right] \frac{1}{2} \left[u_{3}(m, n+1) + u_{3}(m, n) \right] \Delta t$$

$$+ D(n + \frac{1}{2}) \frac{1}{2} \left[E_{x}(m, n+1) + E_{x}(m, n) \right] \Delta t \qquad (6.22)$$

$$u_3(m, n+1) = u_3(m, n) - C_-(n + \frac{1}{2}) \frac{1}{2} \left[E_x(m, n+1) + E_x(m, n) \right] \Delta t$$
$$\frac{1}{2} \left[u_2(m, n+1) + u_2(m, n) \right]. \tag{6.23}$$

The five coupled scalar equations above permit to simulate the electromagnetic field propagation inside the sample without any assumptions neither on the field or on the matter.

6.4 The Soliton Solution of the MB Equations

In this section, we look at the localized solution for the Maxwell-Bloch system. As it can be demonstrate, the only form of light localization that can propagate in a resonant medium is the Self-Induced Transparency (SIT). This is an intense ultra-short pulse that, under certain conditions, can travel undistorted in strongly absorbing media [5–10]. Intrinsically to exist, a SIT transports an inversion of population between two energy levels. In fact, in the intense-signal limit, in which the medium relaxation times are sufficiently longer than the pulse duration and the period of interaction, the Rabi flopping behavior is predominant. It predicts that, if a sufficiently strong signal with a duration T such that, $\Omega_R T = 2\pi$, where Ω_R is the Rabi frequency, the required traveling inversion of population is achieved. In fact, the " 2π pulse", during its going through the system, flips the completely absorbing medium into a completely inverted one and again into the initial completely absorbing configuration, all that within a Rabi oscillation, so no energy losses are present. The pulse travels unattenuated and a complete population inversion is transported in the strongly absorbing medium, as described by the soliton solution of the Maxwell-Bloch equations [11, 12]. Hence, the SIT is the only pulse that carries a population inversion and it is the only stable pulse in the self-consistent interaction between radiation and matter: this is a direct consequence of so-called the Area Theorem (see for example [13]).

Now, we only sketch the main steps, used to obtain the SIT equation: the starting point is the Maxwell-Bloch system. Then, we assume the near-resonant condition $|\omega-\omega_0|\ll\omega_0$ where we remind that ω_0 is the central transition frequency and hence, the polarization is inhomogeneously distributed. It allows to assume that the overall polarization is weak compared to the intensity of the electric field. By doing the Slowly Varying Envelope Approximation (SVEA) and the multi-scale expansion, we obtain the MB equation in the SVEA approximation for the retarded time $\xi=t-z/v_g$ and space variable $z,\ v_g$ is the pulse velocity:

$$\left[\frac{\partial}{\partial z} + \left(\frac{1}{c} - \frac{1}{v_g}\right)\frac{\partial}{\partial \xi} - i\mu\right]A = kB \tag{6.24}$$

$$\partial_{\xi}B = \frac{AN}{2} \tag{6.25}$$

$$\partial \xi N = -\left(B^*A + BA^*\right),\tag{6.26}$$

where we call A the (slowly-varying) electric field, B is the atomic polarization and N is the population invertion, μ is the detuning from resonant frequency ω_0 , $k = (4\pi\omega_0 N d^2)/c\hbar$, d is the dipole moment, and c the vacuum light velocity.

This system admits a localized solution when the SIT-pulse area satisfies the "existence curve":

$$\frac{A_{pulse}}{2\pi} = \frac{\Omega_R \tau_p}{2},\tag{6.27}$$

where A_{pulse} is the pulse area and τ_p is its duration. This relation means that a 2π pulse makes a complete two-level transition from the ground state to the excited one and back again to the ground state in one Rabi period $T_R = 2\pi/\Omega_R$, maintaining the shape of the excited pulse (the profile of the inversion population also remains constant). The envelope profile has a secant shape and depends on the four solitonic parameters, β (the amplitude), X (the pulse position), Ω (the detuning from the resonance frequency) and θ (the pulse phase),

$$A(z,t) = 2\beta \operatorname{sech} (\beta(\xi - X)) \exp(-i\Omega\xi + i\theta). \tag{6.28}$$

Ziolkowski and coworkers [2] investigated the MB system without invoking any approximations, the SIT soliton has been shown to propagate undistorted beyond the SVEA approximation. In the next chapter, we will do the same procedure by introducing also randomness and we will look at analytical perturbed soliton solutions (in the SVEA approximation) and at numerical ab-initio solutions, describing the general behavior of localized wave-forms in disordered resonant media.

References

- 1. Shen YR (1976) Rev Mod Phys 48:1
- 2. Ziolkowski RW, Arnold JM, Gogny DM (1995) Phys Rev A 52:3082
- 3. Slavcheva G, Arnold JM, Wallace I, Ziolkowski RW (2002) Phys Rev A 66:063418
- 4. Slavcheva G, Arnold J, Ziolkowski R (2004) IEEE J Sel Top Quantum Electron 10:1052
- 5. Dodd R (1982) Solitons and nonlinear wave equations. Academic, London
- 6. McCall SL, Hahn EL (1969) Phys Rev 183:457
- 7. McCall SL, Hahn EL (1967) Phys Rev Lett 18:908
- 8. Mantsyzov B, Mel'nikov I, Aitchison J (2004) IEEE J Sel Top Quantum Electron 10:893
- 9. Mel'nikov I, Aitchison J (2005) Appl Phys Lett, vol 87
- 10. Rosanov NN, Kozlov VV, Wabnitz S (2010) Phys Rev A 81:043815
- 11. Lamb GL (1971) Rev Mod Phys 43:99
- 12. Maimistov AI, Basharov AM, Elyutin SO, Sklyarov YM (1990) Phys Rep 191:1
- 13. Allen L, Eberly L (1975) Optical resonance and two-level atoms. Wiley, New York

Chapter 7

Disordered Maxwell-Bloch Equations

As done in the section concerning non resonant nonlinearities, we introduce spatial disorder to investigate the fascinating regime of interaction between light and matter when the two competing light localizing mechanisms (nonlinearity and disorder) are effective on the same spatial scale [1–3]. The nonlinearity allows the propagation of a localized wave-form (the SIT soliton) while the disorder can induce the spatial confinement of the wave in characteristic narrow regions of the sample (the Anderson localization phenomenon). The outgoing response of the electromagnetic field has an intriguing feature: the interaction of a SIT soliton with Anderson localizations provides a valuable route for a two-level laser-like action.

7.1 Introduction

In a two-level laser medium at thermal equilibrium, the distribution of the ratio of atoms in each state is given by the Boltzmann distribution:

$$N_2/N_1 = \exp\frac{-(E_2 - E_1)}{k_B T},\tag{7.1}$$

where N_1 and N_2 are the number of atoms respectively in the lower state with energy E_1 and in the excited state with energy E_2 , T measures the thermodynamic temperature and k_B is the Boltzmann constant. Since $(E_2 - E_1)/k_BT$ is always positive, it follows that a population inversion in which N_2 is larger than N_1 at the thermal equilibrium is not achievable, specially in optical-frequency regime. Working with standard lasers, in which the output signal is time-indipendent, prevents the possibility to produce a two-level population inversion $N_1 > N_2$ and obtain an amplifier. At the best, by assuming to use a sufficiently strong pumping wave, the population in the excited level becomes equal to that one of the ground state $(N_1 = N_2)$, resulting in two-level saturation, when the medium will be transparent. This implies that for activating a two-level laser emission, there is the need to work in a transient (out-of-equilibrium) regime in which (7.1) is not longer valid. In fact,

if a very strong electromagnetic field is applied, it is expected that specific dynamics of the interaction between the pump wave and active media might induce some metastable phenomenon of population inversion, being on timescales faster than the molecular relaxation ones [4–6]. It would be interesting and very useful for laser physics to create an amplifier directly working between just two-levels to reduce all the energy losses related to the usage of additional non-radiative decay levels, otherwise needed to activate the desired population inversion. If it was possible to transfer in the system a stable population inversion profile, as an ideal two-level amplifier, and localize it in some resonant cavity, we would have a real two-level laser. But this idea cannot work in linear steady-state regime in which, as we have seen, the only manner to achieve a population inversion is by exploiting the fast non-radiative decays and using more than two-levels.

To do this, it is necessary to invoke some non-linear out-of-equilibrium phenomenon in the field of coherent resonant interaction processes of matter and pulsed radiation: the SIT soliton can travel undisturbed in strongly absorbing media and can be employed for such a purpose; the SIT represents a traveling population inversion.

To find a way to localize a SIT pulse in the active system in order to create a resonant cavity, which confines the soliton and generates laser-like action is the goal of this chapter. The easiest way to localize the light is by using a photonic crystal. Thanks to the specific properties of this structure, the electromagnetic propagation is already blocked along fixed directions and the amount of disorder necessary to create some localized states is limited [7, 8], especially in one-dimension. We consider a one dimensional structure with disordered spatial regions formed by resonant cavities that generate overlapping localized modes, the Anderson localizations, resonant with the input soliton. A system like this is also called a "stochastic resonator", [9, 10] and its mechanism is underlying the behavior of random lasers [11–17].

We have considered a one-dimensional photonic crystal with a band gap in a fixed range, determined by the specific structure of the alternating refractive indexes. Then, a SIT soliton at frequency within the photonic band gap is generated and is reflected by the ordered medium. By adding disorder, localized modes near the band edges of the spectrum are created with tails inside the forbidden gap [18]. The SIT pulse will becomes resonant with some Anderson localizations in the gap [8, 19] and a slowing-down of the light is numerically observed and analytically confirmed for certain characteristics both of the structure that of the pulse. By adding disorder and increasing the scattering strength, it is possible to observe by the simulations reported below that the soliton is first slowed and finally trapped in a specific spatial region of the medium in which the coupling with the spatially localized states is largely enhanced [20]. Once the soliton is localized in the cavity, laser emission directly by the two-levels atoms is achieved.

In this chapter, we employ analytical and numerical approaches, the first making use of a perturbative analysis of the SIT equations, the second with the support of massively parallel numerical calculations of the full MB equations. The starting point of both ways is the use of the Maxwell-Bloch system that describes, as seen in the previous chapter, the interaction processes between the electromagnetic field (Maxwell's equations) and the two-levels medium, whose polarization is modeled

7.1 Introduction 63

by the Bloch's system. First, a random perturbation is added and the role of the disorder in the soliton propagation is theoretically analyzed in the perturbative limit. In later section, we numerically examine both the perturbative and the non-perturbative regimes by using a parallel Finite Difference Time Domain (FDTD) code [21] and we look at the radiation-matter dynamics in several scenarios.

7.2 Soliton Perturbation Theory in Resonant Media

We first address the role of a random perturbation [22, 23] on a two-level 2π pulse by the reduced Maxwell-Bloch (MB) equations.

The MB equations with retarded time $\xi = t - z/v_g$ and space z (v_g is the velocity of the SIT pulse) read as

$$\left[\frac{\partial}{\partial z} + \left(\frac{1}{c} - \frac{1}{v_g}\right)\frac{\partial}{\partial \xi} - i\mu\right]A = kB + S_1 \tag{7.2}$$

$$\partial_{\xi}B = \frac{AN}{2} + S_2 \tag{7.3}$$

$$\partial_{\xi} N = -(B^*A + BA^*) + S_3,$$
 (7.4)

being: A the (slowly-varying) electric field, B the atomic polarization and N the population invertion, $S_{1,2,3}$ the perturbations, μ the detuning from resonant frequency ω_0 , $k=(4\pi\omega_0Nd^2)/c\hbar$, d is the dipole moment, and c the vacuum light velocity. Let $\vec{A}=\vec{A}_s+\vec{A}_1$ with \vec{A}_1 a perturbation and $\vec{A}_s=(A_s,B_s,N_s)$ the soliton:

$$A_{s} = u\mathcal{E} = \frac{2\beta\mathcal{E}}{\cosh(w)}$$

$$B_{s} = p\mathcal{E} = \frac{\beta^{2}}{\beta^{2} + \Omega^{2}} \left[\tanh(w) - \frac{i\Omega}{\beta} \right] \frac{\mathcal{E}}{\cosh(w)}$$

$$N_{s} = n = -1 + \frac{2\beta^{2}}{\beta^{2} + \Omega^{2}} \frac{1}{\cosh^{2}(w)}$$
(7.5)

where $w = \beta (\xi - X)$ and $\mathcal{E} = \exp\{-i\Omega(\xi - X) + i\theta\}$, $\mu \equiv \Omega k/(\beta^2 + \Omega^2)$. β , X, Ω , θ are the amplitude, position, detuning, and the phase of the soliton, being $1/v_g = 1/c + k/(2\beta^2 + 2\Omega^2)$. The linearized system is

$$\left(\partial_z \vec{A}_1\right) \times \mathcal{I}_1 = \mathcal{L}_1(\vec{A}_1) + \vec{S}_p, \tag{7.6}$$

where $\mathcal{I}_1 = \operatorname{diag}(1, 0, 0), \ \vec{S}_p$ is the perturbation and

$$\mathcal{L}_{1}\left(\vec{A}_{1}\right) = \begin{pmatrix} i\mu A_{1} - \left(\frac{1}{c} - \frac{1}{v_{g}}\right) \partial_{\xi} A_{1} + kB_{1} \\ -\partial_{\xi} B_{1} + \frac{1}{2} \left(A_{1} N_{s} + A_{s} N_{1}\right) \\ \partial_{\xi} N_{1} + 2\Re(B_{s}^{*} A_{1} + B_{1}^{*} A_{s}) \end{pmatrix}. \tag{7.7}$$

Taking the SIT pulse resonant with the medium ($\Omega = \mu = 0$), we derive equations for its parameters by first introducing the auxiliary functions [22] $\vec{f}_X = \partial_X \vec{A}_s$, $\vec{f}_\theta = \partial_\theta \vec{A}_s$, $\vec{f}_\beta = \partial_\beta \vec{A}_s$ and $\vec{f}_\Omega = \partial_\Omega \vec{A}_s$, and letting

$$\vec{A}_1 = \vec{f}_X \delta X + \vec{f}_\beta \delta \beta + \vec{f}_\theta \delta \theta + \vec{f}_\Omega \delta \Omega + \vec{a}_R, \tag{7.8}$$

where $\delta X(z)$, $\delta \theta(z)$, $\delta \beta(z)$ and $\delta \Omega(z)$ are the time-dependent perturbations to soliton parameters and \vec{a}_R is the radiation term $(\vec{a}_R = 0 \text{ hereafter, as it rapidly spreads and is absorbed. We let <math>\vec{S}_p = ([V_B(z)p + iV_A(z)u]\mathcal{E}, 0, 0)$, such that $\langle V_{A,B}(z)V_{A,B}(z')\rangle = \langle V_{A,B}^2\rangle\delta(z-z')$, where $V_{A,B}$ are the electric field and polarization perturbation. Letting the adjoint functions [22] $\vec{f}_\theta = i\vec{f}_\beta$, $\vec{f}_\beta = -i\vec{f}_\theta$, $\vec{f}_\Omega = -i\vec{f}_X$, $\vec{f}_X = i\vec{f}_{\Omega_X}$, such that $(\vec{f}_a, \vec{f}_b) = \mathcal{N}_a\delta_{a,b}$, with a and b two parameters in $(X, \Omega, \theta, \text{ or } \beta)$; we have $\mathcal{N}_\theta = \mathcal{N}_\beta = -1/(3\beta^2)$ and $\mathcal{N}_X = \mathcal{N}_\Omega = -2\pi\beta - 1/(3\beta)$. Projecting over \vec{f}_k we get

$$\delta \dot{X} = -k/\beta^3 \delta \beta + V_B(z)/2\beta^2, \quad \delta \dot{\theta} = -k/\beta^2 \delta \Omega + V_A(z) \tag{7.9}$$

and $\delta \dot{\beta} = \delta \dot{\Omega} = 0$, which gives

$$\langle \delta X(z)^2 \rangle = \frac{\langle V_B^2 \rangle z}{4\beta^4}.$$
 (7.10)

Equation (7.10) describes the random fluctuations of SIT solitons in the limit of small uncorrelated disorder, and states that they grow linearly with the propagation distance, and decay when increasing of the soliton power: as the velocity of the soliton is reduced, its random walking becomes more pronounced. This result describes an index perturbation with weak index-contrast, as shown below in Figs. 7.2a, 7.3a, b and c for ϵ_{r1} and ϵ_{r2} , in the comparison with FDTD simulations. Specifically, Eq. (7.10) predicts that slower SIT solitons are those mostly affected by disorder, and hence they are expected to interact more effectively with Anderson states also in the high index contrast regime. As we numerically show in the following (Figs. 7.2b, 7.3c for ϵ_{r3} , 7.4 and 7.5), as the strength of disorder increases (when the theoretical analysis reported above is not expected to the valid), this leads to localization and laser-like action.

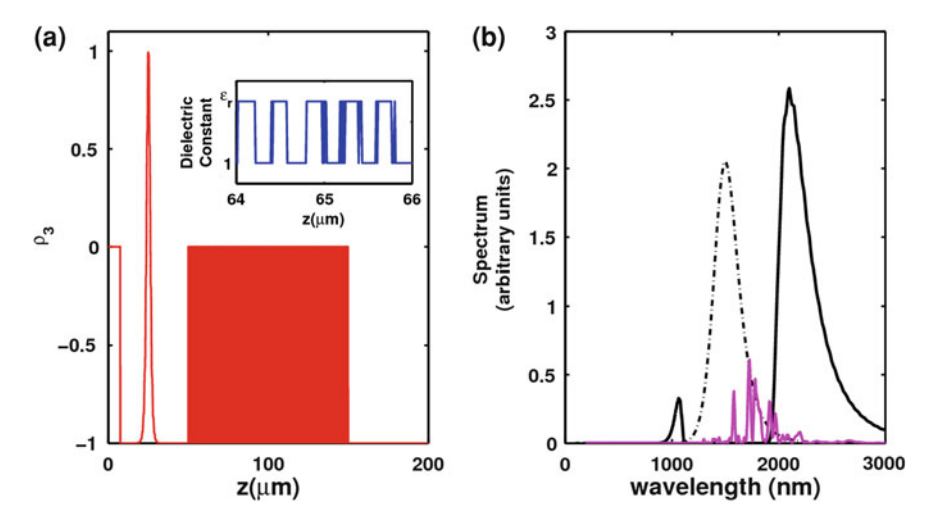


Fig. 7.1 a The simulation region is 200 μ m long, the homogeneous two-level medium extends from 7.5 to 50 μ m. The disordered two-level medium ($\epsilon_r=1$) extends from 50 to 150 μ m; the initial population is equal to $\rho_{30}=-1$ and randomly alternated by a dielectric non-resonant medium with a different refractive index ($\rho_{30}=0$, $\epsilon_r=11$), as shown in the inset. A snapshot of the SIT pulse is shown before impinging on the structure; **b** SIT pulse spectrum for $\tau=100$ fs (*dashed line*); spectrum of a transmitted short pulse *without* the resonant medium showing the photonic-band gap (*continuous line*, $\gamma=0$); transmitted spectrum *in absence* of resonant medium with $\gamma=0.5$ showing the disorder induced resonances in the forbidden band

7.3 Anderson Localization in Resonant Media

Following Ref. [21], we numerically solve the one-dimensional full MB equations by a parallel FDTD algorithm and study the evolution of the SIT pulse in a non-linear disordered SIT medium; we denote as ρ_3 the population inversion of the FDTD equations (corresponding to N in Eq. (7.3) when adopting the rotating wave approximation) and E is the real-valued electric field, whose slowly-varying complex envelope is A in (7.2). Note that we use a different notation for the field here because the FDTD equations are more general that the reduced MB Eqs. (7.2, 7.3) [21].

As sketched in Fig. 7.1, the SIT pulse propagates into the grid from the left boundary (z=0), from vacuum ($z<7.5\,\mu\mathrm{m}$) to a homogeneous SIT medium (atom density $N_{atoms}=10^{24}~\mathrm{m}^{-3}$); its carrier frequency is resonant with the medium $\omega_0=2\pi f_0$, with $f_0=2\times10^{14}~\mathrm{s}^{-1}$, and the pulse duration τ is chosen to satisfy the 2π area theorem. The relaxation time of the density matrix equations are $T_1=T_2=1.0\times10^{-10}~\mathrm{s}~(T_{1,2}\gg\tau)$. The initial population inversion in the SIT medium is $\rho_{30}=-1$, while in the dielectric layers $\rho_{30}=0$ and the two-level atoms are not present. We neglect absorption in the dielectric layers because much smaller than in the resonant two-level system. The input pulse, with peak $E_0=(2\hbar/d)\beta$, enters the two-level medium, initially set in the ground state $\rho_{30}=-1$, and generates the SIT soliton, which, after propagating in the homogeneous resonant region, interacts

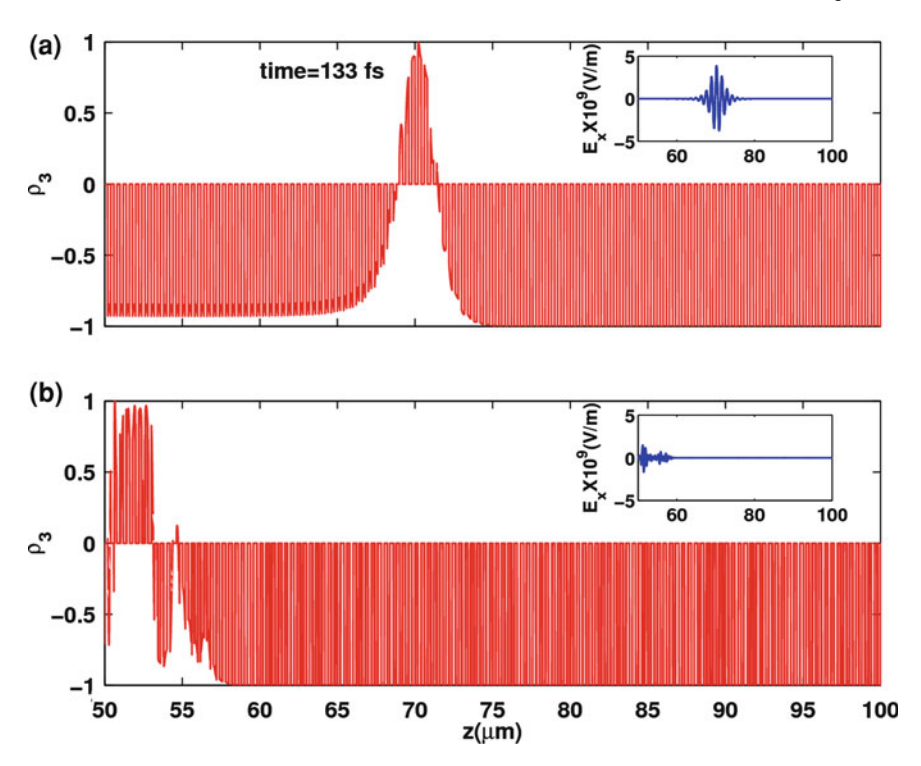


Fig. 7.2 SIT population inversion ρ_3 in a the low-index case ($\epsilon_r=1.5,\ \gamma=0$, analogous results for $\gamma>0$) and in b the high index case ($\epsilon_r=11,\ \gamma=1$), where surface Anderson states are excited. The insets show the corresponding E profiles. ρ_3 appears periodically modulated as $\rho_3=0$ in the dielectric layers with $\epsilon_r>1$

with the random structure as shown in Fig. 7.1. The total length of the structure is 200 μ m, the random active medium extends from 50 to 150 μ m, where we add a fixed degree of disorder by inserting slices of a non absorbing medium with relative permittivity ϵ_r . The disordered structure is created by introducing random layers in the homogeneous two level medium. The degree of disorder is quantified by a parameter γ : the relative permittivity distribution has a square-wave profile from 1 to ϵ_r (inset in Fig. 7.1a) given by the sign of the function $\sin(2\pi z/d + 2\pi\gamma\zeta)$, with ζ a uniform deviate in [0, 1] extracted in each point of the grid. If $\gamma = 0$ an ordered periodical structure is attained: the dielectric layers are equidistant, with constant width 200 nm and period 400 nm (d = 400 nm) and displays a band-gap centered at ω_0 overlapped with the spectrum of the SIT soliton (see Fig. 7.1b).

For $\gamma=0$, increasing ϵ_r creates a one dimensional band-gap structure; for $\gamma>0$, increasing ϵ_r enforces the effect of disorder, and as shown in Fig. 7.2b in the absence of the two-level system; the localized states first appears in proximity of the band-edge of the ordered structure. We use this approach to selectivity create a distribution of Anderson states with a spectrum superimposed to that of the input SIT pulse. In the

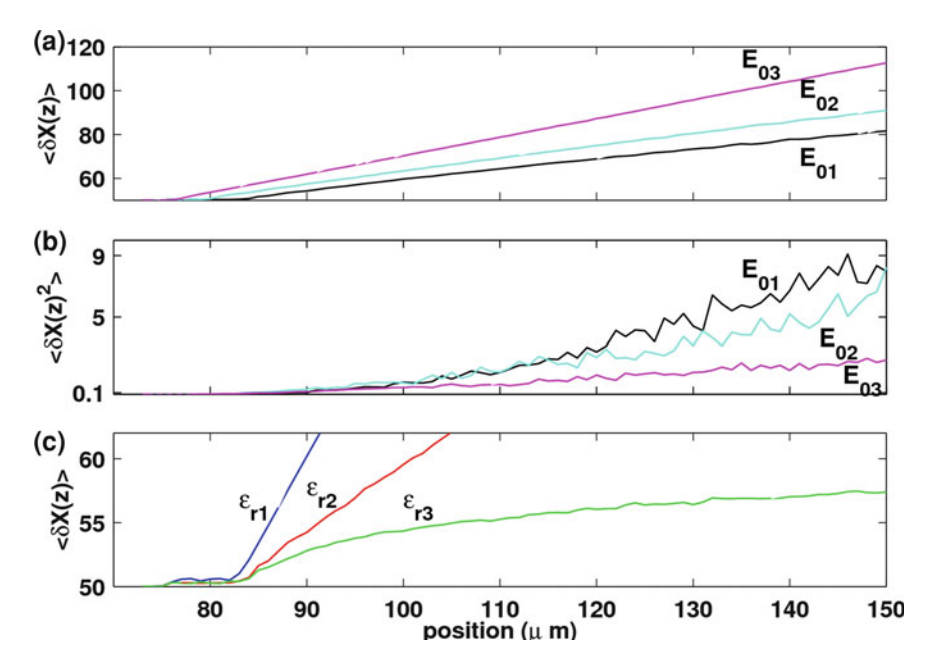


Fig. 7.3 a SIT pulse trajectories calculated for $\gamma=0.1$, $\epsilon_r=6$, for three different initial pulse amplitudes $E_{01}=4.2186\times 10^9\,\mathrm{V/m}$, $E_{02}=4E_{01}$, $E_{03}=8E_{01}$; **b** corresponding standard deviations; **c** SIT pulse trajectories for three relative permittivities $\epsilon_{r1}=2.5$, $\epsilon_{r2}=6$, $\epsilon_{r3}=11$ when $E_0=E_{01}$. Note that the curves for $\epsilon_{r1,2}$ are cut (they proceed as *straight lines*) for comparison with the case ϵ_{r3} . The results are averaged over 100 realizations of the disorder

following, the described disordered structure is embedded in a two-level system and SIT solitons are launched in the homogeneous region ($z < 50 \,\mu\text{m}$) and then interact with the random system ($z > 50 \,\mu\text{m}$). Non-solitonic pulses are rapidly absorbed and do not propagate.

Figure 7.2 shows a temporal snapshot of the population inversion distribution in low index ($\epsilon_r = 1.5$, $\gamma = 0$) ordered case and in the high index disordered case ($\epsilon_r = 11$, $\gamma = 1$): in the former case, the wave propagates with limited distortion and the inversion population is transported through the medium, in agreement with what expected by the perturbation theory reported above (analogous results for low index-contrast $\epsilon_r \cong 1$ are obtained for $\gamma > 0$, see Fig. 7.3b, c); in the latter case, the spatial distribution of the inversion population localizes in proximity of the input face of the sample. This shows that surface Anderson states are involved in the process [20]; as we will report in future work multiple SIT pulses can be employed to enlarge the trapped inversion region.

Panels a, b in Fig. 7.3 show the trajectories and the corresponding standard deviation of the SIT pulse, calculated for different input peak values and for a fixed strength of disorder. In the low index contrast disordered case, following the previous theoretical analysis [see Eq. (7.10)], as the initial peak value increases, the soliton

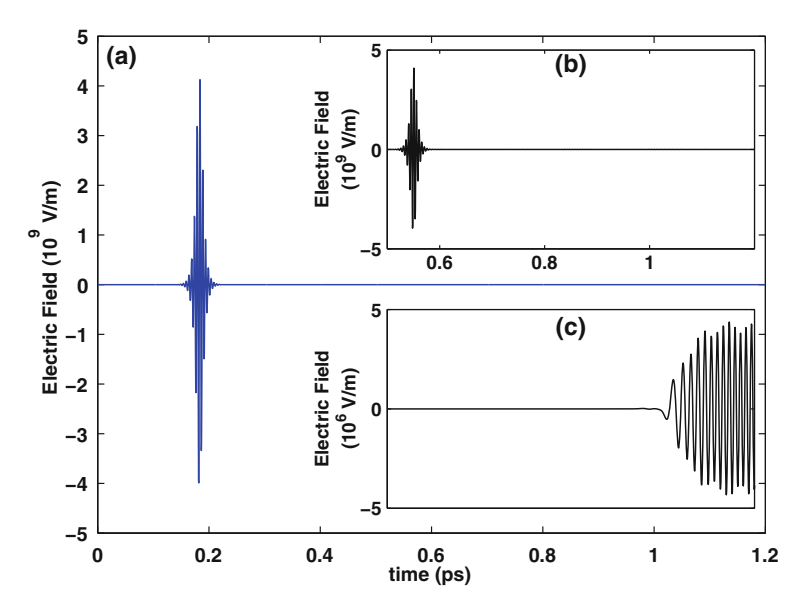


Fig. 7.4 a Temporal profile of the input SIT-pulse with $\tau = 100 \ fs$ and $E_0 = 4.2186 \times 10^9 \ V/m$; b transmitted pulse without disordered structure; c emitted signal for an highly scattering medium ($\epsilon_r = 11, \ \gamma = 1$) The horizontal scale in panels b, c is overlapped with panel a

propagates faster in the structure, and the slope in Fig. 7.3a increases and the corresponding fluctuations are reduced (Fig. 7.3b). Conversely, slow solitons perform a more pronounced random walk in the disordered structure. As the index contrast is increased (beyond the regime of validity of the perturbational approach reported above), this allows a localization processes as shown for ϵ_{r3} in Fig. 7.3c displaying soliton trajectories for different strengths of the disorder (fixed γ and increasing ϵ_r). In the cases ϵ_{r1} and ϵ_{r2} the trajectories proceeds as straight lines, denoting a propagating pulse, conversely for ϵ_{r3} the trajectory bends and the soliton slows down and is trapped. In the other words, in the low-index contrast case, the soliton displays a weakly perturbed motion; as the strength of disorder increases (when increasing ϵ_r with fixed γ), its trajectory becomes more fluctuating, until the wave gets localized; correspondingly the system starts emitting laser-like radiation, as a population inversion region is formed in correspondence of an optical cavity.

Figure 7.4 shows the output of the device for low and high index contrast for a fixed γ . For a small ϵ_r the input SIT pulse in 4a is transmitted as shown in 4b, where the pulse exits at about 0.5 ps. On the contrary, for high ϵ_r , the pulse is trapped in the structure and, after a transient, the output (in Fig. 7.4c) corresponds to a laser-like emission from the two-level system. Note the difference in the vertical scale: for Fig. 7.4b all the energy is transmitted, while for Fig. 7.4c, it is partially reflected (see also Fig. 7.5) and partially trapped in the light-emitting localized states.

In Fig. 7.5a, we show the reflected temporal signal, comprising of the portion of the SIT pulse, which is not trapped in the disordered structure and is reflected (large

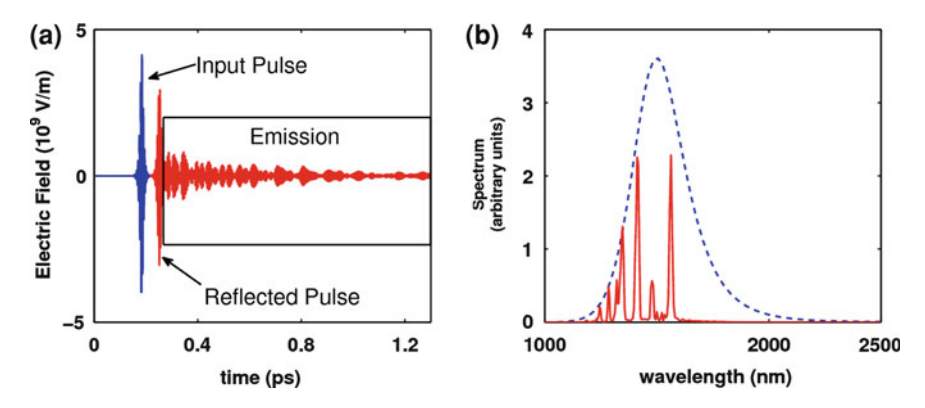


Fig. 7.5 a Temporal profiles of the reflected electric field in the highly scattering case in Fig. 7.4c, including the input pulse, its reflected fraction, and the subsequent two-level laser emission; **b** corresponding spectrum (*continuous line*) compared with the input SIT pulse (*dashed line*)

peak around 0.3 ps), and the subsequent emission from the population inversion trapped in the disorder medium; its spectrum in 5b displays characteristic peaks signaling the excited Anderson localizations with frequencies in the forbidden gap. The energy trapped in the localized modes decay with their characteristic lifetimes (of the order of 0.5 ps).

In this chapter, we have generalized the results of the previous non-resonant section to a resonant disordered system. We investigated the interaction of a SIT soliton (nonlinear localized wave-form) with Anderson localizations (light localization due to disorder) through theory and parallel Maxwell-Bloch simulations. We have shown that an increasing scattering strength of disorder progressively slows down the soliton, up to blocking the pulse in the random system. This process is accompanied by the excitation of modes in a disordered cavity in the presence of population inversion. This results into a two-level laser-like action. The interplay between various forms of light localizations, namely solitons and Anderson states, can hence lead to novel processes of light-matter interactions in complex systems.

References

- 1. Schwartz T, Bartal G, Fishman S, Segev M (2007) Nature 446:52
- Shadrivov IV, Bliokh KY, Bliokh YP, Freilikher V, Kivshar YS (2010) Phys Rev Lett 104:123902
- 3. Conti C, D'Asaro E, Stivala S, Busacca A, Assanto G (2010) Opt Lett 35:3760
- 4. Svelto O (1982) Principles of lasers. Plenum Press, New York
- 5. Allen L, Eberly L (1975) Optical resonance and two-level atoms. Wiley, New York
- 6. Einstein A (1917) Physikalische Zeitschrift 18:121
- 7. López C (2008) Nat Phys 4:755
- 8. Conti C, Fratalocchi A (2008) Nat. Physics 4:794

- 9. Ambartsumyan R, Basov N, Kryukov P, Lethokov S (1996) IEEE J Quantum Electron 2:442
- 10. Lethokov VS (1968) Sov Phys JETP 26:835
- 11. Leuzzi L, Conti C, Folli V, Angelani L, Ruocco G (2009) Phys Rev Lett 102:083901
- 12. Conti C, Leonetti M, Fratalocchi A, Angelani L, Ruocco G (2008) Phys Rev Lett 101:143901
- 13. Cao H, Jiang X, Ling Y, Xu JX, Soukoulis CM (2003) Phys Rev 67:161101R
- 14. Wiersma DS (2008) Nat Phys 4:359
- 15. El-Dardiry RGS, Mosk AP, Muskens OL, Lagendijk A (2010) Phys Rev A 81:043830
- 16. Andreasen J et al (2010) ArXiv e-prints 1001.4671
- 17. Bamba M, Pigeon S, Ciuti C (2010) Phys Rev Lett 104:213604
- 18. John S (1984) Phys Rev Lett 53:2169
- 19. John S (1987) Phys Rev Lett 58:2486
- 20. Szameit A et al (2010) Opt Lett 35:1172
- 21. Ziolkowski RW, Arnold JM, Gogny DM (1995) Phys Rev A 52:3082
- 22. Folli V, Conti C (2010) Phys Rev Lett 104:193901
- 23. Kozlov VV, Matsko AB (2000) J Opt Soc Am B 6:1031

Chapter 8 Glassy Behavior of Laser

The thesis so far has treated the relative feedback between nonlinearity and disorder in the radiation-matter interaction processes by using a perturbative approach for what concerns the theoretical analysis. Furthermore, we dealt with a limited number of localizations. In the Chap. 7, for example, we studied the interaction of a single localized wave-form (just one soliton) with the surface Anderson localizations. We have treated both nonlinearity that disorder as a perturbation. One can argue if is it possible to study the emerging phenomena by treating nonlinearity and disorder on the same level. What happens if we simultaneously consider the light-matter interaction when a large number of localizations are taken into account? Is it possible to employ some method dealing with physical systems with multiple bodies? In order to apply the mean-field theories for many bodies systems, we treat with a standard Random Laser (RL). Later we discuss with details the physical features of this kind of laser, for now it is enough to know that a RL is an optical device sustaining laser action in a disordered medium. This system presents a large number of electromagnetic modes with overlapping resonances. So the RL displays all the features we are looking for: many disorderly distributed states interacting in a nonlinear manner. We are dealing with a complex system and we need an analytical framework able to treat the multi bodies problem. Through some approximations, it is possible to express the interacting light in the disordered resonant system via very general equations, relating to a mean-field spin-glass model [1]. The Spin-Glass theory is an approach to obtain the dynamical and thermodynamical behaviors of a complex system. We solve our model with the replica method, a subtle trick for which the physical system is replicated n-times in order to calculate the partition function and all the physical observables. By operating on the degree of disorder and nonlinearity (through the energy furnished to the system), we are able to obtain the phase-diagram of the RL,

describing the very interesting complex landscape of behavior of the nonlinear waves in random systems.

8.1 Introduction

The number of different disciplines converging in the field of disordered lasers is impressive; random lasers embrace photonics [2], wave-transport and localization [3–6], spin-glass theory [7], random-matrices [8], soft- and bio-matter [9–11], nonlinear and quantum physics [12–18]. Notwithstanding the several theoretical and experimental investigations [19, 2], many are the open issues and the development of the field cannot be compared with that of standard lasers (SL), even if the first theoretical prediction of RL [20] is dated not very far from the first theoretical work on SL [21]. In this respect, a comprehensive theory of stimulated emission able to range from ordered to disordered lasers will be certainly an important step. This theory should be able to parametrize the strength of disorder and should predict specific regimes attainable in SL and RL. The literature dealing with the two kinds of lasers is still largely disjoint. Furthermore, nano-structured lasers unavoidably display some degree of disorder due to fabrication tolerances; hence, understanding the effect of randomness in the light emission has important practical relevance. The main question addressed in this chapter is: consider a SL operating in mode-locking (ML) and progressively increase the amount of structural disorder, at which value should one expect that the mode-locking is frustrated? Which kind of states are expected? Through the spin-glass theory [1], we derive a phase-diagram unveiling the interplay between randomness and nonlinearity and identify different phases characterized by not-vanishing *complexity*, which measures the number of energetically equivalent ML states. Previous theoretical work has dealt with the two regimes: the ordered case where the ML is demonstrated to be given by a ferromagnetic-like transition [22–24] and the completely disordered limit [7]. The former case being relevant to fiber or dye/solid-state standard passive ML [25]; the latter being more oriented on stimulated emission in the presence of multiple scattering [19, 26]. Our analysis unifies the scenario and is based on the following steps: (1) perform a statistical average of the disordered free-energy of the system; (2) identify the order parameters; (3) evaluate the free-energy; (4) build the phase-diagram; (5) compute the complexity.

Our main finding in this chapter can be summarized as follows: the self-starting ML process maintains its standard "ferromagnetic" character (i.e. an abrupt transition from a continuous wave operation to a pulsed regime) as far as the structural fluctuations are sensitively smaller than the average value of the mode coupling coefficients. Conversely, for large disorder the transition acquires a glassy character and the complexity is not vanishing; this implies that there exists a large number of ML states distributed in a given free energy interval and large fluctuations from pulse to pulse are expected. Also an intermediate regime occurs: a *random ferromagnet*, i.e. ferromagnetic behavior with a non-zero complexity.

8.2 The Model 73

8.2 The Model

We start from the Hamiltonian for the coupled mode equations in standard lasers [27],

$$\mathcal{H} = \sum_{m} \gamma_{m} a_{m} a_{m}^{*} + \sum_{s-p+q-r=0} \gamma_{spqr} a_{s} a_{p}^{*} a_{l} a_{m}^{*}, \tag{8.1}$$

for the amplitudes a_m for the cavity modes. In absence of disorder $\gamma_{spqr} = \gamma$, that is the difference between the saturable absorption and the gain constants. For self-starting passive ML $\gamma < 0$. Without loss of generality, we assume that the spatial distribution of the gain medium is randomized. Correspondingly γ_{spqr} is taken as a random variable with mean γ and variance measuring the strength of disorder. The linear term in Eq. (8.1) is diagonal because of the mode-orthogonality (not valid for open systems). Letting $a_m = A_m \exp(i\phi_m)$, and taking the mode-amplitude A_m as quenched, under general hypotheses [27, 28] and a straightforward rescaling, the mode-phase dynamics of a RL can be cast into a dynamical problem with a random Hamiltonian

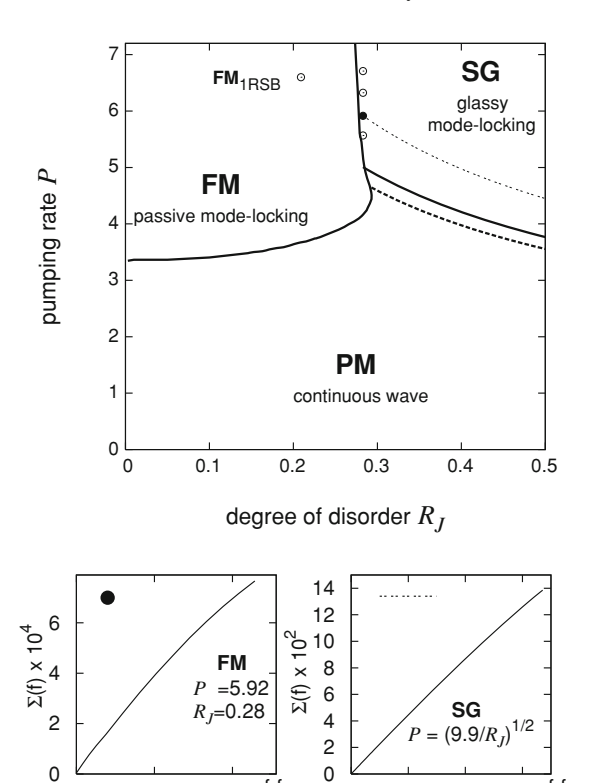
$$\mathcal{H}_{J}[\phi] = -\sum_{\substack{i_{1} \prec i_{2}, j_{1} \prec j_{2} \\ i_{1} \prec i_{1}}}^{N} J_{ij} \cos(\phi_{i_{1}} + \phi_{i_{2}} - \phi_{j_{1}} - \phi_{j_{2}})$$
(8.2)

where N is the number of electromagnetic modes, ϕ_i are their phases, $\mathbf{i} = (i_1, i_2)$ and the quenched couplings have a Gaussian distribution with $\overline{J_{ij}} = J_0/N^3$ and $\overline{(J_{ij} - \overline{J_{ij}})^2} = \sigma_J^2/N^3$. The overbar denotes the average over the disorder, which is quantified by the ratio $R_J \equiv \sigma_J/J_0$. The limit $R_J \to 0$ ($R_J \to \infty$) corresponds to the ordered (disordered) case. The normalized pumping threshold for ML is $\mathcal{P} = \sqrt{\beta J_0} = \sqrt{\bar{\beta}/R_J}$, where $\bar{\beta} = \beta \sigma_J$ and β is the inverse temperature [28]. In our units, when $R_J \to 0$, $\mathcal{P} = \mathcal{P}_{ord} \cong 3.339$ (see Fig. 8.1), in agreement with the ordered case [7]¹; as detailed below, the deviation from this value quantifies an increase of the standard ML threshold \mathcal{P}_{ord} due to disorder. The specific value for \mathcal{P}_{ord} will depend on the class of lasers under consideration (e.g. a fiber loop laser or a random laser with paint pigments), but the trend of the passive ML threshold with the strength of disorder R_J in Fig. 8.1 (FM/PM transition line, see below) has a universal character. \mathcal{P} contains J_0 : for a fixed disorder the threshold will depend on the nonlinear mode-coupling.

A factor of 8 has to be considered because of the over-counting of terms in Ref. [7].

0.02 0.04

Fig. 8.1 Phase diagram in the plane (R_I, \mathcal{P}) . Three phases are found: PM (low \mathcal{P}). FM (high \mathcal{P} /weak disorder) and SG (high P/strong disorder). The full lines are thermodynamic transitions, the dashed line represents the dynamic PM/SG transition. The transition line to the FM phase (both from PM and from SG) are obtained using the RS approximation. The circles are exact 1 RSB FM solutions. In the insets complexity vs. free energy curves are plotted in the SG phase (right inset, at $\bar{\beta} = 9.9$; in the main plot: $\mathcal{P} = \sqrt{9.9/R_J}$, tiny-dashed line) and in the FM phase next to the SG/FM transition (left inset, at $R_J = 0.28, \ \mathcal{P} = 5.92; full$ circle in the main plot). The latter is two order of magnitude smaller



8.3 Averaged Free Energy

The average free energy is calculated with the replica trick [1]. By considering n copies of the system, Eq. (8.2), the free energy averaged over the disorder can be computed as

0.0005

0

$$\beta \Phi = -\frac{1}{N} \overline{\log Z_J} = -\frac{1}{N} \lim_{n \to 0} \frac{\overline{Z_J^n} - 1}{n}.$$
 (8.3)

0.001 $f-f_{eq}$

The thus *replicated* partition function, $\overline{Z_I^n}$, takes the form

$$\overline{Z_J^n} \propto \int \mathcal{D}\mathbf{X} \exp\left[-nNG(\mathbf{X})\right] \sim e^{-nNG(\mathbf{X}_{\mathrm{SP}})}$$
 (8.4)

where **X** denotes all the order parameters and the integral is evaluated by means of the saddle point approximation. Spin-glass systems described by more-than-two-body interactions, cf. Eq. (8.2), are known to have low temperature phases provided by a "one step" Replica Symmetry Breaking (1RSB) Ansatz [29, 30]. Under this Ansatz, taking the $n \to 0$ limit, $\beta \Phi$ reads

$$\beta \Phi = -\frac{\bar{\beta}R_{J}}{8} |\tilde{m}|^{4} - \frac{\bar{\beta}^{2}}{32} \left[1 - (1 - m) \left(|q_{1}|^{4} + |r_{1}|^{4} \right) - m \left(|q_{0}|^{4} + |r_{0}|^{4} \right) + |r_{d}|^{2} \right] - \Re \left[\frac{1 - m}{2} \left(\bar{\lambda}_{1} q_{1} + \bar{\mu}_{1} r_{1} \right) + \frac{m}{2} \left(\bar{\lambda}_{0} q_{0} + \bar{\mu}_{0} r_{0} \right) - \bar{\mu}_{d} r_{d} - \bar{\nu} \tilde{m} \right] + \frac{\lambda_{1}^{R}}{2} - \frac{1}{m} \int \mathcal{D}[\mathbf{0}] \log \int \mathcal{D}[\mathbf{1}] \left[\int_{0}^{2\pi} d\phi \exp \mathcal{L}(\phi; \mathbf{0}, \mathbf{1}) \right]^{m}$$
(8.5)

where $\mathbf{0} = \{x_0, \zeta_0^R, \zeta_0^I\}, \mathbf{1} = \{x_1, \zeta_1^R, \zeta_1^I\}, \mathcal{D}[\mathbf{a}]$ is the product of three Normal distributions and

$$\mathcal{L}(\phi; \mathbf{0}, \mathbf{1}) \equiv \Re \left\{ e^{i\phi} \left[\bar{\zeta}_1 \sqrt{\Delta \lambda^R - |\Delta \mu|} + \bar{\zeta}_0 \sqrt{\lambda_0^R - |\mu_0|} \right] + x_1 \sqrt{2\Delta \bar{\mu}} + x_0 \sqrt{2\bar{\mu}_0} + \bar{\nu} \right] + e^{2i\phi} \left(\bar{\mu}_d - \frac{\bar{\mu}_1}{2} \right) \right\}$$
(8.6)

with $\Delta\lambda = \lambda_1 - \lambda_0$, $\Delta\mu = \mu_1 - \mu_0$. We define the following averages over the action $e^{\mathcal{L}}$, cf. Eq. (8.6): $c_{\mathcal{L}} \equiv \langle \cos \phi \rangle_{\mathcal{L}}$, $s_{\mathcal{L}} \equiv \langle \sin \phi \rangle_{\mathcal{L}}$. The values of $\lambda_{0,1}, \mu_{0,1}, \mu_d$ and ν are

$$\lambda_{0,1} = \frac{\bar{\beta}^2}{4} (q_{0,1})^3; \quad \mu_{0,1} = \frac{\bar{\beta}^2}{4} |r_{0,1}|^2 r_{0,1}$$
 (8.7)

$$\mu_d = \frac{\bar{\beta}^2}{8} |r_d|^2 r_d; \qquad \nu = \frac{\bar{\beta} R_J}{2} |\tilde{m}|^2 \tilde{m}$$
 (8.8)

The remaining parameters are obtained by solving the self-consistency equations:

$$q_1 = \langle \langle c_{\mathcal{L}}^2 \rangle_m \rangle_{\mathbf{0}} + \langle \langle s_{\mathcal{L}}^2 \rangle_m \rangle_{\mathbf{0}}$$
(8.9)

$$q_0 = \langle \langle c_{\mathcal{L}} \rangle_m^2 \rangle_{\mathbf{0}} + \langle \langle s_{\mathcal{L}} \rangle_m^2 \rangle_{\mathbf{0}}$$
 (8.10)

$$r_1 = \langle \langle c_{\mathcal{L}}^2 \rangle_m \rangle_{\mathbf{0}} - \langle \langle s_{\mathcal{L}}^2 \rangle_m \rangle_{\mathbf{0}} + 2i \langle \langle c_{\mathcal{L}} s_{\mathcal{L}} \rangle_m \rangle_{\mathbf{0}}$$
(8.11)

$$r_0 = \langle \langle c_{\mathcal{L}} \rangle_m^2 \rangle_{\mathbf{0}} - \langle \langle s_{\mathcal{L}} \rangle_m^2 \rangle_{\mathbf{0}} + 2i \langle \langle c_{\mathcal{L}} \rangle_m \rangle_{\mathbf{0}} \langle \langle s_{\mathcal{L}} \rangle_m \rangle_{\mathbf{0}}$$
(8.12)

$$r_d = \langle \langle \langle e^{2i\mathbb{E}} \rangle_{\mathcal{L}} \rangle_m \rangle_{\mathbf{0}}; \quad \tilde{m} = \langle \langle \langle e^{i\mathbb{E}} \rangle_{\mathcal{L}} \rangle_m \rangle_{\mathbf{0}}$$
 (8.13)

where

$$\langle (\ldots) \rangle_m \equiv \frac{\int \mathcal{D}[\mathbf{1}](\ldots) \left[\int_0^{2\pi} d\phi e^{\mathcal{L}(\phi;\mathbf{0},\mathbf{1})} \right]^m}{\int \mathcal{D}[\mathbf{1}] \left[\int_0^{2\pi} d\phi e^{\mathcal{L}(\phi;\mathbf{0},\mathbf{1})} \right]^m}$$
(8.14)

$$\langle (\ldots) \rangle_{\mathbf{0}} \equiv \int \mathcal{D}[\mathbf{0}](\ldots)$$
 (8.15)

The overlap parameters $q_{0,1}$ are real-valued, whereas $r_{0,1}$, r_d and \tilde{m} are complex. "One step" parameters $X_{0,1}$ (X=q,r) enter with a probability distribution that can be parametrized by the *replica symmetry breaking parameter m*: $P(X) = m\delta(X-X_0) + (1-m)\delta(X-X_1)$.

8.4 Complexity

The resulting ten independent parameters that can be evaluated by solving Eqs. (8.9)–(8.13) must be combined with a further equation for the parameter m. This is linked to the expression for the *complexity* of the system, i.e. the average logarithm of the number of states of the system present at a given free energy level f. The complexity can be computed, e.g. as the Legendre transform of the replicated free energy, Eq. (8.5):

$$\Sigma = \min_{m} \left[-\beta m \Phi(m) + \beta m f \right] = \beta m^{2} \frac{\partial \Phi}{\partial m}$$

$$= \frac{3}{4} \beta^{2} m^{2} \left(|q_{1}|^{4} + |r_{1}|^{4} - |q_{0}|^{4} - |r_{0}|^{4} \right)$$

$$+ \int \mathcal{D}[\mathbf{0}] \log \int \mathcal{D}[\mathbf{1}] \left[\int_{0}^{2\pi} d\phi \exp \mathcal{L}(\phi; \mathbf{0}, \mathbf{1}) \right]^{m}$$

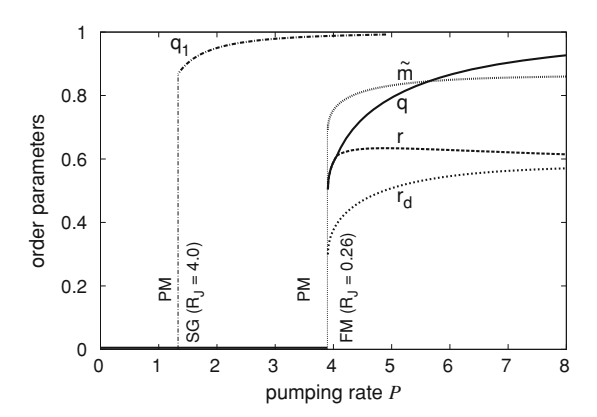
$$- m \int \mathcal{D}[\mathbf{0}] \langle \log \int_{0}^{2\pi} d\phi \exp \mathcal{L}(\phi; \mathbf{0}, \mathbf{1}) \rangle_{m}$$
(8.16)

where the single state free energy $f = \partial (m\Phi)/\partial m$ is conjugated to m. Since the above expression is proportional to $\partial \Phi/\partial m$, equating $\Sigma = 0$ provides the missing equation to determine the order parameters values.

8.5 The Phase Diagram

By varying the normalized pumping rate \mathcal{P} and the degree of disorder R_J , we find three different phases, as shown in Fig. 8.1. For low \mathcal{P} and R_J the only phase present is completely disordered: all order parameters are zero and we have a "paramagnet" (PM); the laser emission is expected to be given by a noisy continuous wave emission, and all the mode-phases are uncorrelated. The PM exists everywhere in the whole plane (R_J, \mathcal{P}) , becoming thermodynamically sub-dominant as \mathcal{P} and R_J increase. For large disorder, as \mathcal{P} grows, a discontinuous transition occurs

Fig. 8.2 Discontinuity of the order parameters at the transition point in \mathcal{P} . Left jump in q_1 at the PM/SG ($R_J = 4.0$). Right discontinuous \tilde{m} , r, q, r_d at the PM/FM transition ($R_J = 0.26$). In the FM phase the thermodynamics is computed in the RS approximation ($q_1 = q_0 = q$, $r_1 = r_0 = r$)



from the PM to a spin-glass (SG) phase in which the phases ϕ are frozen at given values, though not displaying any ordered pattern in space. First, along the line $\mathcal{P}_d = \sqrt{\bar{\beta}_d/R_J}$ ($\bar{\beta}_d = 6.322$), a dynamic transition occurs. Indeed, the lifetime of metastable states is infinite in the mean-field model and the dynamics gets stuck in the highest lying excited states. The thermodynamic state is, however, still PM. Across the full line (cf. Fig. 8.1) $\mathcal{P}_s = \sqrt{\bar{\beta}_s/R_J}$ ($\bar{\beta}_s = 7.094$) a true thermodynamic phase transition occurs. The order parameter q_1 discontinuously jumps at the transition to a non-zero value $q_1 > q_0 = 0$ and $\tilde{m} = r_0 = r_1 = r_d = 0$ (see Fig. 8.2). The SG phase exists for any value of R_J and $\bar{\beta} > \bar{\beta}_s$. However, for small R_J , a random ferromagnetic (FM) phase turns out to dominate over the SG and the PM phases. The transition line PM/FM is the standard passive ML threshold (see e.g. [27, 31]) and from Fig. 8.1 we see that it takes place at growing \mathcal{P} for increasing R_J .

To precisely describe the FM phase in the 1RSB Ansatz we have to solve eleven coupled integral equations [Eqs. (8.9)–(8.13) and $\Sigma=0$, cf. Eq. (8.16)]. In the region where this FM_{1rsb} phase is thermodynamically dominant, however, the PM and the SG solutions also satisfy the same set of equations. Starting the iterative resolution with random initial conditions, determining the SG/FM_{1rsb} and the PM/FM_{1rsb} transition lines becomes numerically very demanding. An approximation is obtained by considering the Replica Symmetric (RS) solution for the FM phase (FM_{rs}). This reduces the number of independent parameters to seven ($q_1=q_0,\ r_1^{R,I}=r_0^{R,I},\ r_d^{R,I}$ and $\tilde{m}^{R,I}$). The corresponding transition line is shown in Fig. 8.1. The exact FM phase is provided by a 1RSB solution and some sampled points are represented by the circles in the phase diagram.

The 1RSB ansatz also enables to determine the not-vanishing extensive complexity, which signals the presence of a large quantity of excited states with respect to ground states. This also implies the occurrence of dynamic transitions besides the thermodynamic one, as anticipated. These take place between PM and SG, where the state structure always displays a non-trivial $\Sigma(f)$, and in the FM phase, though the magnitude of Σ turns out to be smaller. In the left inset of Fig. 8.1 we show,

e.g. $\Sigma(f)$ in the FM_{1RSB} phase at $(R_J, \mathcal{P}) = (0.28, 5.92)$. This has to be compared with the SG complexity at the same temperature that is sensitively larger and does not depend on the "disorder/order ratio": the maximum complexity drops of about two orders of magnitude at the SG/FM_{1rsb} transition, thus unveiling a corresponding *high to low complexity transition*.

In summary, in this chapter, we have seen how the nonlinearity-disorder interplay can be analytically studied, by treating both on the same level of importance. By using the spin-glass theory, we are able to analytically include in a single treatment the underlying physics of the laser action phenomena when an increasing degree of disorder is present. We can obtain the phase diagram for these optical devices, displaying three thermodynamic phases: the standard mode-locked phase (ferromagnetic-like), the paramagnetic phase (continuos wave emission) and the glassy mode-locking phases. The phase diagram permits a complete overview of the laser physics and predicts the mode-locking-like transition for the random laser (the glassy phase).

Our results can be experimentally tested in a variety of different physical systems, from laser powders to standard laser cavities, and are relevant for any disordered nonlinear interaction process. The ML dynamics is expected to be strongly affected by the existence of several valleys in the free energy (i.e. a not vanishing *complexity*). In this respect, lasing in disordered system is an important framework for investigating out of equilibrium dynamical systems, including quantum effects.

References

- Mézard M, Parisi G, Virasoro MA (1987) Spin glass theory and beyond. World Scientific, Singapore
- 2. Cao H (2003) Waves in random media and complex media, vol 13, p R1
- 3. John S, Pang G (1996) Phys Rev A 54:3642
- 4. Lubatsch A, Kroha J, Busch K (2005) Phys Rev A 71:184201
- 5. Wiersma DS, Vanalbada MP, Lagendijk A (1995) Nature 373:203
- 6. Lepri S, Cavalieri S, Oppo G, Wiersma D (2007) Phys Rev A 75:063820
- 7. Angelani L, Conti C, Ruocco G, Zamponi F (2006) Phys Rev Lett 96:065702
- 8. Beenakker CWJ (1998) Phys Rev Lett 81:1829
- 9. Zhang D et al (1995) Opt Commun 118:462
- 10. Polson RC, Vardeny ZV (2004) Appl phys lett 85:1289
- 11. Siddique M, Alfano RR, Berger GA, Kempe M, Genack AZ (1996) Opt Lett 21:450
- 12. Florescu L, John S (2004) Phys Rev Lett 93:013602
- 13. Deych LI (2005) Phys Rev Lett 95:043902
- 14. Tureci HE, Ge L, Rotter S, Stone AD (2008) Science 320:643
- 15. Patra M (2002) Phys Rev A 65:0403809
- 16. Hackenbroich G, Viviescas C, Elattari B, Haake F (2001) Phys Rev Lett 86:5262
- 17. Berger GA, Kempe M, Genack AZ (1997) Phys Rev E 56:6118
- 18. Conti C, Leonetti M, Fratalocchi A, Angelani L, Ruocco G (2008) Phys Rev Lett 101:143901
- 19. Wiersma DS (2008) Nat Phys 4:359
- 20. Ambartsumyan R, Basov N, Kryukov P, Lethokov S (1996) IEEE J Quantum Electron 2:442
- 21. Schawlow AL, Townes CH (1958) Phys Rev 112:1940
- 22. Haken H (1978) Synergetics. Springer-Verlag, Berlin
- 23. Weill R, Rosen A, Gordon A, Gat O, Fischer B (2005) Phys Rev Lett 95:013903

References 79

24. Angelani L, Conti C, Prignano L, Ruocco G, Zamponi F (2007) Phys Rev B 76:064202

- 25. Haus HA (2000) IEEE J Quantum Electron 6:1173
- 26. Cao H, Jiang X, Ling Y, Xu JX, Soukoulis CM (2003) Phys Rev B 67:161101R
- 27. Gordon A, Fischer B (2003) Opt Comm 223:151
- 28. Angelani L, Conti C, Ruocco G, Zamponi F (2006) Phys Rev B 74:104207
- 29. Gardner E (1985) Nucl Phys B 257:747
- 30. Crisanti A, Sommers H-J (1992) Zeit Phys B 87:341
- 31. Gordon A, Fischer B (2002) Phys Rev Lett 8:103901

Chapter 9 The Granular Laser

In the last chapter, we have seen how to analytically treat the interplay between non-linearity and disorder in the framework of the spin glass theory. The emerging results show how the increasing degree of disorder can drastically change the underlying thermodynamics by switching the optical device from a standard laser to a random one while controlling the furnished energy permits to observe the nonlinear emerging phenomena, like the mode-locked transition. By an experimental point of view, the latter mechanism is much simpler to control and hence the related literature is much wider than the former one. Here, we want to visually demonstrate through a set of experiments that the random laser emission depends not only on the furnished energy, the nonlinear processes, but primarily on the structural informations, that is the degree of disorder inside. In order to study how random laser features are affected and controlled by the state of the motion of the sample, and then on the disordered considered configuration, we have to choose the more appropriate physical system. Here, we use shaken granular materials.

9.1 Introduction

In random lasers (RL) stimulated emission is achieved by disorder-induced light scattering [1]. RL were reported in colloidal systems, composed by small particles suspended in thermal equilibrium in a solution, or in materials exhibiting a fixed disorder, achieved, e.g. by porous systems or nano-fabrication. RL in shaked grains were not reported. Granular materials (sands, powders, seeds, cements, etc.) [2–4] are an extensively studied branch of statistical mechanics, with several important applications in chemistry or engineering. Phenomena like the occurrence of spontaneous onset of convection, segregation of mixtures, emergence of patterns and granular waves, non-equilibrium stationary states, glassy relaxations have been considered by several authors, also driven by relevant industrial and technological applications [2–4]. These very simple systems, composed by agglomerations of mesoscopic particles that, in specific regimes, are characterized by a large number of metastable

states and an extreme sensitivity (e.g. in the transmission of sound) on the microscopic arrangement of grains. Their properties are not substantially affected by thermal phenomena, but can be controlled by using mechanical solicitations, as shear and shaking, being one of the paradigms of the statistical mechanics of disordered system and still lacking of general and universal theoretical descriptions. Granular gases [5], i.e. gases of massive particles in rapid movement undergoing inelastic collisions, are obtained by putting under mechanical oscillation a material composed by grains. In the presence of a driving solicitation, a gravity-sedimented ensemble of grains switches, above a critical mechanical energy, from a solid-like state to a gaseous one, whose essential feature is the strong enhancement of fluctuations and the non-equilibrium character [6, 7]: even in such a dilute configuration, regions with very high density may appear. Such a state can only be maintained by continuously furnishing mechanical energy to system. This circumstance may have relevant implications when considering the RL, which happens when energy is furnished to the system not only mechanically but also optically by employing a light-emitting active medium, as described below. The specific and characteristic arrangements of the shaken grains not only can alter the RL features, but, in the gaseous-like phase, may also lead to a novel form of laser emission in a dynamical random structure, which can be controlled by acting on the external mechanical solicitation. Such a situation is not achievable in formerly considered RL; indeed, in the fixed disorder case [1], the specific structure cannot be externally changed, while the formerly adopted colloidal random lasers were realized by mixing an active medium (laser dyes as RhodamineB) [8] and powders of dielectric high-index nano-particles, [9–12], which are too light to exhibit a switchable granular behavior, or were not considered under shaking. Various authors also investigated RL by metallic nano-particles [13–16], however, so far, only particles with diameters of the order of tens of nanometers were considered, which, as in the cases discussed above, do not exhibit granular behavior, while not being substantially affected by gravity. In these systems, thermal equilibrium largely limits the kind of observable fluctuations with respect to out-ofequilibrium granulars. In this chapter, we consider a granular system composed by metallic grains with millimeter size, able to macroscopically change its structural features when the status of motion is altered. We study how the dynamic structural phases affect the RL emission. As we will see, we find that an alteration of the state of motion of the grains forming the disordered laser cavity dramatically changes the laser emission, and sustain novel and competitive forms of RL. We first do an overview of random lasers, then we show the experimental setup and characterize a typical diffusive random laser in order to give a reference system. Finally, we present the experiments on the granular laser and we relate our conclusions.

9.2 Introduction to Random Laser

The term LASER is the acronym for Light Amplification by Stimulated Emission of Radiation. The Laser emission is hence the result of a piloted process of interaction between radiation and matter. The pivotal units of a laser are two, mutually needful:

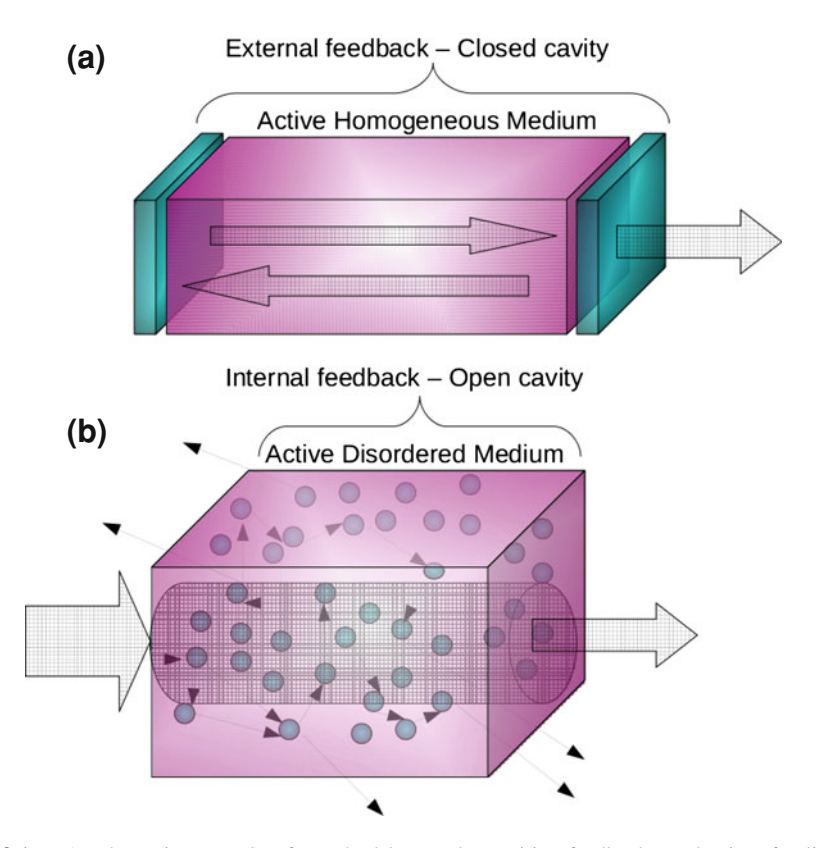


Fig. 9.1 a A schematic example of standard laser. The positive feedback mechanism for light amplification is supplied by an external closed resonant cavity. **b** The active medium contains the scattering elements that provide the internal and spatially distributed positive feedback

active medium and positive feedback. The active medium supports the amplification of light through stimulated emission thanks to the optical feedback element that partially traps the traveling light and forces it to repeatedly cross the active region. The positive feedback can be created externally to the active medium, and correspondingly the resonant cavity is closed, on the contrary the cavity can be open and the feedback is internally distributed, e.g. by optical scattering. The working principle of the first one is by exploiting the first order radiation-matter interaction, that is the emission/absorption processes and prevent, as much as possible, the second order term, the scattering events. In the second kind of laser, instead, the use of an open cavity implies to mix together optical feedback and optical gain (see Fig. 9.1). We need to use a "second-order" medium in which the scattering process supplies the positive feedback. It is evident that, in this case, the losses are higher and the laser threshold rises due to the pronounced light diffusion. In the first kind of laser, the amplifying element is homogeneous as much as possible to avoid light scattering

processes, we want a "first-order" medium 1 ; this is commonly referred to as standard laser. Usually, the amplifying medium is placed between two reflecting (one partially) mirrors, which forms a closed optical cavity (in the specific example of Fig. 9.1, it is a Fabry-Perot cavity). The light travels back and forth between the mirrors and the longitudinal modes sustained by the cavity are amplified in the gain region. The constructive interference condition, $kL+\phi_1+\phi_2=2\pi n$, determines the resonance frequencies. Hence, the frequency and the output direction of the beam are determined by the cavity geometry, being L the length of the resonator and ϕ_1 , ϕ_2 the phases due to reflection by the mirrors. Once the optical gain of the resonant modes exceeds their cavity losses, the laser emission is achieved.

In the second type of laser, the scattering processes are usually determined by inserting disorder into the active region, the resulting device is commonly referred to as a random laser [1, 17, 18]. Light diffusion with gain was initially studied by Letokhov [19]. In fact, Letokhov was the first to introduce the idea of a stochastic resonator: an open cavity containing a multiple scattering medium. Depending on the typology of scatters, the cavity can support a large number of overlapping modes in a specific frequency range. If gain is supplied to the system, this nonresonant feedback can sustain laser-like action. The light is both amplified and multiply scattered. We could say, for sake of synthesis, that the random lasing process is an instability of the amplification of light, when this is enhanced above a critical value, and occuring in the presence of adequate multiple scattering events in a disordered medium. In a nutshell, the light, in order to be amplified inside an open disordered cavity, has to be retained as long as the laser threshold is reached. In practice, there exist two ways to realize this condition: to induce light to make a long random walk through the sample (the diffusive random laser) or to create closed loops between scatterers in which light can be trapped for long time, determined to the gain length (the localized random laser). The way the disordered sample works, depends on the relative scale of randomness and sample size with respect to the wavelength. This can be explained by defining some relevant length scales:

- 1. Amplification: in order to describe the amplification processes through stimulated emission, two related lengths are defined; the gain length l_g and the amplification length l_{amp} . The first one is the path length necessary for the light to be amplified in intensity by a factor e; l_{amp} is the average value of l_g on all the possible gain paths between scatterers. In an ordered medium, l_{amp} equals l_g .
- 2. Scattering: in a random medium, one of the most important physical quantities is the strength of disorder. The scattering mean free path l_s gives the average distance between two consecutive scattering events. The transport mean free path l_t is the average distance over which the propagation direction of the incident light is completely randomized.

When $L \gg l_t \gg \lambda$, the scattering processes can be treated within the diffusive approximation; here L is the size of the sample and λ is the wavelength. The

We use "first order" to denote the fact that scattering is neglected, indeed scattering events in the light-matter interaction Hamiltonian appears at second-order.

amplification length can be written as $l_{amp} = \sqrt{Dt}$, where D is the diffusion coefficient and t is the time. In a three-dimensional (3D) system, $D = vl_t/3$ and $l_{amp} = \sqrt{\frac{l_t l_g}{3}}$, where v is the velocity of the light in the medium. The "photon-particles" move in the sample by making a sort of Brownion motion. The light propagation can be described by introducing a gain term in the diffusive equation [20]:

$$\frac{\partial I(\mathbf{r},t)}{\partial t} = D\nabla^2 I(\mathbf{r},t) + S(\mathbf{r},t) - \tau_i I(\mathbf{r},t), \tag{9.1}$$

where $I(\mathbf{r}, t)$ is the diffusive light intensity, S is the source of diffusing light and τ_i is the characteristic time over which the diffusing light is absorbed by the sample. This is the reason for which this kind of laser is also called "random laser with diffusive feedback" [8, 21, 22]. Every time the light is scattered, is also amplified. So, after N scattering events, the light leaves the samples, having covered a mean distance $d = l_s \times N$. The amount of amplification increases with d. So the overall gain depends linearly by the covered distance d that is dependent on the size L of the sample. Hence, in a 3D system, the gain is linearly dependent on the total volume of the sample. To the other side, the losses are determined by the flux of energy leaking out the sample boundaries; it can be easily shown that they depend linearly on the area of the boundary surface. As a result, a critical volume exists such that the overall gain exceeds the losses [19]. The system becomes hence "unstable" and starts emitting coherent radiation.

The condition for the second kind of random lasers is for $k_e \times l_s \sim 1$, where k_e is the effective wave-vector of the light into the sample. As the strength of disorder increases, the mean free path becomes shorter, and the scatterers lye on distances comparable with the wavelength. In very strong scattering regime, the light is trapped inside the sample. In fact, when the scatterers are closer than one wavelength, each scattering events cannot be considered independent with of the others (as it happens in the diffusive regime). In this scenario, the light beam keeps memory of its phase during scattering and there exists a not vanishing probability that the multiply scattered waves propagate in opposite directions along the same closed loops (see Fig. 9.2). This leads the counter-propagating waves to interfere constructively with each other in such a kind of cavity. The resonance modes, sustained by these closed paths, promote the localization of light. In fact, by adding enough gain to overcome the losses through the boundaries of the localized resonance zones, it is possible to observe the presence of narrow intense peaks in random lasing spectra [23]. In the localized regime, the eigen-modes, coupled with the closed paths, decay exponentially in space on a characteristic distance ξ , which measures the spatial extension of the region in which the light is trapped and gives the size of the resonant micro-cavities. This kind of localized modes are often referred to as the Anderson localization of light [24].

In summary, by increasing the strength of disorder beyond a threshold related to the scattering length, the probability of looped paths inside the sample increases, the interference events become predominant, a transition from a diffusive regime, in

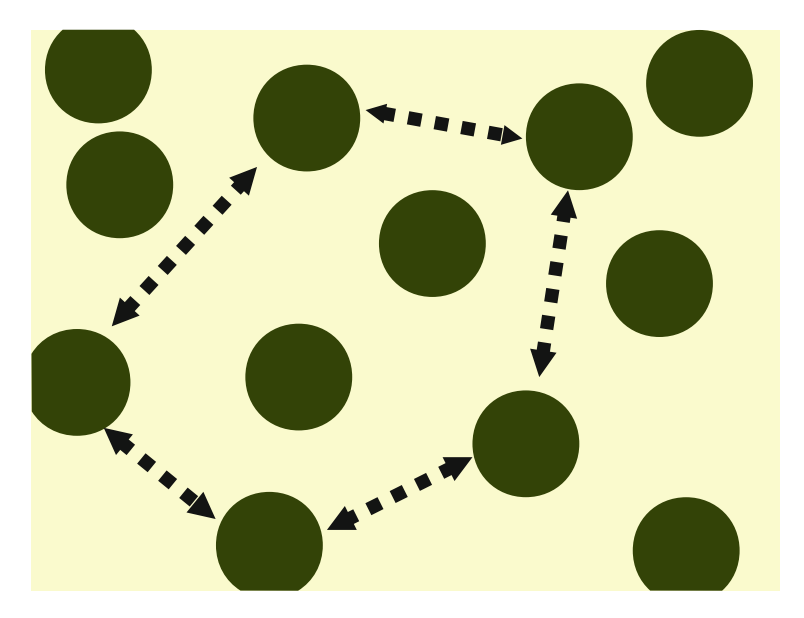


Fig. 9.2 Closed random light path. The light can be trapped inside the sample and can constructively interfere, resulting in localized lasing emission once the gain is supplied

which the light spreads over the whole sample, to a localized one can be observed. The latter resonant phenomenon gives name to this second class of random lasers, i.e. "coherent random lasers".

9.3 Experimental Setup and Procedures

In order to implement our ideas about a granular laser that, due to its specific nature, is able to change its emission spectrum with the state of motion, we have employed an experimental setup, sketched in Fig. 9.3 and explained with details in the following.

The basic idea of our experimental study is as follows. The random laser is a photonic device in which the positive feedback for coherent emission is enhanced by diffusion ("incoherent" random laser) and strong scattering ("coherent" random laser) of the incident light, related to the presence of disordered scatterers in the active medium. The emitted spectrum depends on the strength of the disorder. If we find a way to affect the disorder configuration, we can change the scattering mean free path of light inside the sample. By varying the path length of the incident light with respect to the wavelength, it is feasible to switch from a diffusive random laser to a localized one. The considered way to obtain a sample with controllable disorder is to use a granular material subjected to an external applied force.

In this section, we discuss the experimental setup and the used procedures.

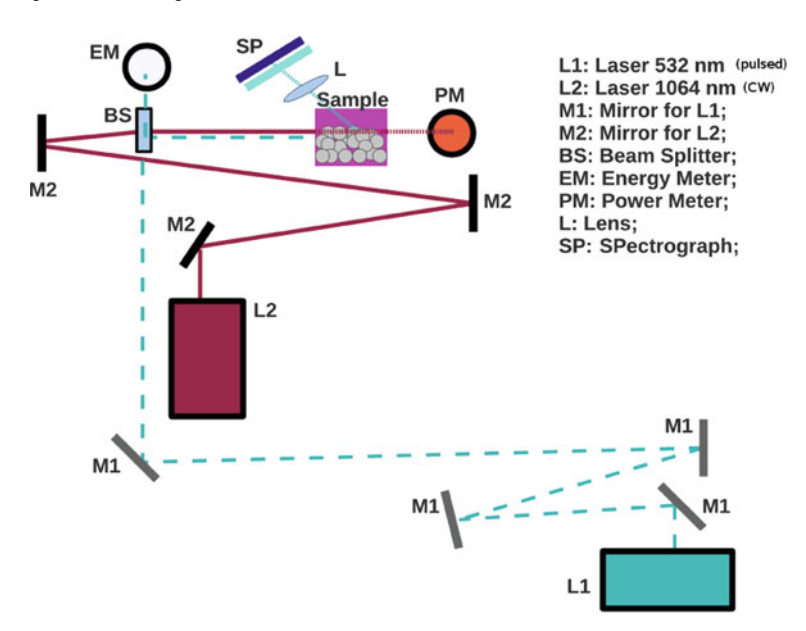


Fig. 9.3 Scheme of the experimental setup

In the first subsection, we describe the optical arrangement for the static analysis (continuous line in Fig. 9.3) with the continuous laser source. In the second one, we will analyze the experimental setup for the light emission study with the pulsed laser (dashed line in Fig. 9.3).

9.3.1 Continuous Wave Analysis

Here, the leading purpose is to draw a "phase-diagram" for the granular material furnishing the status of aggregation of the grains when an external force is applied. So, we measure the transmitted power of an incident continuous light beam by varying the amplitude of oscillations applied to the sample and the height of the input light with respect to the bottom vibrating plate. In this way, it is possible to obtain information about the internal structure and the collective arrangement of the grains (and hence about the density) in the couette, when it is still or put into motion.

We have used a continuous laser source (a IR 1,064 nm Laser, L2 in Fig. 9.3), the input beam is steered across the sample by using 45° dielectric mirrors. The sample is put on a vertically vibrating "plate", obtained by a sound woofer, such that we can vary the amplitude and the frequency of the oscillations through an audio amplifier. We have chosen a woofer that allows to generate the low acoustic frequencies, a range of values in which the granular response is maximized. All the structure is

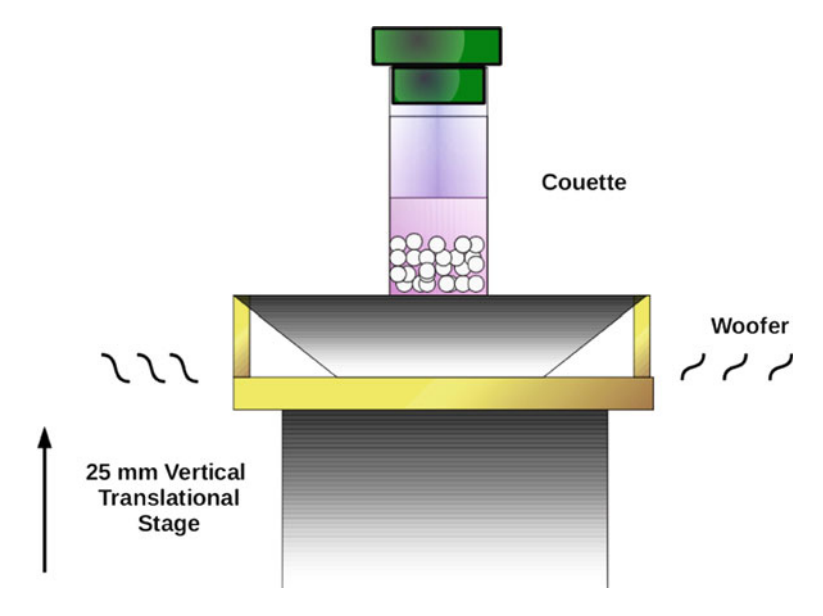


Fig. 9.4 Scheme of granular shaking device. The *vertical* translational stage is motorized and controlled by software

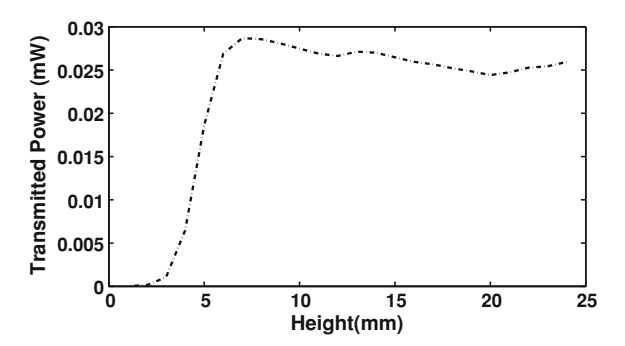
placed on a vertical motorized translation stage having a 25 mm translational range (see Fig. 9.4).

The transmitted intensity is detected by an optical power meter detector that is placed beyond the sample (Fig. 9.3). We control by software the optical instruments by using a $Matlab^{\circledR}$ Routine through which we can synchronously move the translational stage with the sound sent to the loudspeaker, by driving the bottom basis of the sample by using a sinusoidal acoustic signal. For the static analysis, we follow three "protocols" for each sample.

Protocol 0—Measurement of the height of the granular

Once the sample is put in the couette, the first analysis must furnish the precise height of the granular with respect to the basis of the couette. In fact, as we will see, this is a fundamental information for what concerns the "phase-diagram" of the granular sample. This is a measure taken when the sample is still. We fix the height of the laser beam at the basis of the couette when the vertical translation stage is at the ending point (25 mm outstretched). We record the transmitted power and then, we decrease of 1 mm the height of the stage and hence, respectively, the laser beam advances of 1 mm in the lower zone of the sample. We correspondingly record the power. In this way, the sample is vertically scanned; when the light beats the granular medium, no transmitted power is detected, conversely as the last layer of grains is surpassed, the incident light is entirely transmitted. The transition between these two regimes is

Fig. 9.5 The transmitted power from the ZnO powder versus the height of the beam laser with respect to the bottom of the solution sample



almost discontinuous, the smoothing depending on the size of the laser spot which is 3 mm² (an example is given in Fig. 9.5).

Protocol 1—Measurement of the resonance frequency

We find the frequency at which, once in motion, the sample can maximally oscillate, for a given amplitude in order to access the highest dynamic range in our setup. This is apparently a measure that depends only on the instrumentation that we use to send an oscillating force to the sample (see Fig. 9.4). Whenever we change the sample, we repeat this protocol in order to guarantee that the response function of the acoustic apparatus is always the same.

This kind of measure is as follows. We fix the height of the laser beam approximately just above the top layer of the granular particles. This is the zone of maximum sensitivity to an external solicitation, because it is the one with fewer spatial constraints. We start at rest, we record the transmitted power. Then we send, through a $Matlab^{\textcircled{\$}}$ Routine, a sinusoidal signal $y=a\sin(\frac{2\pi fx}{F_s})$, where $F_s=8,192\,\mathrm{Hz}$ is the sample frequency, f is the signal frequency and $x=1:n_x$ is a time-vector with $n_x=TF_s$, T being the overall sound duration. We make a frequency scan ranging from 10 to 100 Hz. For what concerns the amplitude of the signal, values of |y| are in the normalized range [0,1], as determined by the used sound-card of the pc. The amplitude is kept low, at 0.1, in order to better distinguish the resonance zone. In fact, for small stimulations, the top layer of the sample will vibrate slightly and the transmitted signal remains almost unperturbed. When we achieve the resonance zone, the top layer is significantly moved. The superficial grains will jump on the surface, intercepting the passing laser beam and blocking it. Correspondingly, the transmitted power is affected.

Once we increase the frequency and go over the resonance zone, the oscillations return small and the signal is again transmitted. So, by plotting the transmitted power versus frequency, the resonance frequency is found (in Fig. 9.11 we show an example).

² The laser spot is measured by a scanning blade technique

Protocol 2—The "phase-diagram" of the granular

Once known the height of the sample in the couette and the resonance frequency, so we can determine what we indicate as the "phase-diagram" of the sample. In the protocol 2, we do two scanning loops in the height and in the oscillation amplitude. We fix the frequency at the resonance value, approximately at 70 Hz. We send the sound with several values of amplitudes, chosen in the range [0, 1]. For every fixed value of amplitude, we make a vertical scan of the couette and record the transmitted power for each height. In this way, we will have several curves of the transmitted power versus height at different oscillation amplitudes. By studying the trend of the superimposed curves, it is possible to find those values of amplitude for which the sample switches in behavior from a blocked or frozen state to a gaseous one. In fact, when the vibrating force is low, only the top layers can vibrate. The transmitted power has a similar trend with respect to the static case, with almost discontinuous transition by noise to the input power value, in correspondence of the height of the sample in the couette (as in Fig. 9.12, see the curves at small oscillation amplitudes). When the sound amplitude grows and the oscillations become larger, also the deeper grains (those at the bottom of the couette) can move by following the acoustic signal. The top density reduces, the grains are spread in a wider volume and the chances for the input beam to go through the couette decrease because the probability to intercept a grain becomes larger. The transition between the on/off values becomes smoother and smoother (as in Fig. 9.12, see the curves at larger amplitudes). There exists a threshold in the amplitude value, for which the grains can explore all the volume of the couette and the input beam is stopped at all heights. Here we are in the gaseous phase (in Fig. 9.12, the curves for a > 0.1.)

9.3.2 Laser Emission Analysis

The aim of the laser emission analysis is to explore how the random laser spectra by a granular system can change when an external vibrating force is applied on the sample. We expect that an alteration of the state of motion of the grains forming the disordered laser cavity dramatically changes the optical properties of the sample. In fact, the vibration does not only change the configuration of disorder, but, modifying the internal arrangement of the grains on larger volumes, increases the mean free path and affects the diffusion of light inside with respect to the case in which the grains are deposited and tightly packed. But, if, on the one hand, the motion can promote the diffusive random lasers, because light can more easily enter the sample, on the other hand it is possible that, as the amplitude of the oscillation is increased, the grain distance increases and cavities can be created. In this regime, we expect something similar to the localized random laser.

The experimental setup is sketched in (Fig. 9.3), the turquoise dashed path identifies the pulsed light beam. The sample on the woofer is optically pumped by using a frequency-doubled output of a pulsed Q-switched Nd:YAG laser ($\lambda = 532$ nm) with

a 10 Hz repetition rate (the pulse duration is 7 ns). The emitted radiation from the input face is collected by a diffuser and sent to a spectrograph with an electrically cooled CCD array detector (operating temperature -70° C.) The energy of the laser beam is controlled by acting on the flash lamp delay of the laser and by using non-reflective neutral filters. A measure of the incident laser light is obtained by using a broadband no-polarizing 50% beam splitter that splits the beam in two branches, one on the sample and the other one on the energy meter. We use high power dielectric mirrors optimized for 532 nm wavelength in order to steer the beam in the setup.

Protocol 3—The lasing oscillations

By using the phase-diagram obtained above, we optically excite the sample both in static that in motion in order to study the emission spectra. As a rule, we fix the position of the 532 nm pump beam with respect to the height with reference to the static curve (at the bottom, in the middle of the sample, at the top and above the deposit). For each height, we choose several amplitudes, corresponding to the blocked and to the gaseous phase. For these positions and oscillation amplitudes, we send the 532 nm pump beam with an increasing energy and retrieve the emission spectra (as, e.g. in Fig. 9.7).

In the following, we will study how the state of motion for a specific sample can change the scattering length and affect the optical features of the system. To this aim, we will first compare, in the same conditions, two samples. The first one is a reference model, a "standard" random laser, obtained by a colloidal system that is always in the same "granular phase" when it is mixed with the active medium (when at the rest and vibrated). The second one displays two phases, blocked and gaseous, depending on the applied acoustic signal. The easiest way to create these two samples is varying the diameters and the densities with respect to the active medium. In the next chapters, we call the former "the diffusive random laser" and the latter "the granular random laser".

9.3.3 Oscillation Amplitude Calibration

In the following chapters, we use a normalized parameter a in order to describe the oscillation amplitude of the woofer. Hence, a corresponds to a real oscillation. In order to measure it, we use a piezoelectric accelerometer (Dytran, IEPE ACCELEROM-ETERS, SERIES 3056B, $100 \,\mathrm{mV/g}$). We fix the amplitude a and the frequency f of the sinusoidal signal that we send to the woofer through the $Matlab^{\textcircled{\tiny{\$}}}$ Routine; the volume knob is turned at halfway. Once we measured the half-peak voltage, given a conversion factor for which 1 V corresponds to 10 times the gravity acceleration, we can obtain the spatial displacement corresponding to that chosen a. In fact, given a sinusoidal signal for which the spatial position is $y = A*\sin(2\pi ft)$, the accelerometer measures its maximum acceleration, $\ddot{y}_{\text{max}} = A\omega^2$, in unity of g. So, for example, when a = 0.1, the observed half-peak voltage is $1,500 \,\mathrm{mV}$, that corresponds at 15 times g. Being the frequency set to $70 \,\mathrm{Hz}$ and $A\omega^2 = 15g$, we obtain that A is

equal to 0.76 mm. In the next, the normalized amplitude values will be a = 0, 0.07, 0.1, 0.2, 0.3, for which A = 0, 0.53, 0.76, 1.5, 2.3 mm.

9.4 The Diffusive Random Laser

We consider a sample consisting of Zinc Oxide (ZnO) powder in RhodamineB (RhB). The nanoparticles of ZnO are polydisperses with an average diameter of 100 nm, thus this sample cannot be considered a granular system because, as we have seen, the lower size limit for the particles in granular materials is about 1 μ m. We used 0.358 g of Zinc Oxide and 2.842 g of RhodamineB in order to have a concentration of about 20 mM, a typical concentration for diffusive random laser [8]. We will refer in the following to this sample as the "diffusive sample".

9.4.1 Continuous Wave Analysis

When the sample is at rest, ZnO deposits on the bottom and we can measure the height of the powder in the test-tube. For this sample, this kind of measure is unnecessary because, once the couette is vibrated, the ZnO powder is mixed with the solution and an homogeneous mixture is obtained. We do not have a height-dependent spectral emission. The results obtained so far are the same both in static (once the mixture is obtained) that in motion. Here, we report this analysis for sake of completeness and to give the reader chances to compare all the investigated samples by taking into account all the used protocols.

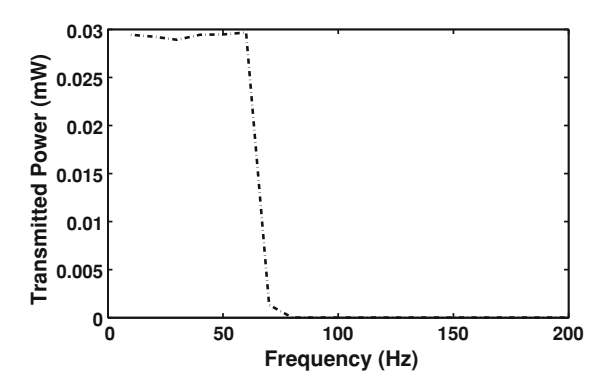
As explained above (protocol 0), the transmitted power of the continuous laser beam through the sample is measured by varying the height of laser beam with respect to the sample with the vertical translation stage. We have used an accuracy of 1 mm, higher accuracy is unnecessary since the laser spot is about 3 mm. The trend of the transmitted power give us the value of the ZnO deposit height.

We report in Fig. 9.5 the measured transmitted power as a function of the laser beam height. As we can be seen, the height of ZnO powder can be set about $h_{ZnO} = 5 \pm 3$ mm, as it can be easily verified by measuring the deposit in the couette by a ruler.

We first followed protocol 1, described in the previous chapter. We set the height of the laser beam with respect to the couette at $z=7\,\mathrm{mm}$, in the more sensible transmission region. Then we performed a frequency scan to detect the resonant frequency of the acoustic setup.

We sent a sinusoidal sound, for $8 \, s$, for a frequency range of $10 \div 200 \, Hz$, with steps of $10 \, Hz$. The amplitude of oscillation is set to 0.1 (see protocol 1, Sect. 9.3 for details). From one vibrating stimulation to another, there is a $2 \, s$ pause, not enough to deposit ZnO.

Fig. 9.6 The transmitted power from the ZnO powder in RhB versus the frequency of the oscillating plate, measured at z = 7 mm



Until the frequency is less than $70\,\mathrm{Hz}$, resonance of the speaker, the vibration is too low to homogeneously mix the ZnO powder in the RhB solution. The transmitted power is about $0.03\,\mathrm{mW}$, as for the still sample (see Fig. 9.5 at $z=7\,\mathrm{mm}$, the power is on $0.03\,\mathrm{mW}$). At $70\,\mathrm{Hz}$, the loudspeaker displays the most pronounced response. The oscillations create an homogeneous mixture after a few seconds, the input laser is scattered by the random medium, and the transmitted power goes to zero (see Fig. 9.6). We have reported here a wide frequency range in order to make indisputable the fact that, once the ZnO is mixed with the RhodamineB and the homogeneity is reached, the further increase of the oscillation frequency does not change the characteristics of the compound and the power measured to the output face remains equal to zero (see Fig. 9.6).

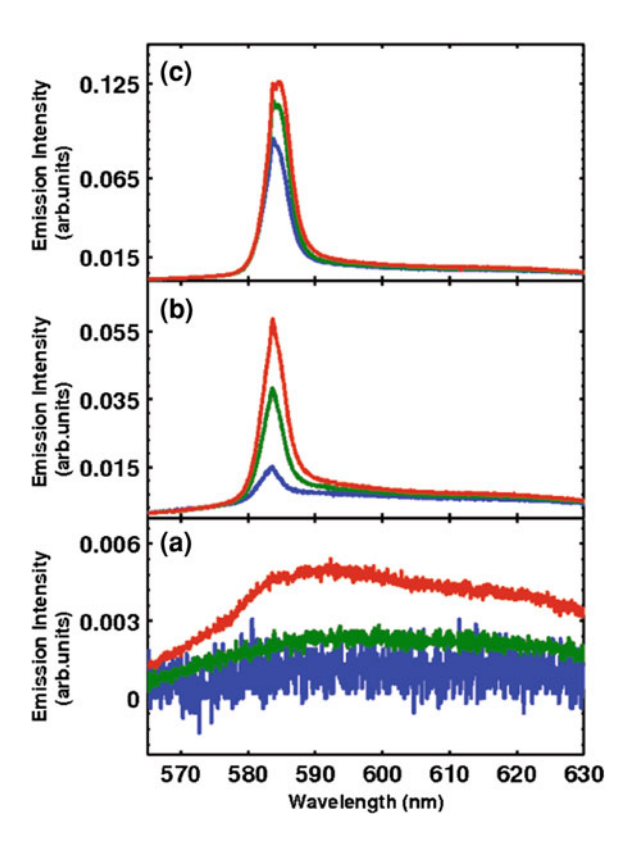
By this analysis, we have a further confirmation that the ZnO solution can not be considered a granular system. As the physical properties are independent of the state of motion, once the sample has been shaken.

At this point, follow the protocol 2 is absolutely not significant. Once the ZnO particles are homogeneously dispersed in the RhodamineB, the transmitted power is always zero, both at high than at low oscillation amplitude. Hence the protocol 2 to determine the "phase-diagram" is not necessary (at variance with what happens for the samples described in the next chapter).

9.4.2 Laser Emission Analysis

The colloidal solution is optically pumped by using a frequency-doubled pulsed Nd:YAG laser ($\lambda = 532 \, \mathrm{nm}$) with 10 Hz repetition rate, as described in Chap. 3. Because, for this low concentration, there is no dependence of the instantaneous disordered configuration, we have captured the emitted spectrum with an exposure time of 1 s. So, the resulting spectrum is the average response for ten pump pulses. The spectral resolution is about 0.3 nm. Figure 9.7 shows the emission spectra for various pump energies. It can be seen that there exists a laser threshold. At low pump

Fig. 9.7 The emission spectra from the RhodamineB dye solution with ZnO disperse nanoparticles (100 nm) with a concentration of 20 mM. The input pump pulse energy is respectively from *bottom* to the *top*, a 0.09, 0.14, 0.47 mJ, b 0.69, 1.29, 1.67 mJ, c 2.32, 2.83, 3.36 mJ. The amplitude of the spectra has been scaled up by factor of, respectively, 1, 2, 4, 6, 8, 10, 12, 14, 16

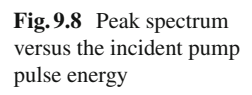


energy (Fig. 9.7a), the spectrum consists of the typical homogeneously broadened fluorescence peak.

As the incident pump pulse energy is increased and the laser threshold is reached, a drastic narrowing of the emission spectrum is observed (Fig. 9.7b), corresponding to an optical gain exceeding the total loss. A main peak appears at about 582 nm and, as it can be seen in Fig. 9.8, the peak intensity of the emitted radiation increases abruptly and, correspondingly, the spectral line-width of the emission spectra is shrunk (see Fig. 9.9).

The dramatic growth of the peak intensity and the simultaneous reduction of the spectral waist are the typical behaviors of the diffusive random laser, as reported for the first time by Lawandy et al. [8].

We made use of this sample as a pivot of the typical and well-known behavior of a diffusive random laser. In fact, having a reference model will serve to guide for our investigations of the granular samples described in the next chapter. The comparison between the diffusive random laser and the granular random laser will direct our interpretations of the new physical phenomena emerging in the latter.



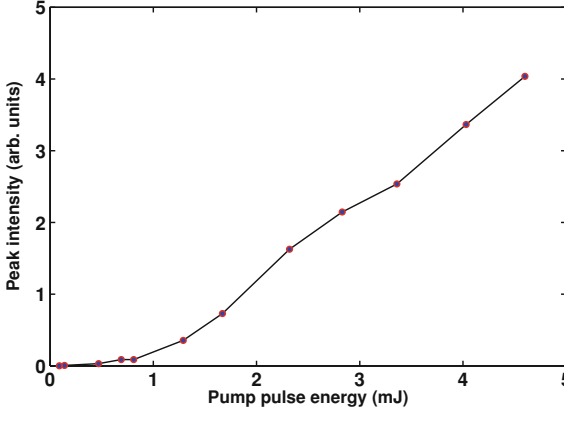
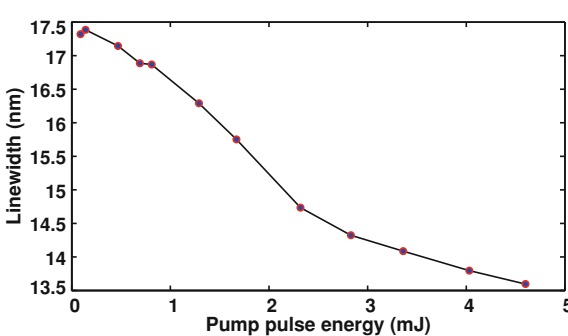


Fig. 9.9 The emission spectral waist, calculated as the standard deviation, versus the pump pulse energy



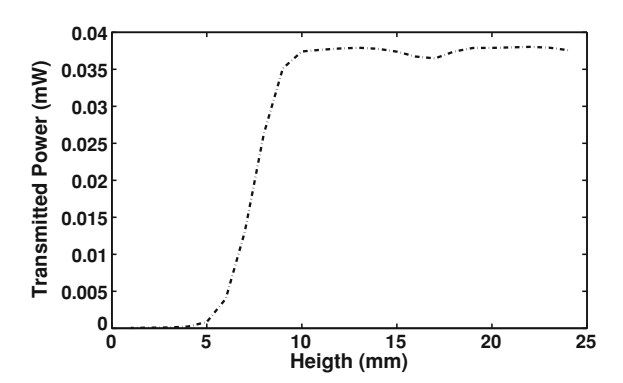
9.5 The Granular Random Laser

Being a random laser a laser device in which the emitted radiation is the achievement of a "feedback mechanism, based on a *disorder-induced* light scattering" [1], our purpose is to study what can happen if we create a random laser with tunable disorder, specifically by using a granular system in a dye solution with an external applied force that modifies the structural arrangement of the grains. In this chapter will report on a transition from an incoherent random laser to a coherent one, that is continuously achievable in a granular sample by a variation of the state of motion. An absolutely new phenomenon appears in which the two types of laser compete in a very interesting disorder-dependent way.

In the following, we will denote as the "granular" sample the sample done by solid amagnetic steel spherical grains (diameter of 1 mm) immersed in a solution of water and RhodamineB (1 mM) and placed in a squared couette with edge $L=1\,\mathrm{cm}$ and height $h=3\,\mathrm{cm}$. We have used 5.23 g of metal particles (about 1,300 grains) and 3.93 g of RhodamineB.

The sample can be considered a granular material. However, following the relevant literature, this system was not previously considered for random lasing. In fact, the

Fig. 9.10 The transmitted power from the metallic particles of size 1 mm in RhodamineB, versus the height of the beam laser with respect to the bottom of the granular sample. The system is at rest



typical colloidal random lasers are realized by mixing an active medium (laser dyes as RhodamineB) and powders of dielectric high-index particles, supporting multiple scattering to provide the positive feedback of the radiation in an open cavity.

Various authors also reported evidences of random lasers by metallic nanoparticles [13–16]. However, so far, only particles with diameters of the order of tens of nanometers were considered. These kinds of systems do not exhibit intersecting granular behavior.

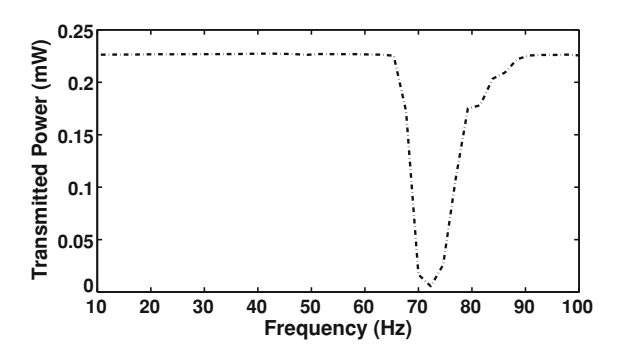
Conversely, we looked for a system able to macroscopically change its structural characteristics by the state of motion. Neither a liquid nor a solid sample or a colloidal one should have this peculiarity, so we have choose a granular material initially composed by metallic grains with millimeter sizes. In such a system, we can study the result of a complex interplay between amplified light in the presence of disorder and the collective nonlinear behavior of a structurally tunable ensemble of grains.

9.5.1 Continuous Wave Analysis

We first consider the measurement of the height of the metallic particles in the sample (protocol 0, see Sect. 9.3 for details). As shown in Fig. 9.10, the metallic grains are deposited to the bottom plate for a height of $h_{Al} = 8 \pm 3$ mm.

We then set the height of the granular with respect to the input beam to $z=8\,\mathrm{mm}$ in order to perform the frequency scan in the region mostly affected by spatial displacements of the particle top layers. The amplitude of oscillation is set at halfway, a=0.5. The frequency scan is a sample-independent measurement, the resonance frequency is in general only determined by the loudspeaker. However, the use of a loudspeaker to oscillate a couette is not its typical application and it is easy to break the internal resistor with the consequent damping of the oscillations. Therefore, for safety, before starting any vibrating experiments, we test the woofer, by repeating the protocol 1, reported in Fig. 9.11. As can be seen by comparing this plot with Fig. 9.6, there is a drastic difference between the colloidal sample and the granular

Fig. 9.11 The transmitted power from the metallic particles of size 1 mm in RhodamineB, versus the frequency of the vibrating plate, measured at the edge region of the granular sample, z = 8 mm



one. For the latter, a threshold above which the grains are homogeneously mixed is not present and the transmitted response shows a specific resonance.

As before, we use a sinusoidal sound with a duration of 8 s. Between two successive sounds, there is a temporal pause of 2 s. The frequency range is $10 \div 100$ Hz and the frequency step is 10 Hz.

As shown in Fig. 9.11, the resonance is around 70 Hz, as also reported before.

We then consider the most important step of the structural "continuous wave" section (protocol 2), in which we retrieve the phase-diagram of the granular material.

We first set the frequency of the vibrating plate at 70 Hz, corresponding to the resonance in Fig. 9.11, and by turning the volume knob of the audio amplifier at a value such that any amplitude saturation in the vibrating dynamics or any damage related to high-volume sound is avoided. Then, we place the vertical translational stage at the starting point and for a fixed amplitude of the oscillations of the bottom plate, a vertical scan is made until the ending point of the stage is reached after 2.5 cm. For every height, we send a sound for 4 s followed by a pause with a duration long enough to allow the translational stage to arrive to the succeeding programmed position.

In Fig. 9.12, we show the transmitted power for five different oscillation amplitudes. There exists a threshold value, around $a\!=\!0.1$, for which the system realizes a transition from a blocked to a gaseous state. In fact, in the former configuration, the sinusoidal sound is not enough to move the whole granular and the particles of amagnetic steel remain deposited at the bottom. Only the top layer particles are vibrated as can be observed by a direct observation of the couette. The intensity of the transmitted light abruptly changes when varying the height of the light beam with respect to the measured height of the granular. However, the transition is smoother with respect to the static case (see Fig. 9.10) because, due to the motion of the top layers, the grains are spread in a effective larger volume, the density is effectively reduced but being sufficient just one grain to reflect the input light, the mean transmitted power passing through the couette is lower than the still case at the same height (compare the red curve of Fig. 9.12, $a\!=\!0.07$, with the static case of Fig. 9.10 between $8 \div 13$ mm.).

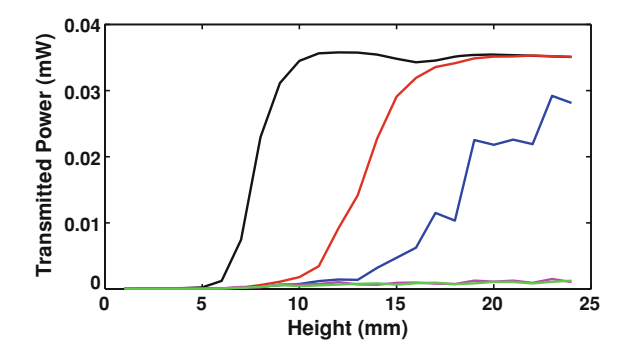


Fig. 9.12 The transmitted power from the metallic particles of size 1 mm in RhodamineB (the granular sample), versus the height of the beam laser with respect to the bottom of the granular sample for five different amplitudes of the vibrating applied force, from the *top* to the *bottom* respectively a = 0.01 (black line), 0.07 (red line), 0.1 (blue line), 0.2 (green line), 0.3 (magenta line)

Once the system has made the transition and the granular is in the gaseous phase, the grains are scattered in the whole available volume (the couette) and the mean transmitted power goes to zero at all heights (the green and magenta lines of Fig. 9.12). In this situation, the strength of disorder is high: this is expected to be an interesting scenario for the appearance of coherent multiple scattering processes and, in the next section, we study the spectrum of the emitted light for this sample at rest and put into motion.

9.5.2 Laser Emission Analysis

We verbatim follow the guidelines of protocol 3, described in Sect. 9.3.

Initially, we use an exposure time of 1s in order to retrieve a mean emission spectrum (we have ten pulses per second from the pump 532 nm Laser).

In Fig. 9.13 we show various spectra, for various heights and oscillation amplitudes. This provide an overall picture of the attainable experimental regimes. Below we will analyze the specific behaviors.

Bottom region

Let us to examine what happens in the deeper layers of granular (see Fig. 9.14). We set the height of the incident pulse to $z=3\,\mathrm{mm}$. With the reference to the phase-diagram analysis, drawing a vertical line to $z=3\,\mathrm{mm}$ in Fig. 9.12, it can be seen that, for all the amplitudes, the transmitted power is always equal to zero. Hence in the deep granular, there is no difference between the several amplitudes of oscillation. By increasing the amplitude of oscillation, we pass from a high density state to a lower density configuration. But on average, there will always be some grain that will stop the optical transmission. This does not imply that the mean density is

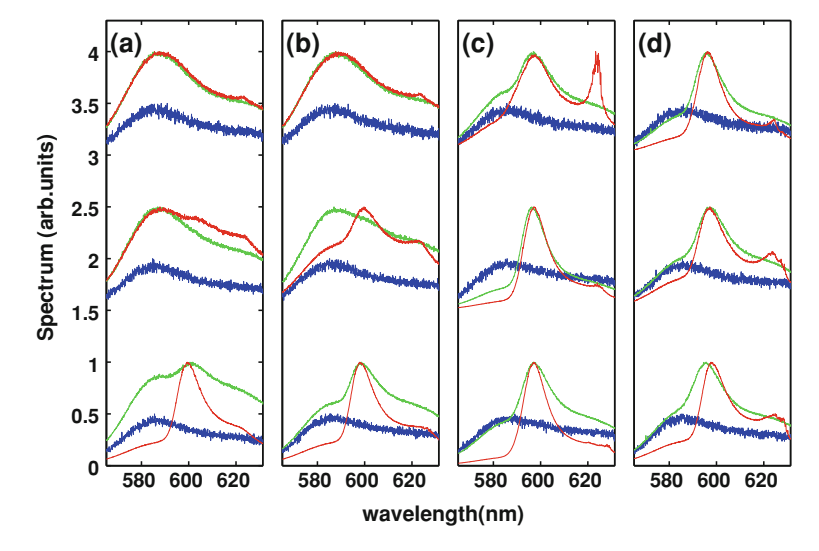


Fig. 9.13 Emission spectra for a granular sample of metallic particles in RhodamineB. Panel **a** corresponds to an oscillation with a=0 (sample at rest), **b** a=0.07, **c** a=0.1 and **d** a=0.2. In each panels, the three *bottom* spectra correspond to z=3 mm (inside the granular, at rest), the three *middle* spectra to z=7 mm (border zone at rest), and the *top* spectra to z=13 mm (outside the granular, at rest). For each z, we show the spectra for three different excitation energies [0.04 mJ (*blue line*), 1.6 mJ (*green line*) and 3.8 mJ (*red line*)]. The spectra are arbitrarily scaled for the sake of comparison

Fig. 9.14 Sketch of the couette at low amplitude, the *arrow* indicates the position of the beam with respect to the bottom when the sample is at rest



almost the same in all four cases but merely that the probability that, during the measuring time, a sphere of radius 1 mm can pass into a cylinder of radius 1.5 mm and length 10 mm (the linear dimension of the couette) is always nearly one. At a first glance, when considering the laser emission, there should be the same mean shape of the emitted spectra for the various oscillation amplitudes, however we expect that there will also exist some differences between the case at rest, in which the spheres are densely stacked together and the case in which, due to the strong oscillations, the interstices between neighboring spheres are increased. In Fig. 9.15, we report the emitted spectra, as measured for two different energy. As it can be seen, except for the blue line of panel (a), once the pumping energy is fixed, the spectra are quite similar.

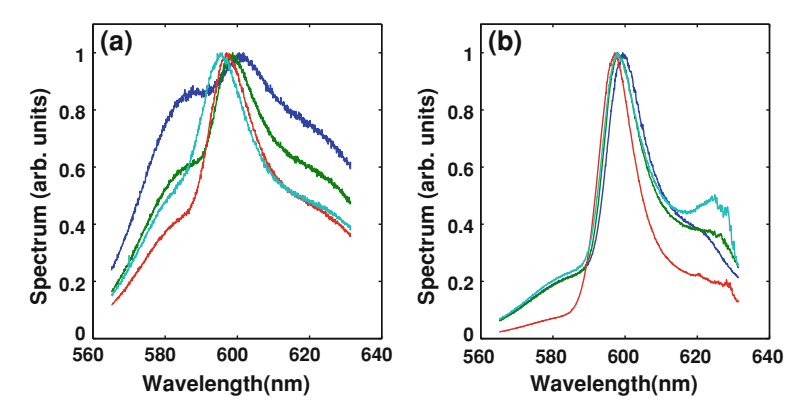


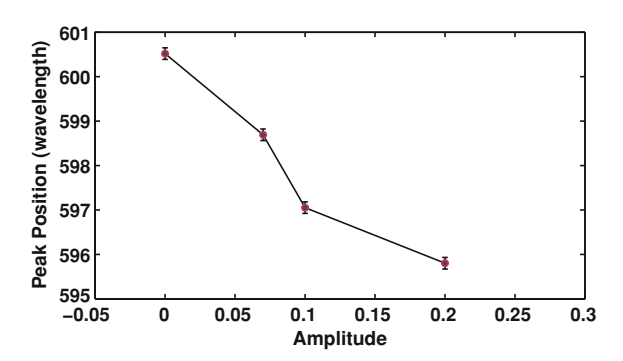
Fig. 9.15 Spectra of emission for granular sample of metallic particles in RhodamineB at z = 3 mm at pumping energy of 1.6 mJ (a), and 3.8 mJ (b). The *blue line* corresponds to a = 0, *green line* to a = 0.07, *red line* to a = 0.1, *sky-blue line* to a = 0.2

In both cases, we exceeded the laser threshold. A main peak is well visible around 600 nm. By increasing the input pump pulse energy, a narrowing of the spectrum is observable, with an increasing peak intensity [compare panel (a) with panel (b)], as in standard "diffusive" random lasers [8, 25]. However there are some noticeable features related to the variation of the amplitudes: a blue shift of the peak position with the amplitude (compare blue, green, red, sky-blue line), the appearance of a second peak in the high energy case [panel (b)] when the strength of the oscillation is increased (green, red but specially sky-blue lines). In correspondence of the excess threshold for laser at approximately 630 nm [sky-blue line in panel (b)], it is registered a red-shift of the main peak at 600 nm.

In order to explain and understand these emerging spectra, it is worthwhile visualize the arrangement of the grains for the several amplitudes. When the system is at the rest, the grains are deposited one of top of each other in a more or less ordered way. Depending on the particular configuration that the packed hard-spheres have assumed, we can have a variable density in the same portion of volume. We have to focus our attention at the negative of the packed spheres: the interstitial gaps between them forming an interconnecting network of cavities. Here, the light can bounce and diffuse. Hence, we can have two cases: in the first one, the light can pass through interstitial holes and diffuses in the sample. It results in a diffusive random laser emission spectrum. In the other case, as we will see below, the light is reflected by one sphere to another one, keeping a closed loop into an homogeneous reflecting cavity (interstitial holes): a coherent interfering feedback can be activated and discrete narrow peaks emerge in the spectrum.

Back to Fig. 9.15, the blue line of panel (a) is distinct to the other ones because here we are at rest and the energy is still too low to activate lasing in the superficial interstices: the cavities losses exceed the gain. By increasing the energy, however, the laser threshold is reached and the peak is well visible [blue line of panel (b), sample

Fig. 9.16 Position of the diffusive peak versus the amplitude of oscillation for the pumping energy of 1.6 mJ



at rest]. Back to panel (a), by increasing the amplitude, for the same energy, we can observe laser action (see red, green, sky-blue lines) because the increased interstitial network, due to oscillations, involves a correspondent increment of the amount of available active medium. The main peak around 600 nm, in both panels, is hence related to a diffusive behavior of the light into the sample. In order to explain the blue-shift versus the amplitude of the oscillations, we made the following argument based on the propagation of the electromagnetic wave in a medium is described by the electromagnetic wave equation. For monochromatic wave, the angular frequency is inversely related to the refractive index of the medium. It simply means that in a random medium increasing the index contrast tends to lower the electromagnetic resonances. On the other hand, the high-frequency modes are mostly promoted in a low-index contrast medium. By increasing the amplitude of oscillations, we stretch the mean free path of the light. By considering a fixed portion of couette volume, a longer mean free path is equivalent to consider a more diluted system with an effective index contrast kept lower. So, the activated modes, as the amplitude is increased, will be those with a lower wavelength. This may explain the blue-shift of the diffusive peak at 600 nm, reported Fig. 9.16.

Finally, in panel (b) we observe an interesting phenomenon, the appearance of a second peak with the increasing of amplitude (see sky-blue line, $a\!=\!0.2$) at approximately 630 nm. In our view, it can be related to the presence of closed cavities in which the light can constructively interfere, a mechanism different and in some sense competitive with the diffusive process discussed above. Indeed, this kind of laser emission could be compared to the standard random laser localizations, supporting by a random system when the mean free path is comparable with the wavelength: the Anderson states. Here, thanks to the interstitial cavities between metallic spheres, we have an ordered cavity in which the free mean path is much longer than the wavelength. The constructive interference can occur in a standard way, and the laser emission can be observed when the gain exceeds the losses [see sky-blue line of panel (b) in Fig. 9.15]. In correspondence of the activation of this coherent laser, we observe a broadening of the diffusive random laser at 600 nm with a red-shifted peak

Without scatterers inside.

Fig. 9.17 Position of the diffusive peak versus the amplitude of oscillation for the pumping energy of 3.79 mJ

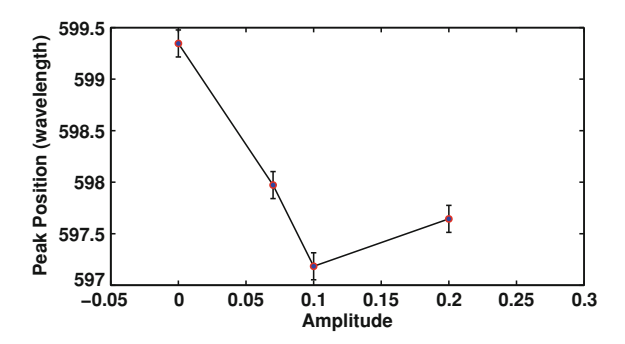


Fig. 9.18 Sketch of the couette at low amplitude, the *arrow* indicates the position of the beam with respect to the bottom when the sample is at rest



[see Fig. 9.19 and compare sky-blue with red line of panel (b) in Fig. 9.15]. This may eventually due to the fact that, when also the localized laser starts to emit, the available energy is distributed between two lasers, and hence the diffusive laser has wider linewidth (Fig. 9.17).

Concluding, at this stage we can conjecture two competing phenomena: interstitial diffusion and interstitial localization. In the granular region, the former appears dominant.

Edge region

In the region of boundary between the metallic spheres and the liquid region of Rhodamine (Fig. 9.18), the emitted spectra are not heavily different with respect to those seen in the section above. In fact in the edge region, the incident pulsed beam can affect mostly the granular or the liquid, depending on the size of the spot, on the beam position with respect to the edge and hence, on the amplitude of oscillations.

If we draw a vertical line in Figs. 9.12 and 9.10 at $z=7\,\mathrm{mm}$, we can see that the transmitted power is approximately equal to the incident power when a=0, while for all other amplitudes it is zero. This implies that, when the sample is at rest or slightly moved ($a=0\,\mathrm{or}\,0.07$), the incident continuous beam is able to cross the sample, going through the RhodamineB. The corresponding measured spectrum is the fluorescence of the RhB, as shown in Fig. 9.19, panel (a) and (b), blue and green lines. However, as before, in the high pump energy case, panel (b), it is sufficient that a small portion of the laser spot invests the granular region to observe a small bump around 600 nm, corresponding to the activation of the diffusive random laser (blue line). At incident pump energy of 1.6 mJ, panel (a), the same occurs to the spectrum

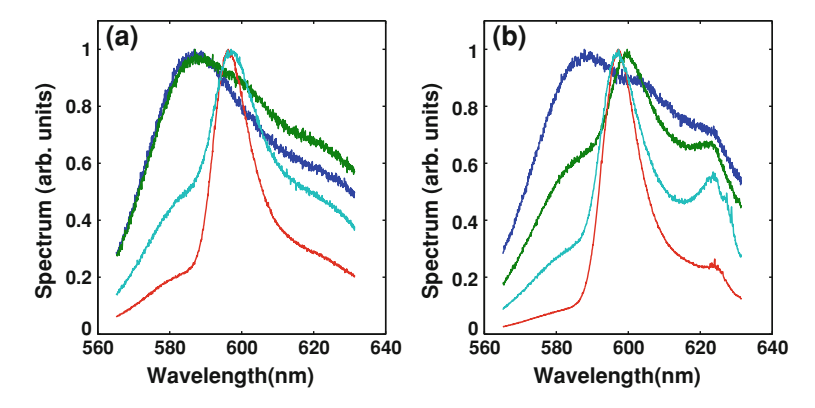


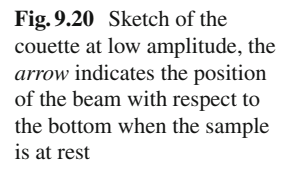
Fig. 9.19 Spectra of emission for GR0 sample in the edge region, at z = 7 mm at pumping energy of 1.6 mJ (**a**), and 3.8 mJ (**b**). In both panel a = 0 (blue line), a = 0.07 (green line), a = 0.1 (red line), a = 0.2 (sky-blue line)

at a=0.07, green line, bump at $600\,\mathrm{nm}$. In fact, a small oscillation allows the beam laser to interact with more grains with respect to the static case. The light start to diffuse through the interstitial holes. By increasing the amplitude of oscillation (red and sky-blue lines), the diffusive laser threshold is largely exceeded, thanks to the increasing availability of active medium, and we can see the characteristic diffusive peak at $600\,\mathrm{nm}$. In these dynamic conditions, an increase of the beam energy support also the localized random laser as shown in panel (b), green, red, sky-blue lines, peaks around $630\,\mathrm{nm}$.

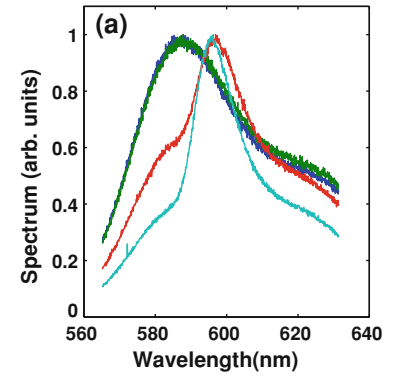
If we compare Fig. 9.15 with Fig. 9.19, we see that in the former case, the diffusive laser threshold is kept lower with respect to the edge case. In fact, in the latter case, a portion of the input energy is lost in the RhodamineB and so strong oscillations are required in panel (a) to reach the proper granular density for diffusive regime. To the other side, however, in the high energy condition, the threshold for localized random laser is lower with respect to the granular region case. This is maybe due to the higher freedom of movement for the grains in the edge region and so, there is a greater explorability of the configuration space and small vibrations are sufficient to reach the condition for interfering scattering emission. Also here, there exists an evident blue-shift for the diffusive peak above the localized laser threshold, and a successive red-shift when the localized regime is enhanced, which we ascribe to the competition between the two lasing phenomena (Fig. 9.19).

Liquid region

Getting into the liquid region (Fig. 9.20), the trend is still the same observed so far. In panel (a) of Fig. 9.21, the broad photoluminescence band is perfectly preserved also at a=0.07 (green line). In fact, the oscillations are not enough strong to drive the metallic grains and intercept the laser beam that is nearly at the top of the couette. The photoluminescence band narrows down, upon increasing the amplitude of the oscillations. The emission spectrum is peaked at $600 \, \mathrm{nm}$. The diffusive random laser







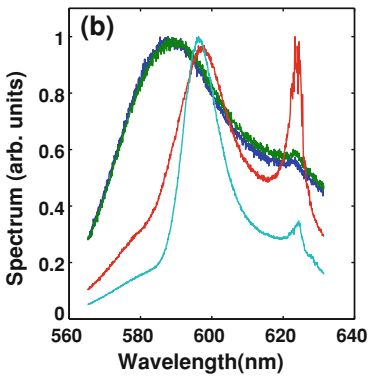


Fig. 9.21 Spectra of emission for GR0 sample in the liquid region, at z = 13 mm at pumping energy of 1.6 mJ (**a**), and 3.8 mJ (**b**). In both panel a = 0 (blue line), a = 0.07 (green line), a = 0.1 (red line), a = 0.2 (sky-blue line)

is enhanced. In panel (b), we observe the appearance of the localized peak also at $a=0,\,0.07$, at 630 nm. This is maybe related to the spot that howsoever is able to intercept a small granular region. Lastly, it must be noted that, although the red line corresponds to a lower amplitude with respect to the sky-blue line, in the former case the localized peak is much more pronounced. This shows that there exists an optimal amplitude of oscillation which corresponds to the best mean free path for the localized lasing. In Fig. 9.22, it is shown the dependence of the peak intensity on amplitude for the diffusive (a) and localized (b) lasers.

For what concerns the trend for the diffusive peak, in panel (a) the peak intensity grows with the amplitude of oscillations, similarly to what happens by increasing the pump energy in standard experiments. This is easily explained by observing that the increasing of the amplitude of oscillations implies an increasing of the interstitial holes. Correspondingly, the available active medium is larger and the threshold for lasing decreases.

On the other hand, for the localized case, panel (b) shows a peak for $a\!=\!0.1$, at which the distances between grains become optimal for interfering scattering and we can observe laser emission. In panel (c) and (d), the relative peak intensities are reported, which confirms the existence of an optimal oscillation amplitude.

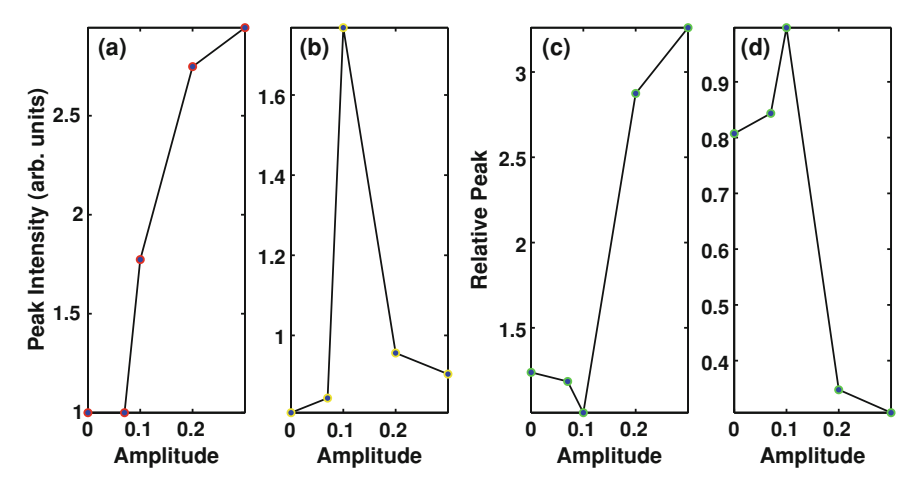


Fig. 9.22 Peak intensity for the diffusive laser (a) and for the localized one (b). In panel (c), we show the ratio between the diffusive peak intensity and the localized one. In panel (d), we show the inverse of (c)

9.5.3 Emission at Constant Power

In order to show that the structural information encoded by laser emission is richer than that obtained by optical transmission via continuous laser source ("continuous wave analysis"), we have investigated the emission spectra at the same constant transmission power for the continuous wave laser. In Fig. 9.23, a horizontal line for a fixed transmitted power is drawn in order to intersect the phase-diagram curves of the granular for several amplitudes. The lines drawn from their points of intersection meet the abscissa axes for different heights. For every intersection point, a couple of values for the oscillation amplitude and pump energy are considered, at which the same transmitted signal corresponds.

We have therefore studied the emitted spectra by the granular sample in these conditions. In the insets, in correspondence to the several intersecting points, the measured emitted spectra are reported at energy 3.8 mJ. Despite the static information⁴ is the same for all three cases, the spectra are not identical. This follows from the fact that the continuous laser source is not affected by the specific instantaneous granular configuration that simply influences the optical transmitted power by stopping the incident beam. The laser emission, indeed, is a resonant phenomenon that dramatically depends on the shape and dimension of the feedback cavity, and hence, the emitted spectra are strongly dependent of the specific structure, generated by fixing amplitude of the oscillations and height of the laser beam.

⁴ i.e. the transmission.

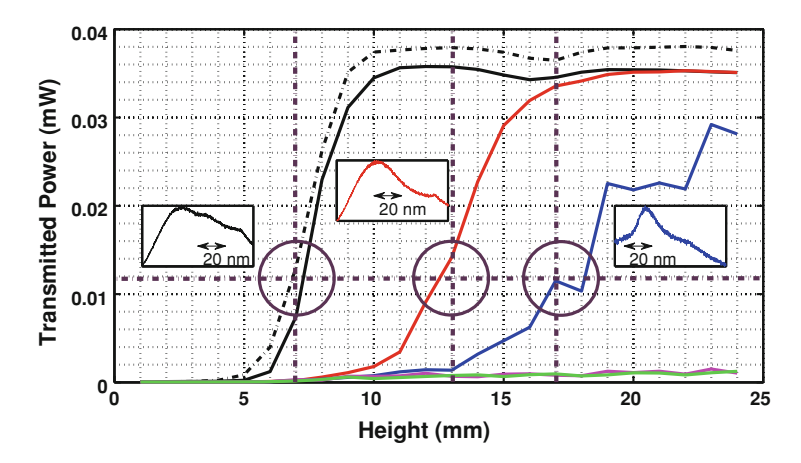


Fig. 9.23 Phase-diagram of the granular sample. The intersecting points of the constant line for fixed transmission power with the granular curves are studied by a dynamical point of view. The insets show the relative spectra. The *black line* corresponds to a = 0.01, *red line* to a = 0.07 and *blue line* to a = 0.1. The chosen heights are accordingly z = 7, 13, 17

9.5.4 Shot-to-Shot Variation

The laser localized emission occurs due the specific random arrangement of the metallic particles. The emitted spectra then depend not only on the input energy, on the height of the beam and on the amplitude of the oscillations, but also on the peculiar history of the random events. We have a statistics associated to the shot-toshot variation and this evidence suggests various conjectures about the explanation of the narrow peaks, observing in the measured spectra. The enhancement of the localized peaks around 630 nm must be related to the presence of multiple interfering processes. In Fig. 9.24, we sketch a light beam caught between three metallic spheres. The light path is $L = L_1 + L_2 + L_3$ and the condition for interference is $kL = 2\pi n$, where k is the wave vector and n is an integer number. In our case, if the above pivotal condition for constructive interference is satisfied, the system makes a transition to a localized state and we observe a peaked spectrum. If the peculiarities of the observed spectra were something related to a single particle phenomenon, we should not have a shot-to-shot variation as indeed shown in Fig. 9.25. This aspect must be related to the instantaneous configuration of the random medium and so, it is a collective phenomenon of the granular.

9.5.5 Sample with Doubled Radius (2 mm)

Henceforth, the next samples will be used jointly to show that the above observed spectra are a coherent phenomenon related to the formation of interference patterns

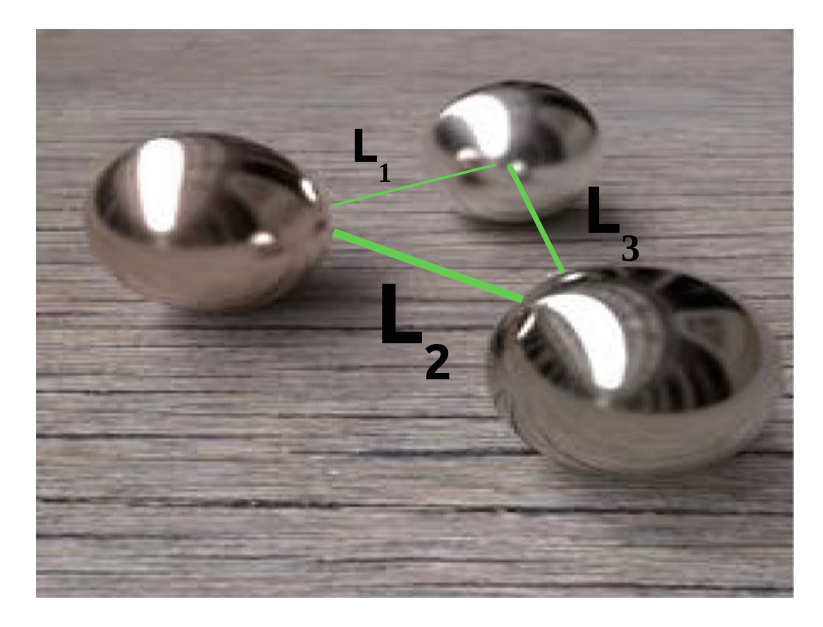
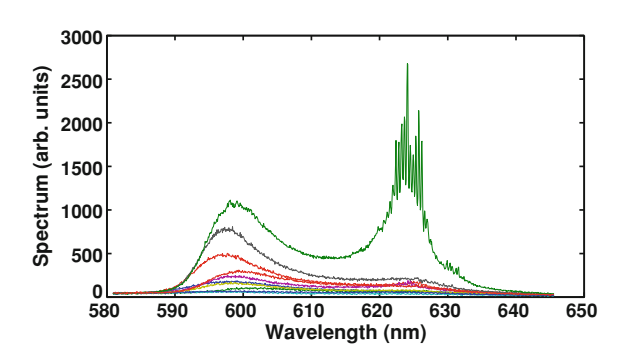


Fig. 9.24 Interference condition

Fig. 9.25 Spectra corresponding to ten pulses for a = 0.1, z = 10. The input energy is $4.6\,\mathrm{mJ}$. Each spectrum is a single shot corresponding to an instantaneous configuration of the granular



of three or more reflecting metallic spheres. We consider a sample with 3.194 g of amagnetic steel spherical grains with a doubled diameter (2 mm) with respect to the above sample in 2.968 g of RhodamineB.

In Fig. 9.26 we show the "phase-diagram" (Protocol 2) for this sample, while in Fig. 9.27 report the observed spectra. The results follows those described above for the smaller particles (1 mm), again displaying the two competitive peaks.

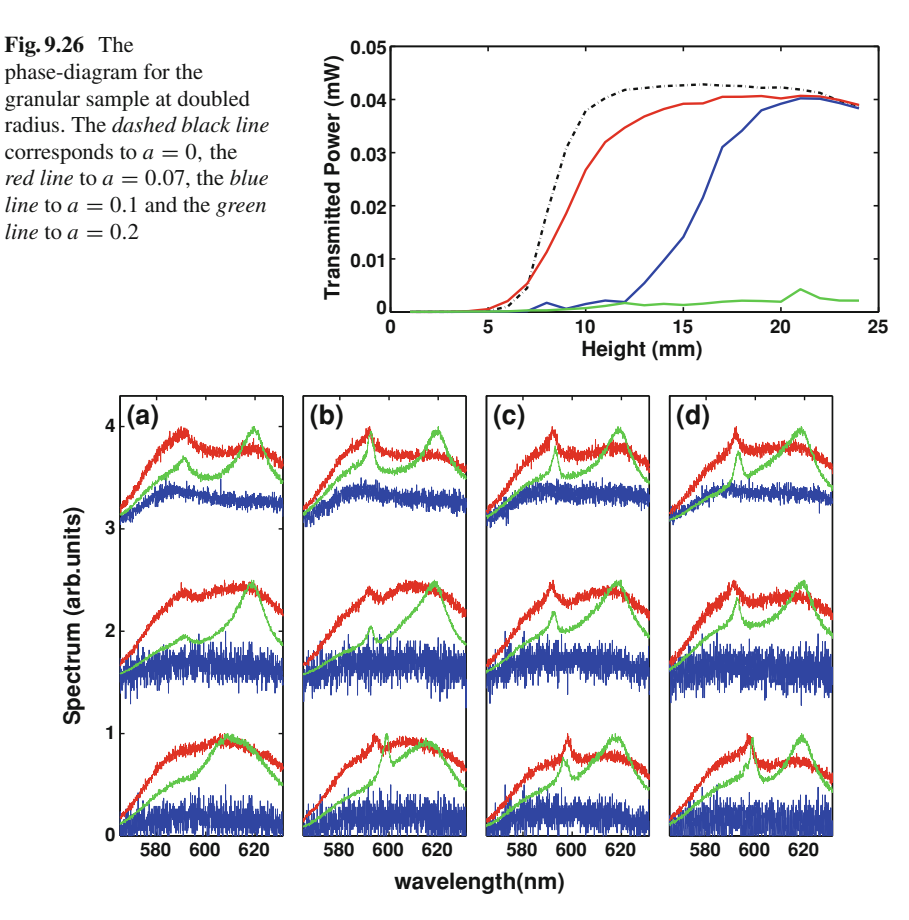


Fig. 9.27 Spectra of emission for granular sample of amagnetic steel spherical particles of size 2 mm, in RhodamineB. Panel **a** corresponds to an oscillation with a=0, **b** a=0.07, **c** a=0.1 and **d** a=0.2. In each panels, the three *bottom* spectra correspond to z=3 mm (inside the granular, at rest), the three *middle* spectra to z=7 mm (border zone at rest), and the *top* spectra to z=13 mm (outside the granular, at rest). Each triad corresponds to three different excitation energy [respectively 0.04 mJ (*blue line*), 1.6 mJ (*green line*) and 3.8 mJ (*red line*)]. The amplitude of the three triads has been shifted up by a factor of 0, 1.5, 3 respectively. The fluorescence band (in *blue*) has been scaled down a factor 0.5

9.5.6 The Two-Dimensional Granular Laser

To show that the reported localized laser emission is indeed a three-dimensional (3D) phenomenon related to interfering scattered light between three or more reflecting spheres, we consider a two-dimensional (2D) granular sample with the grain diameter 1 mm. A thin couette 2.5 cm high and 2 mm deep is chosen in order that the particles

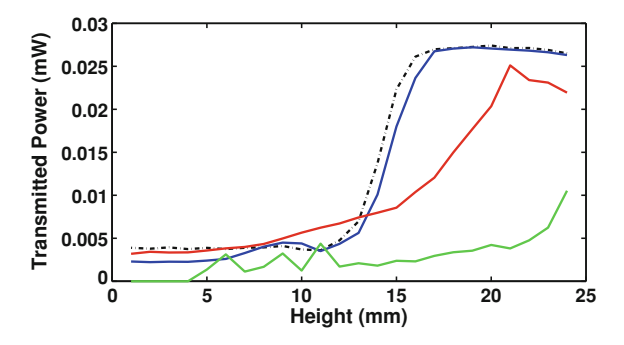


Fig. 9.28 The transmitted power for the two-dimensional granular sample versus the height, for four amplitudes of oscillation a=0 (a), a=0.1 (b), a=0.5 (c), a=1 (d). Here, the volume knob of the audio amplifier is recalibrated with respect to the above experiments, so that the relative amplitudes correspond to different normalized values for a

can be only vertically stacked. The couette device, half-containing metallic particles, is completely filled with RhodamineB.

We repeated all the protocols. For this sample, being a granular medium, there exist two phases, the blocked and the gaseous ones as shown in Fig. 9.28.

For what concerns the dynamical analysis, we went to look for the localized narrow peaks in the gaseous phase. We have fixed three heights of the laser beam with respect to the basis of the couette, in the granular region z = 5, in the edge region z = 16and in the liquid region z = 20 (see the dashed line in Fig. 9.28). For every height, we measure the emitted spectra for several values of input energy, both in the static [panel (a) of Fig. 9.29] that in the gaseous phases [panel (b)]. As it can be seen by the measured spectra, there is not evidence for localized peaks. Hence the additional emission can be ascribed to a specific three dimensional arrangement of spheres, achieved during shaking. This fact also allows to rule out the effect of plasmonic resonances, which are expected to play a negligible rule for the considered size of the grain (1 mm), which is much greater than the wavelength. Plasmonic resonances are indeed know to be relevant for nanoparticles [13–16]. Plasmonic resonances are also rule out by the fact that the localized peak changes from shot to shot (Fig. 2G), and hence depend on the collective configuration of several spheres, and not on the single sphere. The diffusive laser is well observable only in the deep granular once the laser threshold is exceeded.

In Figs. 9.30 and 9.31, we report the behavior of the peak intensity and of the spectral waist in the gaseous phase, at z = 16 mm, which confirm the diffusive character of the observed lasing emission.

By concluding, the fact that in 2D we do not observe localized emission demonstrates that the reported effect, the localized peak of the granular sample reported above, is not due to the single particle (otherwise it should appear in 2D and 3D) but is related to the collective organization of the sample in 3D.

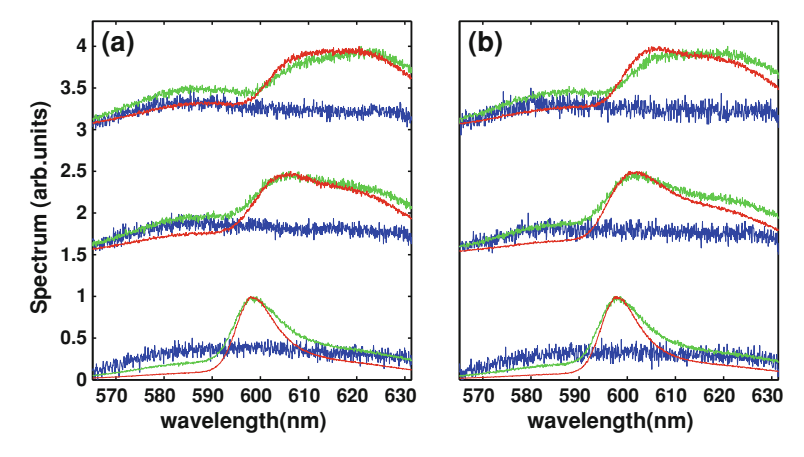


Fig. 9.29 Spectra of emission for the 2D metallic sample. Panel **a** corresponds to the static case while in panel **b** the measured spectra are reported for a = 1, enhanced the gaseous phase. In each panel, the *bottom* triad is for z = 5 mm (granular region), the *middle* triad is for z = 16 mm (edge region) and the *top* one is for z = 20 mm (liquid region). The excitation energies are 0.16, 1.7 and 3.9 mJ (*blue*, *green* and *red lines* respectively). The fluorescence band is scaled down on a factor 0.5 while the amplitudes of the spectra are arbitrarily scaled

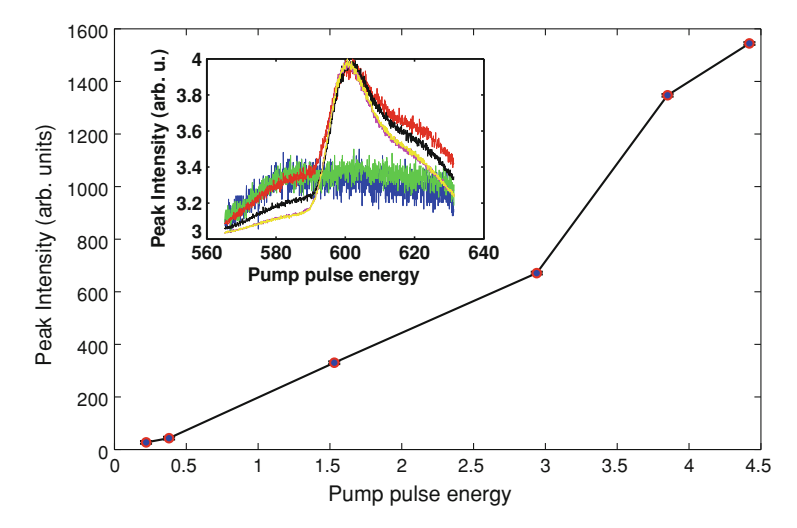
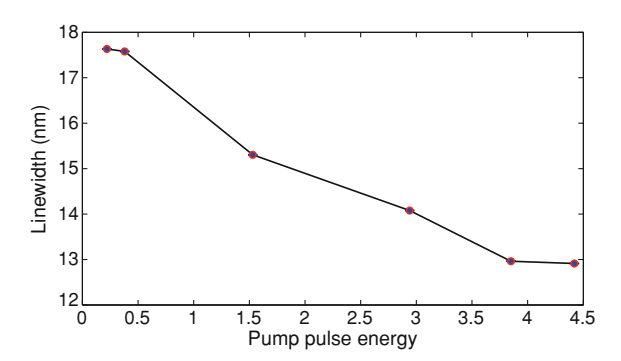


Fig. 9.30 The emission intensity of the peak spectrum versus the incident pump pulse energy. The error bars are included into the marker size. In the inset, the corresponding spectra are reported with 0.22 mJ (*blue line*), 0.38 mJ (*green line*) 1.53 mJ (*red line*), 2.94 mJ (*black line*), 3.85 mJ (*magenta line*), 4.42 mJ (*yellow line*)

Fig. 9.31 The emission spectrum waist, calculated as standard deviation, versus the pump pulse energy



9.5.7 The Heterogeneous Granular Sample

Finally, to show that the localized peak is a coherent phenomenon related to a resonant feedback mechanism, we made an heterogeneous granular sample. The random medium used in this experiment is realized by adding 0.217 g of ZnO powder (100 nm of diameter) to 4.04 g of amagnetic steel spherical grains with size 1 mm. The particles are immersed in 4.0 g of RhodamineB. The ZnO particles introduce a disorder on a length scale much shorter than the dimension of the amagnetic particles. If the light in the pure granular sample could create interfering closed path between reflecting metallic particles, here the presence of ZnO powder breaks the condition of constructive interference, and inhibits the coherent feedback mechanism of the light between adjacent mirrors. By measuring the emission spectra from these samples we found that the localized peak at 630 nm disappears (see Fig. 9.32) and the diffusive one is similar to that observed in the diffusive random laser (see Fig. 9.7). The top spectra of panel (a), related to still sample in the liquid-edge region, show a red shift with a peak around 600 nm due to the fact that, when the sample is at rest, the ZnO is deposited on the bottom and the light is mostly scattered by the metal grains of the top layers (compare these spectra with the edge spectra of Fig. 9.13). When the oscillating force is applied to the bottom of the couette and the heterogeneous granular medium starts to oscillate, the ZnO powder is homogeneously mixed to the RhodamineB and at all heights the dielectric diffusive peak is well visible. The diffusion by the ZnO powder is dominant with respect to the diffusion by metallic particles because the mean free path of the light between scatters is mainly determined by the scattering by dielectric spheres.

We tested various samples with different concentrations of ZnO, in all of the considered cases the diffusive peak due to ZnO dominates, and the localized disappears.

In this final chapter, we have reported on the first experimental evidence of laser emission in granular gases. These results, placed between modern photonics and statistical mechanics, not only demonstrate that RL in granular materials are sensitive to the specific grain distribution and their emission can be controlled by the status of motion of the system, but they also unveil the existence of a new form of random lasing that can be mechanically controlled and competed with the standard RL.

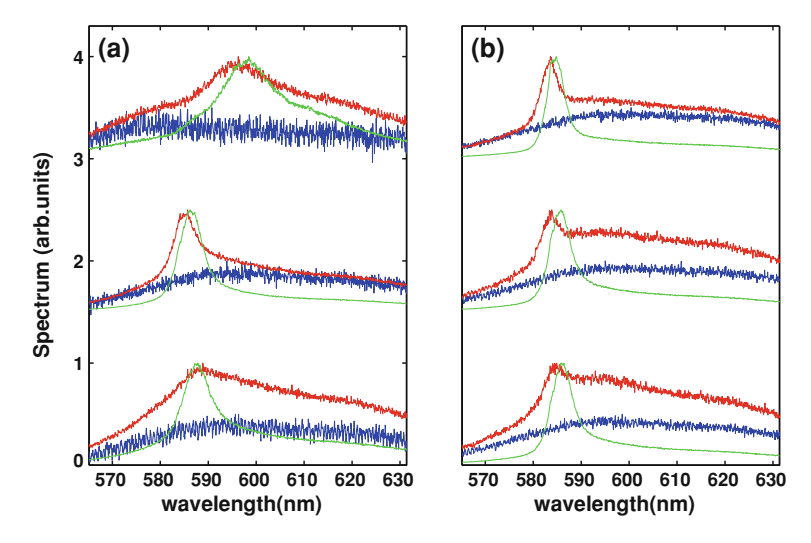


Fig. 9.32 Spectra of emission for heterogeneous granular sample. Panel **a** corresponds to blocked phase, panel **b** to gaseous phase. In each panels, the three *bottom* spectra correspond to beam inside the granular, for the three middle spectra, we are in the border zone, and the *top* spectra are the emitted light in the liquid region above the granular region at rest. Each triad corresponds to three different excitation energies [respectively 0.04 mJ (*blue line*), 1.6 mJ (*red line*) and 3.8 mJ (*green line*)]. Spectra have been scaled by an arbitrary factor for the sake of comparison

These open the way to a variety of further investigations, as light emission in matter under common granular processes like compactification, metastable granular states, mixed systems, accelerated flow under gravity, supercontinuum generation, and the interaction of laser emission with granular waves. The possibility of achieving a controlled non-equilibrium scenario in granular systems provides a variety of novel tools for random photonic devices, and ultimately, for assessing the interplay between the status of motion of mesoscopic matter and light emission.

References

- 1. Cao H (2003) Waves Random Media Complex Media 13:R1
- 2. Jaeger H, Nagel S (1992) Science 255:1523
- 3. Jaeger H, Nagel S, Behringer R (1996) Rev Mod Phys 68:1259
- 4. Poeschel T, Brilliantov N (2003) Granular gas dynamics, vol 624. Springer, Berlin
- 5. Poeschel T, Luding S (2001) Granular gases, vol 564. Springer, Berlin
- McLennan J (1989) Introduction to nonequilibrium statistical mechanics. Prentice Hall, Englewood Cliffs
- 7. Puglisi A, Visco P, Barrat A, Trizac E, van Wijland F (2005) Phys Rev Lett 95:110202
- 8. Lawandy NM, Balachandran RM, Gomes ASL, Sauvain E (1994) Nature 368:436
- 9. Goeuedard C, Husson D, Sauteret C, Auzel F, Migus A (1993) J Opt Soc B 10:2358
- 10. Briskina C, Markushev V, Ter-Gabrielyan NE (1996) Quantum Electron 26:923

References 113

- 11. Cao H et al (1999) Phys Rev Lett 82:2278
- Ryzhkov M, Markushev V, Briskina C, Cao H, (2005) Lasing in powdered ZnO: current state
 of affairs. In: Proceedings of CAOL 2005. 2nd international conference on advanced optoelectronics and lasers, vol 1, pp 72–75
- 13. Dice G, Mujumdar S, Elezzabi A (2005) Appl Phys Lett 86:131105
- 14. Popov O, Zilbershtein A, Davidov D (2006) Appl Phys Lett 89:191116
- 15. Meng X, Fujita K, Zong Y, Murai S, Tanaka K (2008) Appl Phys Lett 92:201112
- 16. Meng X, Fujita K, Murai S, Tanaka K (2009) Phys Rev A 79:053817
- 17. Wiersma DS, Vanalbada MP, Lagendijk A (1995) Nature 373:203
- 18. Wiersma DS (2008) Nature Phys 4:359
- 19. Letokhov VS (1968) Sov Phys JETP 26:835
- 20. Wiersma DS, Lagendijk A (1996) Phys Rev E 54:4256
- 21. Balachandran RM, Lawandy NM, Moon JA (1997) Opt Lett 22:319
- 22. Guerin W, Michaud F, Kaiser R (2008) Phys Rev Lett 101:093002
- 23. Cao H, Ling Y, Xu J, Cao C, Kumar P (2001) Phys Rev Lett 86:4524
- 24. Anderson PW (1958) Phys Rev 109:1492
- 25. Conti C, Leonetti M, Fratalocchi A, Angelani L, Ruocco G (2008) Phys Rev Lett 101:143901

Chapter 10 Conclusions

Investigating the interaction between radiation and matter in the presence of nonlinearity and disorder is the leitmotif of this work.

Over the past few decades, two prominent branches of photonics have been separately developed: soliton theory and Anderson localization of light. Both of these themes deal with the mechanisms of localization of the electromagnetic field resulting from interaction problem between light and matter.

On one hand, solitons are spatially localized light fields, their existence is due to nonlinearity; their are the upshot of coherent balancing between the natural propensity to diffract of a light beam and the focusing effect of nonlinearity.

To the other hand, disorder also induces localization through to the so-called Anderson states; a topic characterized by a huge amount of literature in past years, mostly due to the interdisciplinary character embracing a wide class of disciplines, from optics to computer science, from medical research to quantum mechanics. The Anderson localization needs disorder, as it promotes multiple scattering of light; interference effects hamper diffusive processes and cause wave localization.

A coherent and systematic treatment of the interplay between nonlinearity and disorder, in the regimes where cooperate or where compete for what concerns the localization phenomena is still missing. We wonder whether an hypothetic phase diagram with two control parameters, disorder and nonlinearity, exists. And if so, we expect that the two limit solutions, solitons and Anderson localizations, which are respectively the modes of nonlinearity and disorder, can interact each other in the intermediate regimes. This interaction would give rise to new intriguing phenomena, presenting the features of both. We have studied the effect of disorder on the stability of nonlinear solutions, the solitons, and viceversa, the effect of nonlinearity on the stability of disorder modes, the Anderson states. Nonlocality is additional effect that we used to mediate the interplay between nonlinearity and disorder, while also allowing remarkable technical simplifications.

This work develops by employing analytical, numerical and experimental methods and the analysis covers both the non-resonant and the resonant regimes, embracing issues from nonlinear optics to laser physics.

116 10 Conclusions

Dealing with complex systems, the first step in the development of the theoretical approach is within the perturbative regime when nonlinearity or disorder are treated as perturbations to well-known systems. The application of the methods mutuated by spin-glass theory allowed to extend the theory beyond the perturbative framework, even if at the cost of a substantial increase in the conceptual and mathematical complexity; such an approach allows to derive indeed a phase-diagram in terms of amount of disorder and nonlinearity. Furthermore, the behavior of the electromagnetic field beyond perturbations was studied by a first-principle numerical approach: in the non-resonant regime, we make use of the Beam Propagation Method to solve the Nonlinear Schroedinger equation with randomness; for the resonant regime, a parallel algorithm using a Finite Difference Time Domain (FDTD) scheme is employed to simulate ab-initio the dynamics of the electromagnetic field. Finally, a set of experiments was performed in the resonant regime to characterize the role of a tunable disorder in the random laser emission spectra. The first "granular" laser was implemented in order to study and control the emission phenomena by turning and change the disorder distribution and its strength. Indeed, we use granular matter, for which it is possible to change the state of aggregation under the action of external stresses, thanks to its morphologic characteristics.

The first section of the present work embraces the interaction processes between nonlinearity and disorder in the non-resonant regime, when the nonlinear optical properties of materials are active in their transparency region. In the Chap. 1, we briefly describe the main notions about light propagation in nonlinear systems. We introduce the iconic equation of nonlinear optics, the nonlinear Schroedinger equation (NLS), and we show its localized solutions, the solitary waves. In Chap. 2, we study the dynamics of the solitons in the presence of a perturbative disorder. Through a theoretical and numerical approach, we observe that an increasing degree of non-locality in the nonlinear response of the material acts as a filter on the Brownian motion of the self-trapped waves, averaging out the noise. In the limit of highly non-locality, the random fluctuations of the soliton vanishes. We believe that the obtained results are applicable on a wide range of physical phenomena, as for example Bose-Einstein condensates, thermo-diffusive materials, soft-colloidal matter, liquid crystals, all those materials in which the non-locality can be high. In Chap. 3, the inverse scenery is reported, namely the case in which the disorder is the putative mechanism responsible of the wave trapping, giving rise to the formation of Anderson localizations. The effect of perturbative focusing and defocusing nonlinearities is studied on their stability both in the analytical and numerical framework. We address again the role of non-locality and show that an increasing degree of non locality tends to stabilize the Anderson states. The applicability of this topic is large, primarily in the study of all phenomena working with the propagation of localized wave-forms in strongly disordered systems. In Chap. 4, disorder and nonlinearity live on two distinct length-scales. Now, their mutual interaction favors the activation of solitary waves and their stability. In the second part of this work, we enter the resonant regime. The radiation-matter interaction is active and microscopic. In Chap. 6, we briefly report the basic equations of the problem, the Maxwell-Bloch equations, and we show that also in this regime, under specific conditions, solitary waves can be observed, the

10 Conclusions 117

SIT solitons. Within the same scheme of the first part, in Chap. 7 we initially perturb the soliton dynamics, by introducing random fluctuations of material density. Then, we add structural disorder and we observe the active interaction between the solitary waves and the Anderson states, induced by the presence of disorder. New intriguing features will appear, the coupling between a SIT soliton and Anderson states causes the trapping of the solitary waves in closed cavities in proximity of the Anderson modes, generating a kind of two-level laser device, which coherent emission from the disordered structure can be measured. Chapter 8 shows the generalization of the problem, the active interaction between nonlinearity and disorder, by studying from a theoretical point of view, based on a statistical approach, the phase diagram of lasers. By changing the control parameters, disorder and nonlinearity, into the framework of the Spin Glass theory, the statistical distribution of laser modes is determined and we show as it be possible to switch between the standard and random lasers, simply controlling the degree of disorder and non linearity. In Chap. 9, we implement a new kind of random laser, exploiting the structural characteristics of granular matter. In the presented device, the disorder is easily tunable by changing the external solicitations and the system allows to switch between diffusive random laser emission and the localized one.

In conclusions, in this research, we give a unified view of electromagnetic localization, and we study the two main mechanisms that allow light trapping: disorder and nonlinearity. In particular, we study their interplay between the well-known solitons and Anderson localizations. When this processes act on the same ground, there exists a wide and fascinating class of new phenomena, yet to be discovered, that we have here partially investigate. All of these physics can be used and exploited to increment new technologies and the research driven by localized states of light, from optical communications to medical imaging.